UNIVERSITÀ DEGLI STUDI DI TRIESTE

UNIVERSITÀ DEGLI STUDI DI TRIESTE

XXXV CICLO DEL DOTTORATO DI RICERCA IN SCIENZE DELLA RIPRODUZIONE E DELLO SVILUPPO

PO FRIULI VENEZIA GIULIA – FONDO SOCIALE EUROPEO 2014/2020

DEVELOPMENT AND CHARACTERIZATION OF 3D STRUCTURES AND HYDROGELS BASED ON NATURAL AND MODIFIED POLYSACCHARIDES FOR BIOMEDICAL APPLICATIONS

Settore scientifico-disciplinare: **MED/50 – SCIENZE TECNICHE MEDICHE APPLICATE**

DOTTORANDA
CHIARA PIZZOLITTO

COORDINATORE
PROF. PAOLO GASPARINI

SUPERVISORE DI TESI
PROF. IVAN DONATI

CO-SUPERVISORI DI TESI
PROF. GIANLUCA TURCO
DOTT. PASQUALE SACCO

ANNO ACCADEMICO 2021/2022

UNIVERSITÀ
DEGLI STUDI
DI TRIESTE

UNIVERSITÀ DEGLI STUDI DI TRIESTE

XXXV CICLO DEL DOTTORATO DI RICERCA IN SCIENZE DELLA RIPRODUZIONE E DELLO SVILUPPO

PO FRIULI VENEZIA GIULIA – FONDO SOCIALE EUROPEO 2014/2020

DEVELOPMENT AND CHARACTERIZATION OF 3D STRUCTURES AND HYDROGELS BASED ON NATURAL AND MODIFIED POLYSACCHARIDES FOR BIOMEDICAL APPLICATIONS

Settore scientifico-disciplinare: **MED/50 – SCIENZE TENCICHE MEDICHE APPLICATE**

DOTTORANDA
CHIARA PIZZOLITTO

COORDINATORE
PROF. PAOLO GASPARINI

SUPERVISORE DI TESI
PROF. IVAN DONATI

CO-SUPERVISORI DI TESI
PROF. GIANLUCA TURCO
DOTT. PASQUALE SACCO

ANNO ACCADEMICO 2021/2022

A Bianca, il miglior risultato di questo dottorato

.

PREFACE

This thesis is submitted in fulfilment to the requirements of the Graduate School of Reproduction and Developmental Sciences for the academic title of Ph.D. in Reproduction and Developmental Sciences at the University of Trieste. The work has been carried out mainly at the Department of Life Sciences at the University of Trieste under the supervision of Prof. Ivan Donati and co-supervised by Dr. Pasquale Sacco. Part of the activity was performed at the Biomaterial Lab of the Dental Clinic of Maggiore Hospital under the supervision of the co-supervisor Prof. Gianluca Turco.

The thesis consists of a general introduction, aim of the study and a detailed discussion of results divided into three chapters.

RIASSUNTO

L'ingegneria tissutale si prefigge lo scopo di combinare l'utilizzo di cellule e di scaffold al fine di migliorare, riparare e/o sostituire tessuti ed organi lesionati. La difficoltà nel raggiungimento di questo obiettivo è costituita dalla ricerca di materiali che siano in grado di mimare la complessità della matrice extracellulare (ECM). L'ECM, infatti, è caratterizzata da una forte eterogeneità di componenti e da una natura dinamica, in cui stimoli meccanici derivanti dall'ambiente esterno si trasformano in stimoli biochimici trasmessi alle cellule, andando ad influenzare la risposta cellulare. Tra i materiali più promettenti in grado di mimare la complessa architettura della ECM si possono annoverare i polisaccaridi, specialmente quelli di origine naturale. Il loro utilizzo risulta vantaggioso per diverse motivazioni, tra cui struttura simile a quella di alcune componenti della ECM, scarsa tossicità, alta biocompatibilità e biodegradabilità. Uno dei polisaccaridi di origine naturale più utilizzati è il chitosano, le cui limitazioni, come la sua scarsa solubilità a pH neutro (soprattutto per i classici chitosani commerciali ad alto/medio peso molecolare e basso grado di acetilazione), sono facilmente superabili attraverso il ricorso a modifiche chimiche. Un risultato di quest'ultimo approccio riguarda il CTL, un chitosano modificato mediante l'aggiunta di lattosio, prodotto dall'azienda Biopolife s.r.l. con sede a Trieste ed utilizzato come polisaccaride di interesse in questo progetto di dottorato. Negli anni, diversi studi condotti sul CTL hanno evidenziato le sue proprietà bioattive a contatto con diverse linee cellulari (condrociti, cellule mesenchimali ed osteoblasti in primis), rendendo vantaggioso il suo impiego per lo sviluppo di biomateriali per diverse applicazioni biomediche. Grazie alla presenza di ammine (primarie e secondarie) reattive nel suo scheletro il CTL è in grado di essere reticolato fisicamente e chimicamente portando alla formazione di idrogeli con proprietà meccaniche interessanti. Infatti, è stato dimostrato come il CTL, sfruttando i dioli presenti nelle sue catene laterali, è in grado di formare network dinamici in presenza di reticolanti transienti come l'acido borico. Studi approfonditi sui network a base di CTL e acido borico hanno rilevato proprietà meccaniche simili a quelle della ECM nativa. Tuttavia, la continua riorganizzazione della rete polimerica limita drasticamente le potenziali applicazioni di questi idrogeli come substrati cellulari. Si è reso quindi necessario l'introduzione di cross-linker covalenti per migliorare la stabilità del network. Tra i vari reticolanti covalenti, la genipina è risultata essere un buon candidato, grazie alla sua origine naturale e alla sua dimostrata biocompatibilità.

Il primo obiettivo del progetto è stato lo studio della reazione chimica tra la genipina, reticolante di origine naturale, e le ammine primarie del CTL. Le tecniche analitiche utilizzate sono state principalmente la spettroscopia UV-Vis e il dicroismo circolare. Due tipi di reazione, con relativa

cinetica, sono stati rilevati in presenza di ossigeno: (1) una reazione intercatena che coinvolge due molecole di genipina e due molecole del polisaccaride, e (2) una reazione di una molecola di genipina con un'ammina primaria del polimero, senza però portare ad una reticolazione delle catene. Quest'ultima reazione evolve poi in un'ulteriore reticolazione tra catene, portando allo sviluppo di una colorazione blu del composto, caratteristica dei prodotti contenenti genipina.

La seconda parte del progetto di dottorato prevede l'utilizzo di idrogeli con reticolazione duale utilizzati in questo lavoro come substrati cellulari per la crescita e il differenziamento di cellule mesenchimali da tessuto adiposo (hMSC-AT). Questi "dual cross-link hydrogels" sono composti dal CTL, reticolato attraverso l'uso dell'acido borico, che funge da reticolante temporaneo, e dalla genipina, reticolante covalente di originale naturale. Un'approfondita analisi meccanica di questi substrati ci ha permesso di dimostrare come la presenza del reticolante temporaneo ha un effetto praticamente nullo sul modulo di taglio (shear modulus) ma impatta notevolmente sulla dissipazione dello stress applicato. Sulla base di questi risultati si è quindi valutato l'impatto della dissipazione dello stress sul differenziamento osteogenico di hMSC-AT seminate al di sopra di questi substrati. Questa proprietà del materiale porta a una precoce espressione dei tipici markers osteogenici, come evidenziato dall'analisi di espressione dei geni Runt-related transcription factors (RUNX2), collagene di tipo 1 (COL1A1), osteocalcina (OCN), fosfatasi alcalina (ALP) e formazione di depositi di calcio. I substrati dove il CTL veniva reticolato solo con la genipina, invece, presentavano caratteristiche puramente elastiche e la risposta al differenziamento osteogenico avviene in tempi più lunghi. Da questo studio emerge quindi che la dissipazione dello stress applicato risulta essere un ulteriore parametro da tenere in considerazione nello sviluppo di biomateriali con potenziali applicazioni nel settore dell'ingegneria tissutale ed è un'ulteriore conferma di quanto le proprietà meccaniche vadano a influenzare processi cellulari sia fisiologici che patologici.

Nell'ultima parte del progetto, invece, il CTL e un suo derivato solfatato sono stati utilizzati come matrici per coordinare l'aggregazione cellulare, portando alla formazione di sferoidi, strutture tridimensionali con potenziali applicazioni nel campo della rigenerazione della cartilagine. Studi precedenti avevano già dimostrato che il CTL, a contatto con una coltura primaria di condrociti, induce aggregazione, portando alla formazione di noduli e stimolando la produzione di collagene di tipo 2. In questo progetto ci si è focalizzati su un'analisi dettagliata del ruolo del polimero all'interno di queste strutture. Utilizzando condrociti primari estratti da articolazione di maiale, abbiamo potuto dimostrare che il CTL non solo coordina l'aggregazione cellulare, fungendo da matrice temporanea, ma interagisce fortemente con le componenti cellulari dei condrociti. L'analisi al microscopio a

trasmissione elettronica (TEM), infatti, ha dimostrato che i condrociti sono in grado di internalizzare il polimero all'interno di strutture vescicolari durante i primi giorni di coltura, rimaneggiandolo poi nei giorni successivi. Gli sferoidi formati in presenza di CTL poi si differenziano dagli sferoidi descritti in letteratura (dove predominano le interazioni cellula-cellula) per la presenza di una matrice amorfa tra le cellule. Basandoci poi sulle proprietà bioattive di questo polimero è stato interessante andare a valutare l'influenza del CTL sulla formazione e sul differenziamento condrogenico di sferoidi di cellule mesenchimali da tessuto adiposo. Sferoidi formati da CTL sono stati comparati con sferoidi formati su un coating di agar, per simulare gli sferoidi descritti già in letteratura con predominanza di interazioni cellula-cellula. Anche in questo caso è stata dimostrata la presenza del polimero all'interno della struttura, portando quindi alla formazione di sferoidi più lassi rispetto alla controparte formata in agar. Il risultato più sorprendente, però, è stato quello relativo al differenziamento. Negli sferoidi formati in presenza di CTL è possibile rilevare la presenza di alcuni marker condrogenici già nei primi giorni di coltura. Negli sferoidi formati con agar, invece, il differenziamento condrogenico avviene seguendo le tempistiche classiche descritte in letteratura (circa 21 giorni). Infine, sono stati condotti degli studi preliminari utilizzando dei CTL modificati con solfati per coordinare l'aggregazione di cellule mesenchimali da tessuto adiposo. Gli sferoidi risultanti, però, presentano delle dimensioni molto più piccole rispetto agli sferoidi formati con il CTL standard. La causa di questa variazione di dimensioni è da ricondurre alla parziale degradazione del polimero. Questo risultato preliminare è un'ulteriore conferma del ruolo attivo del polimero CTL nel coordinare l'aggregazione cellulare ed un'eventuale sua degradazione può arrivare a compromettere notevolmente la formazione di aggregati.

ABSTRACT

Tissue-engineering strategies combine cells with different materials to improve, restore or replace damaged tissues. The difficulty in achieving this goal is to find materials that are able to mimic the complexity of the extracellular matrix (ECM). Indeed, the ECM is characterized by a strong heterogeneity in composition and a dynamic nature in which cells are able to transform external mechanical stimuli into internal biochemical response. This process influences cell-fate decisions. Various materials can be used to recapitulate the ECM physical characteristics, although polymers from natural sources are considered the best choice given their good biocompatibility. Natural polysaccharides offer additional advantages such as their structural similarity to the component of the ECM and biodegradability. Chitosan is one of the most important polysaccharides used as biomaterials, but some weaknesses, such as low solubility a neutral pH – characteristics shared for most of commercial chitosans (high-to-medium molecular weight and low fraction of acetylated units, F_A) - limit its applications. To overcome such flaw, chitosan can be chemically modified. An example of these modifications is CTL, a lactose-modified chitosan produced by Biopolife s.r.l. in Trieste, which is of interest as a polysaccharide in this PhD project. The literature has already reported on the bioactive properties of this polymer towards various cell lines (e.g. chondrocytes, mesenchymal stem cells, osteocytes) and its use in the development of biomaterials for biomedical applications. Due to its polycationic nature and the presence of primary and secondary amines, CTL is capable to forming physical and chemical hydrogels with intriguing mechanical properties. CTL has been shown to form transient polymeric networks in the presence of inorganic crosslinkers such as boric acid, where the crosslinking points are constantly breaking and reforming in a highly dynamic fashion. The consequence is a non-equilibrium network endowed with peculiar mechanical properties. However, for long-lasting applications in the field of biomaterials, the introduction of stable connection points is advantageous in order to avoid the continuous rearrangement of the network. A good covalent crosslinker is genipin, a natural aglycone that is often used as a ligand of primary amines for the production of biomaterials due to its low cytotoxicity.

The first part of the project focused on studying of the chemical reaction between genipin and primary amines, using UV-VIS and circular dichroism as analytical tools. The novelty of these studies lies in the fact that all the measurements were undertaken at a pH of 7.4 and physiological osmolarity in the presence of oxygen as well as in oxygen-depleted conditions. Two types of reactions and their kinetics have been uncovered in the presence of oxygen: an interchain binding, which involves two genipin molecules and two polysaccharide chains, and a binding of one genipin molecule to the polymer chain

without chain-chain reticulation. The latter evolves into additional interchain cross-linking, leading to the formation of the well-known blue iridoid-derivatives.

In the second part, dual cross-linked hydrogels consisting of CTL and based on boric acid and genipin as temporary and permanent cross-linkers, respectively, were developed. These networks provide a suitable platform to study the behavior and the differentiation of adipose-derived mesenchymal stem cells (hMSC-AT). Rheological studies on these novel hydrogels have shown that the presence of temporary cross-linkers has a minor effect on the shear modulus but causes an immediate relaxation (dissipation) of the applied stress. This material property promoted osteogenic commitment of hMSC-AT, which was confirmed by the higher expression of characteristic bone markers such as Runt-related transcription factors (RUNX2), type I collagen (COL1A1), osteocalcin (OCN), alkaline phosphatase (ALP) and calcium deposit formation. On the other hand, the cells cultured in purely elastic substrates in which CTL is only cross-linked with genipin, started to differentiate afterwards. Thus, this study shows that stress dissipation is an additional parameter to be considered in the development of biomaterials with potential application in tissue engineering. This represents a further confirmation that mechanical properties influence both physiological and pathological cellular processes.

In the final part of the project, CTL and a Sulphated-CTL were used as a temporary matrix to coordinate cell aggregation and form spheroids, 3D structures with potential application in the treatment of injured cartilage tissue. It has been previously reported that CTL induces the aggregation of primary chondrocytes with the formation of nodules and stimulates the production of type-II collagen. In this project, we focused on analyzing the role of the polymer within these structures. Using primary chondrocytes from pig joint, we were able to demonstrate that CTL not only serves as a temporary matrix for the aggregation of cells, but also interacts very closely with the cells structures. In particular, transmission electron microscopy (TEM) has shown that chondrocytes can internalize the polymer in the first days of culture and remodel it in the following days. Furthermore, these chondro-aggregates differ from the spheroids described in the literature (which are characterized by the presence of cell-cell interactions) by the presence of an amorphous matrix between the chondrocytes. Following the bioactive properties of the polymer described in the literature, the next step was to investigate the influence of the polymer CTL on aggregation and chondrogenic differentiation of hMSC-AT. The spheroids formed in the presence of CTL are compared with the spheroids formed on non-adhesive agar-coated wells. This last type of spheroids is used to simulate the spheroids described in the literature, where cellular interactions predominate. Also in this case

the presence of the polymer in the structures was detected as well as the formation of a loose structure. However, the most striking result was those related to differentiation. In the spheroids formed in the presence of CTL, chondrogenic markers can already be detected in the first days of culture. In contrast, in the spheroids formed with agar, chondrogenic differentiation occurs according to the classical schedule described in the literature (21 days). Finally, preliminary studies were performed with sulfated CTL to coordinate the aggregation of hMSC-AT. However, the resulting spheroids are much smaller than spheroids formed with conventional CTL. The change in size can be explained by the partial degradation of the polymer. This preliminary result once again confirms the active role of CTL in coordinating cellular aggregation, and its degradation can significantly compromise the formation of the aggregates.

LIST OF PAPERS

Pizzolitto, C., Cok, M., Asaro, F., Scognamiglio, F., Marsich, E., Lopez, F., Donati, I., Sacco, P., 2020. On the mechanism of genipin binding to primary amines in lactose-modified chitosan at neutral pH. Int. J. Mol. Sci. 21, 1–17. https://doi.org/10.3390/ijms21186831

Pizzolitto, C., Esposito, F., Sacco, P., Marsich, E., Gargiulo, V., Bedini, E., Donati, I., 2022a. Sulfated lactose-modified chitosan. A novel synthetic glycosaminoglycan-like polysaccharide inducing chondrocyte aggregation. Carbohydr. Polym. 288, 119379. https://doi.org/10.1016/j.carbpol.2022.119379

Pizzolitto, C., Scognamiglio, F., Baldini, G., Bortul, R., Turco, G., Donati, I., Nicolin, V., Marsich, E., 2022b. Bioactive Lactose-Modified Chitosan Acts as a Temporary Extracellular Matrix for the Formation of Chondro-Aggregates. ACS Appl. Polym. Mater. https://doi.org/10.1021/acsapm.2c01613

Pizzolitto, C., Scognamiglio, F., Sacco, P., Lipari, S., Romano, M., Donati, I., Marsich, E., 2023. Immediate stress dissipation in dual cross-link hydrogels controls osteogenic commitment of mesenchymal stem cells. Carbohydr. Polym. 302, 120369. https://doi.org/10.1016/j.carbpol.2022.120369

CONTRIBUTION TO OTHER PUBLICATIONS NOT INCLUDED IN THE THESIS

Sacco, P., Cok, M., Scognamiglio, F., **Pizzolitto, C**., Vecchies, F., Marfoglia, A., Marsich, E., Donati, I. 2020. Glycosylated-Chitosan Derivatives: A Systematic Review. Molecules 25, 1534.

Sacco, P., Furlani, F., Marfoglia, A., Cok, M., **Pizzolitto, C**., Marsich, E., Donati, I., 2020. Temporary/Permanent Dual Cross-Link Gels Formed of a Bioactive Lactose-Modified Chitosan. Macromol. Biosci. 20, 1–7. https://doi.org/10.1002/mabi.202000236

Sacco, P., Piazza, F., **Pizzolitto, C**., Baj, G., Brun, F., Marsich, E., Donati, I., 2022. Regulation of Substrate Dissipation via Tunable Linear Elasticity Controls Cell Activity. Adv. Funct. Mater. 32, 1–12. https://doi.org/10.1002/adfm.202200309

LIST OF ABBREVIATIONS

2D – two-dimensional

3D – three-dimensional

ACI – Autologous Chondrocytes Implantations

ALP – Alkaline Phosphatase

CD – Circular Dichroism

COL-1 – Type I Collagen

COL-2 – Type II Collagen

CS – chondroitin sulphate

CTL – Lactose modified chitosan

DP – Degree of polymerization.

ECM – Extracellular Matrix

FBS – Fetal Bovine Serum

G' – Elastic (storage) modulus

G" – Viscous (loss) modulus

GAGs – Glycosaminoglycans

h – thickness

HA – Hyaluronic Acid

HA – Hyaluronic acid

hMSC-AT – human mesenchymal stem cell from adipose-tissue

ITS – Insulin-Transferrin-Selenium-Sodium pyruvate

MACI – Matrix-induced Autologous Chondrocytes Implantations

MSCs – Mesenchymal Stem Cells;

MTT – 3,4,5-dimethylthiazol-2yl-2,5-diphenytetrazolium bromide

MW – Molecular weight

Ø – diameter

OA – Osteoarthritis

OCN – Osteocalcin

PBS – Phosphate Saline Buffer

$R_{D/G}$ – Molar ratio between glucosamine units of CTL (D) and genipin (G)

RM – Regenerative Medicine

RUNX2 – Runt-related transcription factor 2

SEM – Scanning Electron Microscopy

TE – Tissue Engineering

TEM – Transmission Electron Microscopy

TERM – Tissue Engineering and Regenerative Medicine.

TABLE OF CONTENTS

1. INTRODUCTION

1.1. Tissue engineering: from traditional strategies to current challenges.

Tissue Engineering and Regenerative Medicine (TERM) is an interdisciplinary field that aims to develop biological substitutes to restore, maintain or improve tissue functions. Great expectations are placed on tissue engineering (TE) as most of the strategies currently adopted, such as organ transplants, surgical reconstructions, and mechanical devices are limited by the lack of donors, long-term complications and the inability to fully replicate organ functions (Han et al., 2020; Langner and Vacanti, 1993). TE achieves its goal by combining cells, scaffolds, growth factors and other strategies such as cell-based therapy, gene therapy and immunomodulation (Han et al., 2020). Three strategies are usually used in TERM:

- Complex systems of cells and biomaterials;
- Cell systems (*e.g.*, stem cell transplantation);
- Biomaterial systems that integrate into the body's tissue.

Over the years, much effort has been done to optimize different biomaterials and improve cell attachment, viability, protein uptake and even differentiation (Naqvi and Mcnamara, 2020).

Although TERM has been developed for over 30 years, it is still in its infancy as many fundamental questions remain unanswered. These include the selection of cell sources, the development of tissue-specific materials and the construction of complex organs. In addition, understanding the *in vivo* processes and mechanisms of tissue-engineered materials, their similarities and differences to the development and healing of natural tissue/organs, as well as their transformation and final fate are critical to the field. Answering these questions is essential for the efficacy, stability and safety of the clinical applications of TE materials (Han et al., 2020).

One of the problems that has hampered the full achievement of TERM's goals is the difficulty in finding materials that mimic the complexity of organs and the dynamic nature of the extracellular matrix (ECM). Mimicking the highly organized architecture of tissues and organs is critical for nutrient transfer, oxygen transport and other biological functions such as cell differentiation (Sharma et al., 2019). In recent years, it has therefore been recognized that it is essential to consider the physical environment when developing methods for tissue repair and regeneration (Martinac and Kloda, 2003). Indeed, biophysical cues regulate cell proliferation, the differentiation process, gene expression, protein synthesis and matrix production (Ingber, 2009). Thanks to new evidence and progress, the field of mechanotrasduction has made significant progress in TERM (Naqvi and

Mcnamara, 2020). However, due to the complexity of cell-ECM interactions, this remains one of the greatest challenges for TE. In recent years, however, significant progress has been made to produce artificial matrices that reconstructs dynamic environment. The ideal scaffold should not only support cell growth and maintenance, but also have appropriate mechanical, chemical and biological properties that mimic the native ECM. Therefore, the study of the interaction between cell and biomaterial plays a very important role (Geckil et al., 2010). Among the different materials, hydrogels best mimic both the three-dimensional structure of the ECM and its mechanical properties (Peppas et al., 2006). By choosing biocompatible synthetic or natural polymers and crosslinkers, it is easy to obtain biocompatible hydrogels for TE purposes (Rivest et al., 2007).

1.1.1. Hydrogels as ECM model

Hydrogels are three-dimensional networks formed by hydrophilic polymer chains in a water-rich environment. They possess tunable physical and chemical properties to mimic the native ECM, making them a good candidate for matrices for TE. Under physiological conditions, they are able to absorb water or biological fluids and increase their dry weight from 10-20% to a thousand-fold. Moreover, they can be chemically stable or degrade and eventually dissolve (Zhang and Khademhosseini, 2017).

The classification of hydrogels is based on various factors, such as physical properties, swelling, cross-linking and biodegradation rate. One of the most important differences is between physical and chemical hydrogels. In physical hydrogels, network reticulation is based on physical interactions and can be achieved by electrostatic interactions, hydrophobic association, chain aggregation, crystallization, polymer chain complexation and ion binding or hydrogen bonding (Ullah et al., 2015). These gels benefit from the possibility of reversible bonding, but on the other hand, this property makes them weak and gives them poor long-term stability (Jiang et al., 2014). Chemical gels, on the other hand, are not reversible because they are based on the covalent bond arising from chemical reaction of a crosslinker with the polymer (Ullah et al., 2015). In general terms, chemical gels are more stable and have better mechanical properties. However, the addition of a cross-linking agent may increase the risk of toxicity. The study of cross-linked hydrogels obtained with cross-linking of natural origin is therefore of great interest (Jiang et al., 2014).

Of current interest are also dual-network hydrogels, which combine physical and chemical cross-linking properties and have been developed to overcome the limitations of purely physical and chemical hydrogels (Ullah et al., 2015). A detailed discussion of this last type of hydrogels and a general discussion of the polymers used for gel formation will be given in the following sections and chapters.

1.1.2. Mechanical properties of hydrogels

The mechanical properties of hydrogels are of extreme importance to select them as a substrate that mimic the complexity of the ECM. By tuning the composition of the hydrogels (*i.e.* type and concentration of the polymer, type and concentration of crosslinker, and preparation methods) it is possible to modulate the mechanical behavior of this set of materials. In this section, I will discuss the main mechanical features of hydrogels that have proven to have an impact on cellular response.

1.1.2.1. Stiffness (elastic response)

Stiffness is one of the most important material properties and has been the most studied parameter over the years in relation to cell behavior considering that tissues in the human body exhibit different rigidities. It is defined as the ability of a material to withstand deformation due to an applied load and to return to its original size and shape when the load is removed. Information about the elasticity of a material is obtained by calculating the Young's Modulus (or elastic modulus), starting from the analysis of a stress-strain plot in which the stiffness is represented by the slope of the linear region (Figure 1).

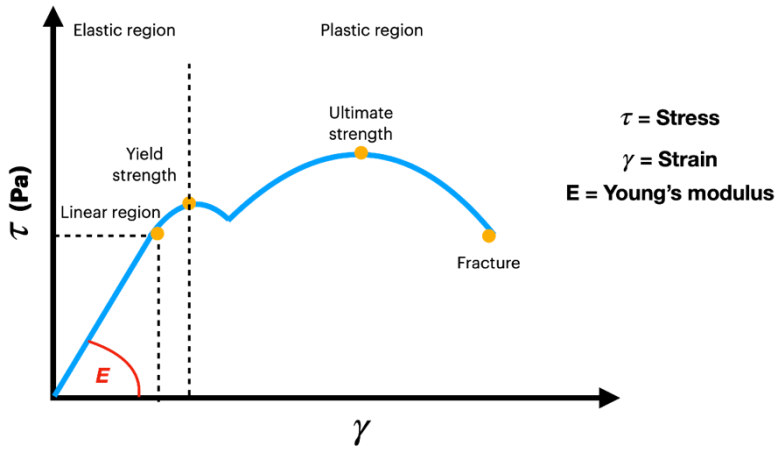

Figure 1. A typical stress-strain curve. This graph shows the change in stress as strain increase. The Young's modulus (E) is defined by the slope of the linear region.

The stiffness of hydrogels is important not only to maintain the stability of the scaffold, but also because it affects cell activities and fate. Indeed, native tissues exhibit stiffness ranging from less than 1 kPa for the brain to several tens of kPa for cartilage and bone (Discher et al., 2009), and a change in stiffness could be associated with some pathologies such as fibrosis and cancer (Leight et al., 2017; Santos and Lagares, 2018).

Transferring this concept to the interaction between cells and the substrate - and thus between matrix and cell – stiffness represents the resistance a cell fells when it deforms its surrounding ECM.

Different studies have shown that stiffness has an impact on cell spreading, shape and formation of focal adhesion both in 2D (Davidson et al., 2019; Engler et al., 2006; Pelham and Wang, 1997) and in 3D conditions (Saraswathibhatla et al., 2023; Yamada and Sixt, 2019). In addition, cell proliferation is slower in soft (non-stiff) substrates. Finally, stem cell differentiation is influenced by the stiffness of the substrate. For example, when polyacrylamide hydrogels (PAA) were used, cell differentiation depended on stiffness: on soft PAA, hydrogels, cells differentiated into adipocytes, whereas on stiff hydrogels, osteoblast differentiation was stimulated (Trappmann et al., 2012). Similar results were obtained under 3D culture (Huebsch et al., 2010).

1.1.2.2. Viscoelasticity

Tissues and ECM also exhibit complex, time- and rate-dependent mechanical behaviors, including viscoelasticity, viscoplasticity, energy dissipation, stress relaxation and nonlinear elasticity (Chaudhuri et al., 2020). Brain tissue is one of the softest and most dissipative viscoelastic tissues (Li et al., 2020). Changes in viscoelasticity have been linked to the progression of diseases, such as brain tumors (Streitberger et al., 2014), aging (Sack et al., 2009), and breast cancer progression (Sinkus et al., 2007). Viscoelasticity is the property of a material that exhibits both viscous and elastic behavior when deformed. Viscoelastic materials are characterized by having both an elastic (storage G') and a viscous (loss G") modulus, each indicating the amount of energy stored or dissipated by the substrate upon deformation. From a mechanical point of view, this means that the total energy transferred to the substrate is partially dissipated by the viscous contribution. Hydrogels are an example of viscoelastic materials. The response of cells to the viscous properties of the ECM and its dissipative environment is a very challenging topic. Cameron and Co-authors have shown that varying G" over two orders of magnitude at constant storage modulus has an effect on cell behavior and differentiation of MSCs (Cameron et al., 2011). Other authors have also demonstrated that viscous dissipation in biological tissues is crucial for correct cell phenotype development and tissue homeostasis (Charrier et al., 2018). By using biomaterials endowed with viscoelastic properties, recent studies have found that, in addition to stiffness, viscoelasticity, viscous dissipation, substrate creep, stress relaxation and energy dissipation have a strong influence on cellular events (Cameron et al., 2011; Charrier et al., 2018; Chaudhuri et al., 2016; Lee et al., 2017; Sacco et al., 2020a).

1.1.2.3. Viscoplasticity

Viscoplasticity is a subgroup of viscoelasticity. Viscoplastic materials exhibit permanent deformation when the applied stress exceeds a “yield-stress” of the material and remain at least partially deformed when the stress is removed (Chaudhuri et al., 2020). The viscoplasticity of a material is measured by

creep-recovery test (Figure 2). During the first part of the test the material is loaded with a constant stress and the increase in deformation is followed over time. In the second part (recovery phase), the stress is removed, and the initial shape of the material is gradually regained over time. A non-zero final strain stands for permanent deformation of the material and accounts for a viscoplastic deformation.

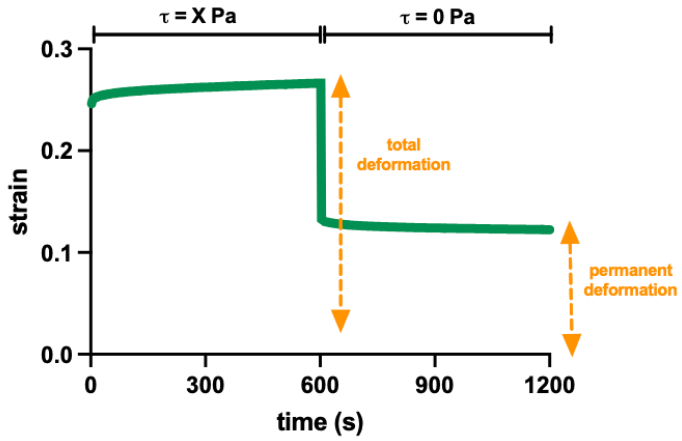

Figure 2. Example of a creep recovery profile; the permanent deformation indicates the degree of viscoplastic deformation.

Viscoplasticity influences the behavior of cells. Grolma et al., have shown that network plasticity controls MSCs spreading through a biphasic relationship dependending on cellular forces. Consequently, plasticity also regulates many ECM adhesion and remodeling genes (Grolma et al., 2020). In addition, Nam et al., have characterized the viscoplasticity of various cell-culture materials and found that materials forming gels through weak bonds showed a marked stress-dependent plasticity. On the other hand, covalent cross-links in a network account for a much strength and diminish plasticity. In the same work the authors demonstrate that cells can remodel their environment by mechanical forces alone, managing to re-orientate and alight fibers in an irreversible way (Nam et al., 2016).

1.1.2.4. Stress relaxation

The last parameter we are interested in is stress relaxation, a common behavior of the ECM. In hydrogels, stress relaxation is the observed time-dependent decrease in stress in response to the application of a constant strain (Figure 3). The commonly measured parameter is $\tau/2$, which indicates the time after which the stress is halved. A short $\tau/2$ (relaxation time) corresponds to a rapid decrease in stress and thus a high energy loss.

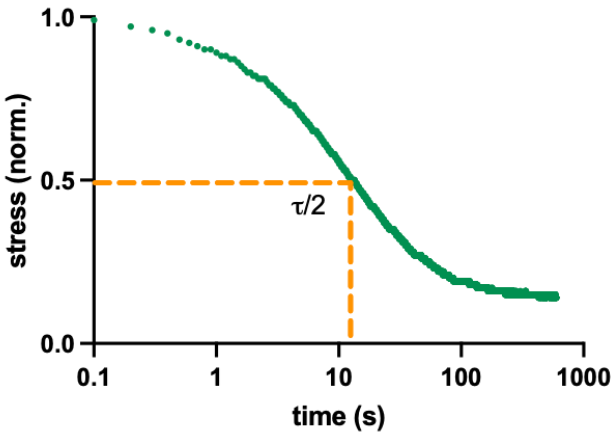

Figure 3. Example of a stress-relaxation profile. τ/2 indicates the time after which the stress is helved.

In general, ionic hydrogels show a faster stress relaxation than covalent hydrogels. Sodium alginate is often used to form hydrogels with tunable stress relaxation. Fast stress relaxation enhances cell spreading, proliferation and osteogenic differentiation, while slow relaxation restricts cell volume and up-regulates genes related to matrix degradation (Chaudhuri et al., 2016; Lee et al., 2017). Hyaluronic acid cross-linked with dynamic covalent bonds and fibrillar type I collagen are used to produce tunable stress relaxation hydrogel that mimics the mechanical and structural cues of native ECM (Lou et al., 2018).

1.1.3. Dual cross-linked hydrogels

As mentioned earlier, one strategy to overcome some of the chemical, physical and mechanical limitations of chemical and physical hydrogels is the use of double cross-linking hydrogels. The interest in such hydrogels is mainly due to two aspects.

On one hand, dual cross-linked hydrogels have been developed to avoid the instability of the physical hydrogel network that limits their long-lasting application in biomedical fields. In this case, the addition of a strong and stable crosslinker can contribute to prevent the continuous rearrangement of the structure. On the other hand, dual cross-linked hydrogels have been developed to overcome some limitations of conventional chemical gels, such as their low fracture toughness and extensibility. In fact, the double cross-linked hydrogel was first proposed by Gong et al., to produce hydrogels with high toughness. To achieve this goal, the introduction of "sacrificial bonds" that dissipate the strain energy without destroying the main network could be a good strategy (Gong, 2010). However, the broken bonds do not recover, resulting in permanent damage. To overcome this, double cross-linked gels with permanent and reversible cross-links have been synthesized. In this latter case, the broken bonds have the ability to reform (Mayumi et al., 2016).

Synthetic hydrogels are generally used for the preparation of dual cross-linked hydrogels. For example, polyvinyl alcohol hydrogels were prepared using glutaraldehyde and borate ions as cross-linking agents. This type of hydrogels showed interesting mechanical properties in terms of viscoelasticity and relaxation time (Mayumi et al., 2013; Narita et al., 2013; Zhao et al., 2017).

1.1.3.1. Dual cross-link hydrogels based on CTL

In the literature, there are also several evidences of double cross-linked hydrogels based on polymers of natural origin. In this type of dual cross-linked hydrogels, the polymer used is CTL, a lactose modified chitosan. While genipin serves as a "permanent" bond for CTL, boric acid serves as a "temporary" linker (Sacco et al., 2020b). Indeed, CTL has recently been shown to form dynamic polymeric networks in the presence of inorganic cross-linkers such as boric acid, due to the presence of diols located on the lactitol flanking moieties. Given the transient nature of the ester bond, the cross-linking points are constantly breaking and reforming. The result is a non-equilibrium network, endowed with peculiar mechanical properties. For example, they exhibit a strain-hardening behavior when the applied stress is increased and self-healing properties. In this respect, the CTL-boric acid system mimics native networks, as does the myosin II or Actin Binding Protein (ABP) on actin (Cok et al., 2018; Furlani et al., 2019b, 2019a; Sacco et al., 2017). However, for long-lasting applications in the field of biomaterials, the introduction of stable junctions is beneficial to limit the continuous rearrangement of the network. Recent findings on dual cross-linked gels based on CTL reticulated *via* both temporary (boric acid-based) and permanent (genipin-based) crosslinkers have revealed a peculiar mechanics of ultimate gels. The strain-hardening effect in the non-linear regime, adaptable strength, toughness, viscoelasticity and energy dissipation, as well as good biocompatibility, have been identified as the main properties of this material that could find application in biomedicine (Sacco et al., 2020b) . Furthermore, by tuning the concentration of the transient crosslinker (*e.g.* boric acid), it is possible to control the immediate stress of the hydrogels and to control the osteogenic commitment of human adipose-derived mesenchymal stem cells (Pizzolitto et al., 2023) .

1.1.4. Genipin

As mentioned above, covalent cross-linkers impart a high degree of stability to the hydrogel. However, they can have a degree of toxicity due to the presence, in the final construct, of unreacted molecules of both the crosslinker and the products formed during the reaction. Therefore, one of the challenges is to achieve the stability of the hydrogels using non-toxic reagents. One of the natural reagents that can also form covalent bonds is genipin (Figure 4). Genipin is a natural molecule obtained from the hydrolysis of geniposide, which is extracted from the fruits of *Gardenia*

Jasminoides Ellis and used in traditional oriental medicine (Fujikawa et al., 1987). Genipin is the compound responsible for the pharmacological activities of *Gardenia*. It can be difficult to extract directly, so it is produced using β-glucosidase. Genipin can also be isolated in large quantities by a microbiological process using *Penicillium nigricans*. The production protocol and quality assessment for genipin have been re-evaluated and established according to modern aspects. The production of genipin uses macroporous resins and silica gel for purification. The conversion of geniposide to genipin reaches 95% under optimized fermentation conditions. This process is cost-efficient and can be applied industrially (Muzzarelli et al., 2016).

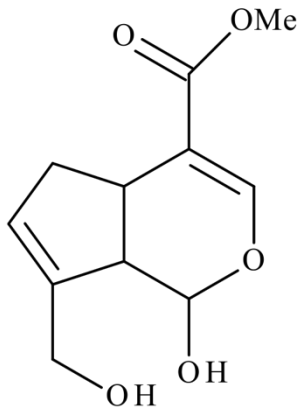

Figure 4. Genipin structure

Genipin is often used as a cross-linking agent because it is less toxic than other covalent cross-linking agents. In particular, genipin is about 1000 times less cytotoxic than glutaraldehyde (Sung et al., 1999). For this reason, genipin is used to produce various biomaterials for TE. For example, geniposide has been used as a novel angiogenic agent for tissue regeneration as it enhanced HUVEC proliferation, migration and tube formation *in vitro* and increased tissue neocapillarity density and hemoglobin content *in vivo* (Huang et al., 2005). Genipin was found to possess anti-inflammatory properties and to protect against Alzheimer's amyloid beta protein toxicity and acute hepatic dysfunction (Koo et al., 2004; Takeuchi et al., 2005). In addition, genipin has been identified as a UCP2 inhibitor that stimulates insulin secretion and improves type 2 diabetes (Zhang et al., 2006). Genipin has also been used as a cross-linking agent for chitosan to prepare various hydrogels and scaffolds. The latter have been used as carriers for drug delivery and tissue regeneration. Chitosan membranes cross-linked with genipin were found to have higher tensile strength and lower swelling ratio, making them a promising material for wound dressings and drug delivery systems (Abitha M Heimbuck et al., 2019; F L Mi et al., 2001; Fwu Long Mi et al., 2001). Genipin has also been used to cross-link chitosan-gelatin mixtures for nerve (Chiono et al., 2008) and bone regeneration

(Georgopoulou et al., 2018). Finally, a chitosan scaffold cross-linked with genipin has been described for use in bone tissue engineering (Dimida et al., 2017). Despite the extensive use of genipin for the production of various materials (Muzzarelli, 2009; Muzzarelli et al., 2016), the reaction mechanism is not yet fully understood. One of the basic features of the reaction between genipin and primary amines is the formation of the blue color (Touyama et al., 1994). Over the years, several possible structures and reaction mechanisms have been proposed. In a fundamental work by Butler et al., based mainly on UV-VIS spectroscopy, a mechanism based on two reaction pathways was proposed: a first and fastest reaction involving a genipin and an amino group of the chitosan, which would then develop into an association between the chains. The slowest second reaction involves a genipin molecule bridging to the chitosan chains by opening the dihydropyran ring and converting the ester bond to an amide (Butler et al., 2003). The behavior of genipin has also been studied experimentally and theoretically by other authors (Di Tommaso et al., 2014, 2013; Touyama et al., 1994)

1.2. Natural Polymer of biomedical interest

Various materials can be used to recapitulate the physical properties of the ECM, although polymers from natural sources are considered the best choice. Natural polymers can originate from many sources: plants, animals and even microorganisms. They are often used because of their biocompatibility, low cytotoxicity and structural similarity to ECM components. They can be chemically modified to overcome their structural weakness and sometimes rapid degradation. Polymers of natural origin that are used for the development of hydrogels include: collagen, hyaluronic acid, alginate, agarose and chitosan and its derivatives.

1.2.1. Collagen

Collagen is used extensively as a natural polymer in the manufacture of biomaterials as it is the most abundant component of the ECM of many tissues (*e.g.* skin, ligaments, cartilage, tendons and bone) (Lee and Mooney, 2001). Collagen fibers are responsible for the elastic and viscoelastic properties of tissues. In addition, non-collagenous components interact with collagen fibers to resist compressive and tensile forces. The deformation mechanism of collagenous structures can be divided into four regions, and the slope of the stress-strain curve increases with load (Sorushanova et al., 2019). Chemical, physical or enzymatic cross-links are used to form collagen hydrogels. Type-I collagen is the main type of collagen used in particular for the production of scaffolds for skin applications. Indeed, collagen-based materials have been developed in various forms for wound healing, such as hydrogels, sponges, powders and films/dressings (Chalimidi et al., 2015; Doillon, 1988; Sargeant et al., 2012). Collagen type I hydrogels also facilitate proliferation, migration and osteogenic

differentiation of bone marrow stromal cells (Hesse et al., 2010). Collagen gels are also a popular platform for neuronal growth due to their natural origin, biodegradability, low antigenicity and good biocompatibility. Using a simple mechanical method, it is possible to orient the collagen fibers within the hydrogel. The result is a unique 3D template that can guide neuronal regeneration (Antman-Passig et al., 2017). Collagen is also used as a tissue culture because of its ability to attach different cell types (Lee and Mooney, 2001). Due to its biocompatibility and low immunogenicity, collagen is also widely used also as a bioink for 3D bioprinting in TE. Collagen-based bioinks are also frequently used in combination with other materials (Osidak et al., 2020). For example, Albanna et al., used a fibrinogen/collagen bioprinted layer with autologous dermal fibroblasts and epidermal keratinocytes and found wound closure, reduced contraction, and accelerated re-epithelization in murine and porcine full-thickness wound models (Albanna et al., 2019). Pure collagen bioink was used to print a construct for osteochondral tissue regeneration in the rabbit knee joint (Shim et al., 2016).

1.2.2. Hyaluronic acid (HA)

HA is a natural linear polysaccharide found in synovial fluid, ECM and connective tissue. It consists of D-glucuronic acid and D-N-acetylglucosamine linked by alternating β-1,4 and β-1,3 glycosidic bonds (Figure 5). It belongs to the glycosaminoglycan family and has a high molar mass, unique viscoelastic and rheological properties and is not sulphated (Kogan et al., 2007).

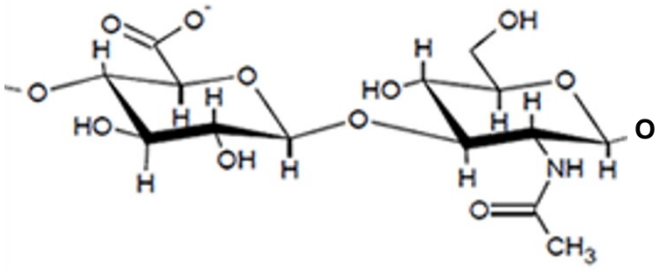

Figure 5. Representation of the chemical structure of hyaluronic acid (HA)

HA can be modified in various ways to alter its properties (Burdick and Prestwich, 2011). Controlling the rate of degradation and improving the mechanical properties of hydrogels based on HA is challenging. Cross-linking and adjusting the concentration of HA are methods to stabilize HA while maintaining its basic properties (Borzacchiello et al., 2015). The chain length and molecular weight (MW) of HA play a role in its biological function, with a high MW HA improving cell viability and wound heling (Law et al., 2013). For example, biodegradable membranes have been developed for the *in situ* release of HA for the healing of surgical intestinal wounds (Scognamiglio et al., 2019).

Various materials based on HA have been used for skincare. In fact, HA has a high capacity to bind and retain water molecules, which contributes to its effectiveness in promoting skin hydration, stimulating collagen and elastin production and reducing the sings of aging (Al-Halaseh et al., 2022). HA has both structural and signaling functions in cellular processes such as inflammation, wound healing and cancer. The protein CD 44 is the most important HA binding receptor and is involved in various physiological and pathological processes, including cancer progression. For this reason, HA hydrogels can be used for the local delivery of antitumor drugs (Dosio et al., 2016).

Finally, one of the most important applications of HA is in the field of cartilage regeneration. Indeed, HA plays an important role as a lubricant in joints, helping to regulate cellular activities and absorb mechanical impacts. However, in inflammatory processes, HA can become thinner and less viscous, leading to joint disorders such as osteoarthritis (OA) or rheumatoid arthritis. The safety and efficacy of HA-based formulations in the treatment of joint diseases has been confirmed in several studies (Legré-Boyer, 2015). The effectiveness is due to its chondroprotective capacity. For example, injections of exogenous HA can relieve pain and maintain viscoelasticity, but therapeutic results are variable (Marinho et al., 2021).

1.2.3. Alginate

Alginate is a commonly used biomaterial for drug delivery and TE due to its biocompatibility, low toxicity, low cost and ease of gelation. It is a block copolymer of two 1→4 linked units: β-D-mannuronic acid (M-block) and α-L-glucuronic acid (G-block) (Figure 6). It is isolated from brown seaweed (*e.g. Laminaria*, *Macrocystis*, *Lessonia*) or bacteria (primarily *Azotobacter* and *Pseudomonas*). The occurrence, proportions and distribution of M- and G- blocks depends on the natural sources. One of the most important properties of alginate is its ability to form an ionic hydrogel when exposed to divalent cations. The most commonly used cation is calcium (Ca^{2+}). The gelation mechanism leads to the formation of the most accredited molecular structures called “egg-box” (Andersen et al., 2012; Donati and Paoletti, 2009). The composition and arrangement patterns of the blocks determine the physiochemical properties of the alginates. The M/G ratio, the block structure and the degree of polymerization of the alginate backbone also influence the gelling behavior (Zhang et al., 2021).

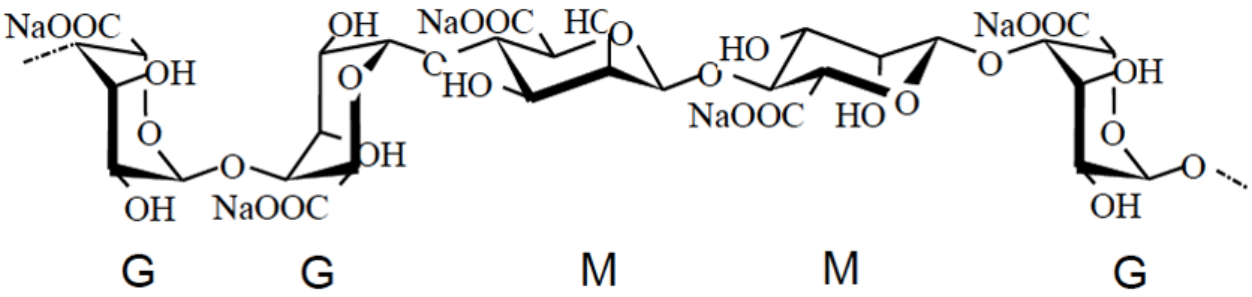

Figure 6. Representation of the chemical structure of alginate

Alginate hydrogels are biocompatible and can be formulated in various physical forms for TE applications (Lee and Mooney, 2012; Sahoo and Biswal, 2021; Zhang et al., 2021). To improve cell adhesion alginate can be modified by peptides (such as arginyl-glycyl-aspartic acid (RGD)) to the polymer (Andersen et al., 2015; Chaudhuri et al., 2015; Jeon et al., 2010). Alginates are popular for wound dressings because of their biocompatibility, non-toxicity and high absorption capacity. They can absorb excess wound fluid, promote wound healing and minimize bacterial infections. However, due to its poor mechanical properties, alginate is usually combined with synthetic polymers to improve its mechanical properties (Zhang and Zhao, 2020). Alginate is also commonly used for drug delivery, especially in oral dosage forms (Lee and Mooney, 2012). Functionalized alginate nanoparticles have been used for cancer immunotherapy (Zhang et al., 2017, 2012). Alginate/hydroxyapatite composite scaffolds have been developed for bone TE (Turco et al., 2009). Alginate can be used in a binary polysaccharide mixture with a lactose-modified chitosan, potentially used for cartilage regeneration (Marsich et al., 2008). Finally, alginate could also be used to produce substrates for mechanobiology studies. In this contest Chaudhuri and co-workers have used alginate polymers to demonstrate the role of stress-relaxation in regulating cell behavior and fate (Chaudhuri et al., 2016, 2015). Recently, methylated alginates have been developed as a platform to investigate the role of compliance of hydrogels with the same shear modulus on cell proliferation and YAP/TAZ localization (Scognamiglio et al., 2023).

1.2.4. Agarose

Agarose is often used as a polysaccharide to form thermally reversible gels. It consists of agarobiose repeating units, a disaccharide of (1,3)-linked β-D-galactopyranose and (1,4)-linked (3,6)-anhydro-α-L-galactopyranose and is derived from red seaweeds (Figure 7).

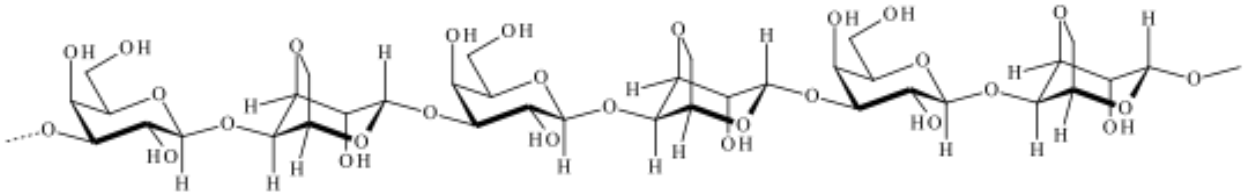

Figure 7. Representation of the chemical structure of agarose

It belongs to the family of thermoresponsive polysaccharides in which the sol-gel transition occurs *via* a special gelation mechanism characterized by high hysteresis. This transition can occur by thermal stimulus alone, so no other chemicals are required (Graham et al., 2019). One of the most important applications of agarose hydrogels is electrophoresis, but they can also be used for drug delivery (Wang et al., 2009) and wound healing applications (Graham et al., 2019). However, agarose is not biodegradable and can inhibit the spontaneous repair process *in vivo*. The physical structure of the gels can be controlled by using different concentrations of agarose, resulting in various pore sizes that influence cell migration and proliferation. However, agarose is generally not suitable for the encapsulation and culture of adherent cells, as it does not allow integration between the cells and the gel matrix(Graham et al., 2019). To improve this interaction, it is possible to bind some oligopeptide domains to agarose (Lee and Mooney, 2001). For example, the oligopeptide domain CDPGYIGSR covalently bound to agarose has been used as a substrate for 3D growth of spinal ganglia (Borkenhagen et al., 1998). Recently, agarose has also been used with CTL to produce a series of semi-interpenetrating hydrogels as a 2D model to study substrate dissipation as a key regulator of cell response (Sacco et al., 2022).

1.2.5. Chitosan and its glycosylated derivatives

Chitosan is a polysaccharide derived from the alkaline N-deacetylation of chitin, the structural components of the exoskeleton of crustaceans. It is a linear polysaccharide consisting of β-(1→4)-linked D-glucosamine (deacetylated, D unit) and N-acetyl-D-glucosamine (acetylated, A unit), randomly ore more block-wise distributed along the polysaccharide chain (Figure 8).

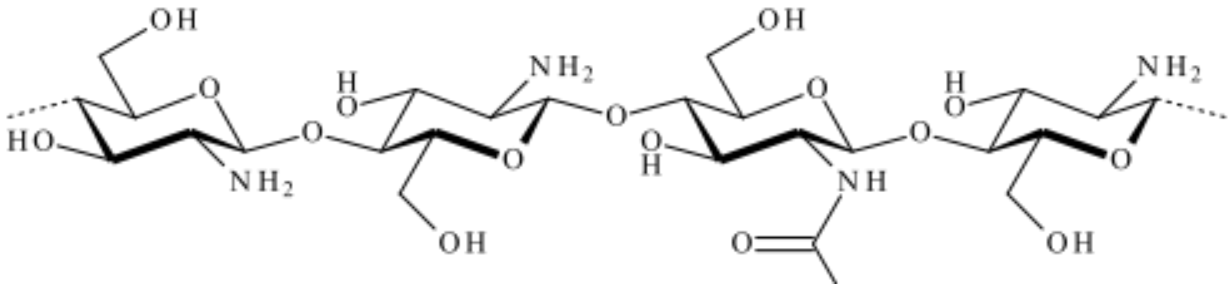

Figure 8. Representation of the chemical structure of chitosan

Thanks to the protonation of the amino groups at the C2 position, it is a water-soluble polymer under acid conditions and behaves like a polyelectrolyte whose charge density depends on its proportion of D units and pH (Sorlier et al., 2001; Strand et al., 2001). Chitosan solubility at neutral pH depends on its molecular weight and the degree of acetylation. In fact, neutral solubility can be improved by increasing the degree of acetylation up to around 60% or reducing the molecular weight, with degree of polymerization (DP<10) (Khong et al., 2013; Sannan et al., 1976; Vårum, K.M.; Ottøy, M.H.; Smidsrød, 1994). Chitin and chitosan do not occur naturally in the gel form. Researchers have proposed physical and chemical cross-linking processes to form chitosan hydrogels. Chemical gels are formed with small molecules that can be toxic, while physical gels are less toxic and can be tailored to have different properties. The sol/gel transition in physical gels can be achieved by varying physical/chemical parameters, such as temperature, pH and ionic strength. Chitosan can interact with ions, small molecules or macromolecules with opposite charges in a typical pH range of 4-6 (Huang and Lapitsky, 2012). One of the main ionic crosslinkers used for ionic crosslinking of chitosan is tripolyphosphate (TPP), but pyrophosphate (PPi) could also be used. However, PPi forms cylindrical macroscopic networks with lower mechanical properties compared to TPP-chitosan hydrogels (Sacco et al., 2016). The mechanical properties of chitosan-TPP gels are influenced by their molecular weight and the degree of acetylation. Different polymer characteristics influence hydrogel behavior when subjected to small/large deformations, modulating stiffness, elasticity and rupture strength of chitosan gels (Sacco et al., 2018b) . In this way, chitosans with different degrees of acetylation and ionically crosslinked with TPP were synthetized. The resulting networks showed viscoelastic and strain-softening behavior at large deformations and differences as to cell adhesion and spreading (Sacco et al., 2020a). Ionotropic gelation has been used to synthesize chitosan structures encapsulating various molecules for biomedical applications. Physical chitosan gels can also form without the use of external gelling agents. Gelation is achieved by modulating the chemical composition of the polymer through a controlled re-N-acylation process. The resulting gels exhibit weak syneresis and swelling phenomena that depend on the pH and ionic strength. The gelling system is proposed for use as an injectable material for periodontal surgical purposes (Gérentes et al., 2002). Chitosan is widely used for the production of various biomaterials due to its biocompatibility and because it does not induce significant responses from the immune system reaction (Molinaro et al., 2002; Thambiliyagodage et al., 2023). In addition, chitosan exhibits antibacterial, antifungal, anti-HIV-1, antitumor and antioxidant properties, which make it suitable not only for biomedical applications but also for water treatment and food industries (Kong et al., 2010; Younes et al., 2014; Zheng and Zhu, 2003). Although chitosan can be safely classified as a good candidate for tissue engineering, some weaknesses related to its physical nature limit its potential application. For example, one of the major

limitations of commercial chitosans is the poor solubility of the biopolymer at neutral pH. To address this, chemical modifications of the starting polymer and grafting of flanking molecules are considered (Sacco et al., 2020).

1.2.5.1. Lactose-Modified Chitosan (CTL)

One of the possible modifications involves the introduction of lactitol moieties into the polysaccharide backbone (Figure 9). This chemical modification can be traced back to the late 1980s, when Yalpani and co-workers established the chemical conditions for the modification of the polysaccharide chain and studied its rheological properties (Yalpani and Hall, 1984). A few years later, Donati *et al.*, re-investigated the synthesis of a lactose-modified chitosan, originally termed Chitlac. Highly deacetylated (89%) chitosan was modified by reductive amination (N-alkylation) with the aldehyde functionally of lactose. About 70% of the free amino groups of the chitosan were modified to obtain the corresponding lactitolated derivative. Structurally, CTL consists of three building β-1→4 linked sugars: glucosamine (D-unit), *N*-alkylated glucosamine (lactitol-substituted D-unit, L-unit) and *N*-acetyl-glucosamine (A-unit) randomly distributed along the polysaccharide chain (Donati et al., 2005). The result of introducing lactitol side chains into the chitosan backbone is a chitosan derivative that is soluble at neutral pH. Further studies on the average structure and dynamics of Chitlac have been carried out to determine the main physicochemical properties and to investigate the orientations of the lactitol side chains of Chitlac, hereafter referred to as CTL (D'Amelio et al., 2013; Esteban et al., 2018).

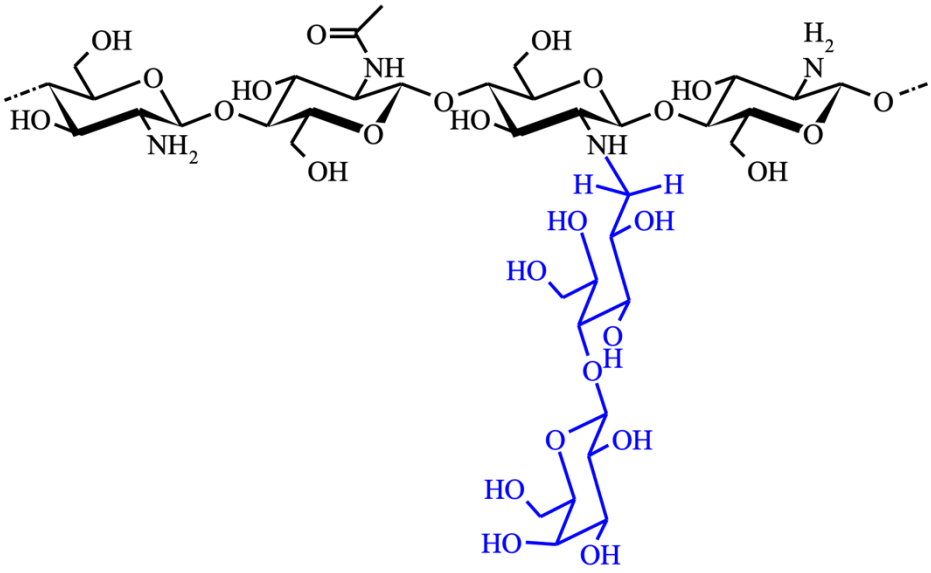

Figure 9. Representation of the chemical structure of lactose-modified chitosan (CTL)

Due to its polycationic nature and the presence of primary amines from the unreacted glucosamine units, CTL could form physical and chemical hydrogels. As mentioned earlier (Section 1.1.3.1), CTL has been shown to form dynamic cross-linked polymeric networks in the presence of inorganic cross-linkers such as boric acid. This transient exhibits a strain-hardening behavior under increasing load, similar to the characteristics of the ECM component such as collagen (Cok et al., 2018; Furlani et al., 2019b; Sacco et al., 2017). CTL can also form dual cross-linked hydrogels with peculiar mechanical properties, where boric acid acts as a transient cross-linker and genipin as a permanent cross-linker (Pizzolitto et al., 2023; Sacco et al., 2020b). CTL could also be used for the preparation of mixtures with alginate and HA, as it can be mixed with polyanions without phase separation (Donati et al., 2011, 2007a, 2007b; Marsich et al., 2013).

In addition to forming the chemical and physical gels, CTL has over the years demonstrated various bioactive properties that make it an interesting natural polymer for the development of biomaterials for tissue regeneration. In particular, CTL was shown to induce the aggregation of articular chondrocytes with the formation of high dimensions nodules (up to 0.5 – 1 mm) within 12-24 hours. It also stimulated the production of type II collagen and GAGs (Donati et al., 2005; Marsich et al., 2008). The localization of CTL at the plasma membrane of isolated chondrocytes and its permanence at the same site even after nodule formation suggest that the process is mediated by specific binding of CTL to the cells, possibly through its β-galactose residues (Donati et al., 2005). Marcon *et al.* confirmed the role of Galectin-1 as a bridging molecule between CTL and chondrocyte aggregates (Marcon et al., 2005). Recently, cell aggregation promoted by lactose derivatives of chitosan was a prerequisite for commitment of adipose-derived stem cells to the chondrogenic lineage (Tan et al., 2008). Furthermore, the use of CTL as a chondroprotective additive in the treatment of osteoarthritis has shown good results in studies on rat models (Salamanna et al., 2019). The potential application of this polymer is mainly due to the fact that the interaction between CTL and chondrocytes is mediated by Galectin-1 (Gal-1) (Marcon et al., 2005). There is increasing evidence that the expression of Gal-1 correlates with the degree of cartilage degeneration, with this protein being specifically present at sites of damage (Osório, 2016). Recent works have shown that treatment of osteoarthritic chondrocytes with lactose inhibits the binding of Gal-1 to the cell surface. In this way, the expression of Gal-1-regulated genes is reduced, leading to a decrease in inflammation (Tarricone et al., 2021, 2020a, 2020b; Toegel et al., 2016). Since it has been demonstrated that CTL is able to inhibit the expression of Gal-1, there is growing interest in the use of this polymer for the production of materials used in the field of cartilage regeneration (Scognamiglio et al., 2020a; Scognamiglio et al., 2020b). Interesting bioactive properties have also been demonstrated towards osteoblast-like cell lines

(Travan et al., 2012), osteogenic differentiation of Dental Pulp Stem Cells (Rapino et al., 2019) and neuronal cells (Medelin et al., 2018).

1.3. Extracellular matrix

The extracellular matrix (ECM) is an essential component of multicellular structures, that provide structural and biochemical support to surrounding cells. The ECM plays an active role in cellular processes such as proliferation, differentiation and migration. The ECM consists of numerous matrix proteins and polysaccharides that support cells and tissues. The proteins can be categorized as structural (such as collagens and elastin) or non-structural (such as fibronectin and laminin). Other important components of the ECM are integrins, growth factors and a group of matrix metalloproteinase (MMPs). The ECM has a 3D structure that can be divided into two forms: the basement membrane and the interstitial matrix. Both forms have a similar basic structure, with collagens forming the main network and non-structural proteins attached to it. These proteins communicate with the surrounding cells via integrins (Kular et al., 2014). The composition of the ECM varies from tissue to tissue. For example, cartilage ECM is mainly composed of type-II collagen, while bone ECM is characterized by type-I collagen and nanocrystals of carbonated hydroxyapatite (Kuhn and Tuan, 2010).

The ECM not only supports the cells, but also exerts biochemical and mechanical stimuli that influence cell phenotype, motility, differentiation and matrix production. In this way, the ECM is not a static network but is subject to constant remodeling, demonstrating its dynamic nature and providing an important source of biomechanical cues (Naqvi and Mcnamara, 2020).

1.3.1. Mechanotransduction

Cells are able to convert external mechanical stimuli from the ECM into intracellular biochemical signals. This process is called mechanotransduction (Ingber, 2006). Alterations in the mechanical environment of the ECM or in the cellular mechanisms for sensing such stimuli have been associated with pathological conditions (Ingber, 2009). Focal adhesions (FA) are the main form of communication between cells and the ECM. FA serves as a vector for the transmission of mechanical signals from the ECM to the cells and the cells respond accordingly by changing their cytoskeletal structure and exerting forces. The main receptors that transmit these signals between the cells and the ECM are integrins. Integrins are a large family of transmembrane α/β heterodimers that bind ECM proteins, including fibronectin and laminin, and are involved in cell signaling pathways. They provide mechanical continuity between the inner and outer environments of cells and act as stretch sensors that trigger signaling pathways through various mechanisms. One of the most important proteins

responsible for triggering and maximizing integrin activation is talin. Integrins are part of a network of matrix components involved in the transmission of mechanical forces, including signaling molecules such as G-proteins, Focal Adhesion Kinase (FAK), Receptor Tyrosine Kinase (RTKs), and Mitogen-activated Protein Kinase (MAPKs), as well as FA proteins (Kular et al., 2014).

1.3.2. Mechanobiology of stem cells

Biophysical stimuli play a crucial role in tissue formation. Mechanical and physical cues are crucial for embryonic tissue patterning and organogenesis (Naqvi and Mcnamara, 2020). Indeed, many developmental events involve extensive collective cell movements and transitory cell shape changes. These are necessary to generate mechanical tension in embryonic tissues that regulate further cell movement and differentiation (Beloussov and Grabovsky, 2006). Mesenchymal stem cells (MSCs) were first discovered in bone marrow and are cells characterized by the ability to differentiate into different cells types, such as osteoblasts, chondrocytes and adipocytes. The ECM environment of MSCs, or the stem cell "niche", is critical to their fate. Mechanical cues from the ECM can control the fate, as the cells require cell-cell and cell-matrix interactions to maintain their potency. Changes in the mechanical properties of the ECM can alter cell shape and intracellular tension, leading to shifts in signaling events that affect gene expression. (Kuhn and Tuan, 2010; Naqvi and Mcnamara, 2020). One of the signals that MSCs can sense through mechanotransduction systems is the stiffness of the ECM. The nuclear factors responsible for translating these signals into biochemical signals that control cell behavior, including growth, differentiation and malignant progression of cancer, are not well understood. However, YAP and TAZ have been identified as nuclear relays for mechanical signals stimulated by ECM rigidity and cell shape. This regulation requires Rho GTPase activity and actomyosin cytoskeleton tension but is independent of the Hippo/LATS cascade (Dupont et al., 2011). The YAP/TAZ pathway plays a crucial role in stem cell biology and is regulated by several upstream pathways. YAP/TAZ localization to the nucleus has been linked to osteogenic differentiation, while cytoplasmic localization is associated with adipogenesis. Abnormal YAP/TAZ activity is associated with several diseases, including atherosclerosis, fibrosis, pulmonary hypertension, inflammation, muscular dystrophy and cancer. FAK also plays a role in regulating cell differentiation and function. For example, FAK and ROCK signaling have been shown to promote osteogenesis, while inhibition of their activity promotes adipogenesis in human adipose stem cells. MAPKs, a family of enzymes, also play a role in mechanotransduction pathways. ERK and p38 are involved in the regulation of differentiation in stem cells, with ERK being activated by mechanical forces via the integrin focal adhesion complexed and the MAPK-ERK signaling cascade. Mechanical stimulation increases matrix mineralization and induces osteogenic differentiation via the ERK signaling pathway.

Similarly, p38-MAPK activation triggered by mechanical loading has been shown to be essential for skeletal formation and osteoblast differentiation (Naqvi and Mcnamara, 2020).

1.4. Articular cartilage

In the final part of this project, CTL is used to coordinate the aggregation of cells. The resulting spheroids display potential application in the field of cartilage regeneration. For this reason, in the following sections I will briefly explain the main features of articular cartilage and its ECM, the problem of cartilage regeneration and the main strategies to overcome this problem, which affects millions of people worldwide (Chen et al., 2012).

Articular cartilage is a special type of hyaline cartilage found in the synovial joints and is between 2 and 4 mm thick. This cartilage provides a low-friction, wear-resistant surface with increased compressive strength, providing a smooth, lubricated surface for diarthrodial joints and protects the subchondral bone (Bhosale and Richardson, 2008; Strecanska et al., 2022).

Water accounts for 65-80% of the wet weight of cartilage and provides nutrition, lubrification, and load-dependent deformation. In osteoarthritis, the water content increases, resulting in reduced load-bearing capacity. Collagen, mainly of the type II, makes up 10-20% of the wet weight and provides tensile strength. Proteoglycans (10-20%) contribute to compressive strength and help maintain fluid and electrolyte balance in cartilage (Buckwalter and Mankin, 1998). Glycosaminoglycans (GAGs) such as hyaluronic acid (HA) and chondroitin sulphate (CS) are the subunits of proteoglycans and have a limited ability to repair themselves, leading to long-lasting injuries and degradation (Bhosale and Richardson, 2008; Gao et al., 2014). Finally, chondrocytes synthesize matrix components and regulate matrix metabolism. They have unique properties, such as no cell-to-cell contacts, a spheroidal shape and high individual metabolic activity (Bhosale and Richardson, 2008). The unique biological and mechanical properties of articular cartilage depend on the structure of the tissue and the interactions between the chondrocytes and the extracellular matrix (Buckwalter and Mankin, 1998). Chondrocytes are responsible for the organization of collagen, proteoglycans and non-collagenous proteins into a specialized tissue that supports the functions described above (Chen et al., 1999). The composition, structure and functions of these cells differ depending on their depth in the cartilage. There are four different morphological zones in the cartilage, arranged from top to bottom:

- superficial zone is the thinnest layer of articular cartilage. The chondrocytes in this zone synthesize high concentrations of collagen and low concentrations of proteoglycans, resulting in a high water content. The parallel arrangement of fibrils provides tensile and shear strength

and disruption of this zone can lead to the development of osteoarthritis (Bhosale and Richardson, 2008).

- Middle zone is a transitional zone between the superficial and deep zones. It forms the largest part of articular cartilage and accounts for 40-60% of tissue volume. The cell density in this zone is lower. Chondrocytes, which are spherical and contain synthetic organelles such as the endoplasmic reticulum, Golgi bodies and mitochondria, are embedded in a rich extracellular matrix. The ECM in this area has larger collagen fibrils, more proteoglycan, especially aggrecan, and less collagen and water than in the previous zone. The interterritorial fibrils are oriented obliquely or randomly to the articular surface, in contrast to the parallel fibrils in the superficial zone (Bhosale and Richardson, 2008; Buckwalter, 1983; Buckwalter and Mankin, 1998).
- Deep zone is separated from the calcified zone by the tidemark, a histological feature characterized by an irregular surface and consisting of thick, horizontal bundles of type I collagen fibers. It forms a dense and structurally strong substrate for the attachment of type II collagen fibrils that extend into the deep zone (Bhosale and Richardson, 2008; Correa and Lietman, 2017).
- calcified cartilage zone is the mineralized zone and contains chondrocytes with a hypertrophic phenotype and low metabolic activity. These cells synthesize type X collagen, which contributes to structural integrity and shock absorption alongside the subchondral bone (Bhosale and Richardson, 2008).

Due to lack of neural, vascular and lymphatic networks, as well as a small population of progenitor cells, cartilage has low regenerative capacity (Vincent et al., 2022). However, chondrocytes can survive under hypoxic conditions because they rely on the passive diffusion of nutrients from the synovial fluid. Cartilage remodeling is a physiological process involving the breakdown of old ECM and the synthesis of new ECM, and the balance between these processes is crucial for cartilage homeostasis (Sophia Fox et al., 2009)

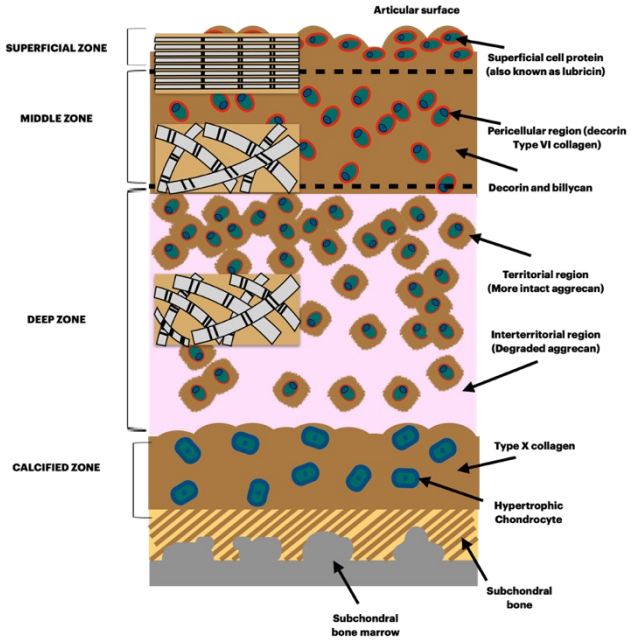

Figure 10. Diagrammatic representation of the general structure of human articular cartilage

1.4.1. Cartilage extracellular matrix

The extracellular matrix (ECM) of cartilage consists primarily of collagen, proteoglycans and other components such as fibulin and elastin. Type II collagen is the primary structural protein and forms a network with other types of collagen. Non-collagenous proteins, including aggrecan and other proteoglycans, provide compressive strength by interacting with the collagen network. In addition, aggrecan interacts with GAGs and HA to provide compressive resistance and shock absorption under load. Other proteoglycans contribute to the complex three-dimensional matrix network. Finally, the ECM is also enriched with water and chondrocytes. This composition gives cartilage its unique ability to pressurize fluid and withstand high cyclic loads. The pericellular matrix directly connects the ECM and chondrocytes and plays a critical role in maintaining the mechanical properties of the cartilage. The interactions between chondrocytes and the ECM regulate various biological processes important for articular cartilage homeostasis and repair, such as cell attachment, growth, differentiation, and survival (Peng et al., 2021).

Cartilage physiology is largely maintained by proper mechanical stimulation during normal activity, with various forces affecting tissue composition and integrity, including compression, tension, shear and hydrostatic pressure (Ofek et al., 2010). Chondrocytes interpret these mechanical signals through mechanotransductive signaling pathways that can trigger either catabolic or anabolic gene expression changes, altering extracellular matrix synthesis (Ofek et al., 2010).

Cartilage remodeling is a physiological process that involves the degradation of the old ECM and the synthesis of the new ECM. The balance between these two processes is crucial for cartilage homeostasis. Pro-inflammatory cytokines can disrupt this balance, leading to cartilage damage and

inflammatory joint diseases such as osteoarthritis and rheumatoid arthritis (Strecanska et al., 2022). The ECM plays a crucial role in controlling tissue morphogenesis and chondrocyte differentiation. Chondrogenesis is the process of cartilage formation from condensed mesenchymal tissue and is regulated by the action of the ECM on the mesenchymal stem cell (Strecanska et al., 2022). In fact, cell-cell adhesion and cell-matrix interactions involving molecules such as N-cadherin and ECM receptors like integrin, are essential for chondrogenesis (Gao et al., 2014). Integrin signaling activates downstream signaling pathways such as MAPK/ERK, PI3K/Akt and Rho family GPTases that regulate cell survival, proliferation, migration and differentiation (Strecanska et al., 2022). Moreover, the expression of integrins changes from healthy to pathological tissue. In normal chondrocytes mainly α1β1, α3β1, α5β1, α10β1, αVβ1, αVβ3 and αVβ5 integrins are expressed. In OA cartilage the levels of α1β1 and α3β1 increase, while α2β1 and α4β1 appear, which are not detectable in normal cartilage (Loeser et al., 1995). The mechanism behind this change in integrin expression in OA tissue is not yet known, but may be related to the release of growth factors and cytokines that stimulate integrin expression, leading to changes in the ECM and promoting chondrocyte hypertrophy (Loeser, 2014).

1.4.2. Cartilage degeneration

As discussed before, articular cartilage has a poor intrinsic ability to self-repair. In early development, fetuses can heal articular cartilage defects effectively without scarring. However, this ability declines soon after birth and is almost completely lost by early adulthood, leading to degenerative diseases that not only affect patient quality of life but also place a financial burden on healthcare systems worldwide (Chen et al., 2012; Correa and Lietman, 2017; Hiligsmann et al., 2014).

Regeneration of articular cartilage can occur after trauma and the healing process depends on the nature of the defects. Partial-thickness injuries receive minimal help from adjacent tissues, while full-thickness injuries produce a response from the vascularized subchondral bone but do not restore the original articular cartilage. The result is a fibrocartilaginous tissue, without optimal mechanical properties (Correa and Lietman, 2017). Articular cartilage injuries can also result from indirect effects of the loading, especially in people who play sports. These injuries are difficult to diagnose and can lead to cartilage and subchondral bone damage (Buckwalter, 1998)

Osteoarthritis (OA) is a chronic degenerative disease that can occur without trauma. In fact, in this case there is an unequal balance between ECM deposition and degradation. In the clinical phase of the disease, the alteration of the synovial membrane is associated with an inflammatory response in which proinflammatory cytokines (TNF-α and IL-1) are present. Inflammation is an important factor

associated with the progression of cartilage loss, especially during the OA process. The consequence are joint pain, swelling and stiffness (Martel-Pelletier, 2004).

1.4.3. Strategies for cartilage regeneration

After damage or loss of articular cartilage, there are different treatment strategies that can be employed. In recent years, thanks to tissue engineering (TE), research has focused mainly on biological healing and cartilage regeneration. This interest is due to the fact that there are still no strategies with effective long-term effects for cartilage repair.

Conventional treatments for cartilage regeneration include:

- Microfracture: used to repair small defects and is based on a spontaneous repair process. In fact, microfractures are created over the underlying subchondral bone. In this way, the subchondral bone releases the progenitor cells from the bone marrow that are responsable for regenerating the damaged tissue.
- Mosaicplasty: involves the transfer of cylindrical autologous osteochondral grafts. In the knee, these grafts are taken from the donors sites and inserted into drilled tunnels in the defective section of the cartilage.
- Autologous Chondrocytes Implantations (ACI): is one of the methods in which the cells are used to repair the cartilage. In this technique, the patient undergoes two surgical procedures. In the first surgery a piece of healthy cartilage is taken. The chondrocytes recovered from the cartilage tissue are expanded in vitro for few weeks. In the second surgery intervention, the autologous chondrocytes are implanted into the defect site of the patient which in then covered by a periosteal graft.
- Matrix-induced Autologous Chondrocytes Implantations (MACI): in this case, the cells are seeded onto a scaffold a few days before implantation.

The successful results of these techniques can be compromised by some drawbacks, such as a two-step surgery for some of them, the limited size of the defect that can be restored, and the formation of fibrocartilage tissue, rich in type I collagen (Choi et al., 2018; Jiang et al., 2020).

Finally, if the articular cartilage cannot be regenerated with any of the previous treatments, total or partial joint replacement can be performed. The damaged joint is replaced with an artificial implant consisting of a metal shell (titanium, stainless steel, or alloys), a piece of polymer (such as polyethylene in order to glide smoothly) and a metal stem. In such cases, there are a few frequently reported complications, including infections, looseness, wear of the implant, where the patient has to undergo revision surgery (Zhang et al., 2009).

1.4.3.1. The role of tissue engineering in articular cartilage repair

The main problem with cartilage regeneration is the difficulty in reproducing both the complex structure of this tissue and the various interactions between its components (Johnstone et al., 2013). The regenerative strategy often involves hydrogels, chondrogenic growth factors and cells (chondrocytes or MSCs). Since 1990, a variety of natural and synthetic hydrogel-forming polymers have been developed (Strecanska et al., 2022).

Natural polymers are selected for their biocompatibility, biodegradability and similarity to ECM cartilage components. For example, several studies have shown that HA promotes chondrogenic differentiation and can support the healing of cartilage in various animal models. Combining HA with MSCs has also demonstrated promising results in slowing the progression of osteoarthritis and reducing inflammation(Johnstone et al., 2013). Similar results are also obtained with CS (Johnstone et al., 2013).

Injectable hydrogels offer a minimally invasive approach to cartilage repair as they are capable of undergoing a sol-gel transition and *in situ* gelation. They can effectively fill irregular erosion sites and be functionalized with bioactive molecules. Gelation is triggered by the sensitivity of the hydrogel to changes in temperature, pH, and ion concentration changes, while another group of injectable polymers relies on chemical cross-linking methods (Johnstone et al., 2013; Kim et al., 2009). Methacrylate gelatin hydrogels have been shown potential to have the potential to promote long-term culture of bone marrow-derived mesenchymal stem cells (BMSCs), chondrogenesis, and glycosaminoglycan (GAG) production (Kim et al., 2009). In addition, injectable hydrogels can be functionalized with bioactive substances, such as TGF-β1 to support chondrogenesis of MSCs (Johnstone et al., 2013).

Finally, devitalized and decellularized cartilage have been studied, with devitalized cartilage showing greater yield stress compared to decellularized cartilage. Methacrylate porcine-derived decellularized cartilage hydrogels demonstrated a stress-strain profile similar to native cartilage when cultured with rat bone marrow-derived stem cells. However, decellularization and digestion may be too harsh for some tissues, resulting in mechanically weak gels not suitable for load-bearing applications, that required additional material modifications (Peng et al., 2021)

1.4.3.2. Scaffold-free strategies

Interest in scaffold-free methods for cartilage regeneration has increased in recent years. This interest is given both by the biocompatibility due to their completely biological nature, and the accurate mimicking of natural cartilage development (Huang et al., 2016). For this reason, a 4th generation ACI has been developed to better replicate natural cartilage before implantation (Hulme et al., 2021).

In this approach, spheroids of neocartilage are implanted without a synthetic matrix (Hulme et al., 2021). Several products have been developed and some of them are already used in clinical practice. Chondrosphere® and RevaFlex™ , for example, are scaffold-free cartilage constructs that offer several advantages over scaffold-based approaches. These constructs are created by culturing chondrocytes at high density so that they adhere to each other and secrete a cartilage-specific matrix, from which solid neotissues eventually form. Chondrosphere® consists of spheroids developed from autologous chondrocytes. They are cultured *in vitro* for 6-8 weeks and then implanted into defects (Jiang et al., 2020). These spheroids can integrate into the defect sites, grow in size and adapt to the shape of the defect (Armoiry et al., 2019; Grevenstein et al., 2021)

RevaFlex™ differs from Chondrosphere® because it is grown for months *in vitro* and appears relatively stiff. These constructs do not naturally adhere to the defects and require fixation with a glue. However, implanting a more mature neocartilage construct allows for consistent control of certain properties. In fact, these more mature grafts also have higher initial mechanical properties, which could allow faster rehabilitation (Medvedeva et al., 2018).

In general, for the formation of spheroids it is necessary to prevent cell adhesion to a surface. Various methods are described in the literature (Białkowska et al., 2020), some of which involve the use of a polymer coating to promote cell aggregation. The table below shows the main methods used for forming spheroids and the principle on which the preparation method is based (Table 1) (Ryu et al., 2019).

Technical method	Properties
Pellet culture	Use centrifugal forces to concentrate cells
Liquid Overlay	Use non-adhesive materials to inhibit cell attachment
Hanging Drop	Use surface tension and gravitational force
Spinner culture	Use conventional force by stirring bars
Rotating Wall Vessel	Use constant circular rotation of vessel
Microfluidics	Use microfluidic flow and materials permeable to soluble factors
Magnetic levitation	Use magnetic force to levitate cells.

Table 1. Summary of the methods described in the literature for the formation of spheroids.

2. AIM OF THE THESIS

In tissue engineering (TE) filed there is an increasing need for biomaterials that mimic the complexity and dynamics of the extracellular matrix (ECM). The difficulty in achieving this goal is the reason for the partial failure of existing TE approaches in replacing living tissues, such as cartilage or bone. In this project, CTL, a lactose-modified chitosan commercially available in pure medical grade provided by Biopolife s.r.l., a company located in Trieste, was used as the main material for the development of innovative hydrogels and three-dimensional structures that mimic the architecture of native tissue. This goal was achieved by taking advantage of CTL's chemical, physical and mechanical characteristics as well as its biological properties. In detail in the first part of the project, CTL is crosslinked with two crosslinkers (boric acid and genipin) to form hydrogels with mechanical properties similar to those of the extracellular matrix. The relationship between some of these mechanical properties and the osteogenic commitment of adipose-derived mesenchymal stem cells was then investigated in a 2D culture system. In the second part, CTL and a Sulphated-CTL were used as a biomimetic matrix that coordinates the aggregation of primary chondrocytes and mesenchymal stem cells to form spheroids, 3D structures with potential benefits for cartilage regeneration. The expected results would improve current knowledge about the interplay between extracellular matrix and cells and allow for potential translation of the present materials to regenerative medicine, including cartilage and bone tissue replacement to mention a few.

3. EXPERIMENTAL SECTION

3.1. CHAPTER 1: Chemical reaction between CTL primary amines and genipin.

3.1.1. Aim of the work

The first part of the project focused on the study of the chemical reaction between CTL primary amines and genipin, using mainly UV-VIS spectroscopy and circular dichroism (CD) as analytical tools.

3.1.2. Materials and Methods

3.1.2.1. Materials

Hydrochloride form of lactose-modified chitosan, CTL (CAS Registry Number 2173421-37-7) was kindly provided by biopoLife s.r.l. (Trieste, Italy). The chemical composition of CTL was determined by ^{1}H NMR spectroscopy and resulted: fraction of deacetylated units (F_D) 0.21, fraction of lactose-modified units (F_L) 0.63, and fraction of acetylated units (F_A) 0.16. The calculated molar mass of CTL repeating unit ($MW_{r.u.}$) resulted 403 g/mol. The physical properties of CTL were determined by viscometry: the intrinsic viscosity, [η], of CTL was measured at T = 25 °C by means of a CT 1150 Schott Geräte automatic measuring apparatus and a Schott capillary viscometer. A buffer solution, composed by 20 mM AcOH/AcNa, pH 4.5, and 100 mM NaCl filtered through a 0.22 μm Millipore cellulose filter (VWR International), was used as solvent. The resulting [η] was 344 mL/g. Given the molar mass of chitosan used in the synthesis process (325 000 g/mol) and its repeating unit (168 g/mol), the molar mass of CTL was estimated to be at around 800 000 g/mol.

Phosphate buffer saline (PBS), lactose monohydrate, glucosamine hydrochloride, ethylamine were purchased from Sigma-Aldrich (Chemical Co. USA). Sodium chloride and hydrochloric acid were purchased from Carlo Erba (Italy). Genipin was purchased from Challenge Bioproducts Co., Ltd (Taiwan). Deionized water was used in all preparations.

3.1.2.2. Preparation of CTL and genipin mixture

Lactose-modified chitosan solutions in PBS at pH 7.4, final polymer concentration in the range 1.9 g/L – 7.5 g/L were added of genipin in PBS at different final concentration in the range 0.04 mM –

0.37 mM. The resulting solution was incubated at 37 °C in the presence of oxygen. Typically, 30 mL of solution containing CTL and genipin were incubated in a cylindrical vessel of 60 cm^3 of volume. At selected time points, an aliquot of the CTL-genipin mixture was collected and analyzed by means of different techniques. In the case of measurements in oxygen depleted conditions extending over 4 h, prior to the incubation at 37 °C the solution of CTL and genipin was ice cooled to slow down the reaction (Pasquale Sacco et al., 2020b) and extensively degassed using a nitrogen flow. For oxygen depleted conditions over 24 h, the solution of CTL and genipin was incubated in a Thermo Scientific Oxoid 2.5 L jar containing an Oxoid AnaeroGen 2.5 L sachet. Glucosamine and ethylamine were used for comparison.

3.1.2.3. Intrinsic Viscosity analysis

Intrinsic viscosity of chitosan and CTL was measured at T = 25 °C by means of a Schott-Geräte AVS/G automatic measuring apparatus and an Ubbelohde-type capillary viscometer (Ø = 0.53 mm). A buffer solution composed of 20 mM AcOH/AcNa, pH 4.5, and 100 mM NaCl was used as solvent (P. Sacco et al., 2018). The intrinsic viscosity [η] values were determined by analyzing the polymer concentration dependence of the reduced specific viscosity (η_{sp}/c) and of the reduced logarithm of the relative viscosity ($\ln(\eta_{rel}/c)$) using the Huggins (equation A) and Kraemer (equation B), respectively:

$$\frac{\eta_{sp}}{c} = [\eta] + k'[\eta]^2 c \qquad \text{(A)}$$

$$\frac{\ln(\eta_{rel})}{c} = [\eta] - k''[\eta]^2 c \qquad \text{(B)}$$

Where k' and k'' are the Huggins and Kramer constants, respectively.

The binding of genipin to CTL in PBS at pH 7.4 was followed at T = 37 °C by measuring the relative viscosity of the solutions at different time points with a capillary viscometer.

3.1.2.4. Circular Dichroism

Circular Dichroism spectra of the CTL-genipin solutions in PBS buffer at pH 7.4 were recorded at different time points using a Jasco J-700 spectropolarimeter in the wavelength range 220 - 450 nm or 220 - 700 nm at T = 25 °C. A quartz cell of 1 cm optical path length was used, and the following setup was maintained: bandwidth, 1nm; time constant 2s; scan rate, 100 nm/min. Two spectra, corrected for the background, were averaged for each sample.

3.1.2.5. UV-VIS analysis

UV-VIS spectra of the CTL-genipin solutions in PBS at pH 7.4 were recorded at different time points at 25 °C in the range from 220 nm to 700 nm with a Shimadzu UV-2450 spectrophotometer. UV absorption of CTL-genipin solutions in PBS at pH 7.4 incubated, in the presence or in the absence of oxygen, at 37 °C for 24 h was recorded with a multiplate reader FLUOStar Omega-BMG Labtech. 150 µL of solution were transferred in a 96-wells multi-well and the absorbance was measured at 600 nm. Eight replicates, corrected for the background, were averaged for each datapoint.

3.1.3. Results and discussion

The binding of genipin to primary amino groups has been widely explored to produce functional structures for drug delivery and biomaterials development (Abitha M. Heimbuck et al., 2019; Xu et al., 2015; Yu et al., 2020; Yuan et al., 2007). In this context, several chemical reactions have been proposed, but all analysis are performed under acidic conditions and mainly with chitosan as polymer containing primary amino groups (Butler et al., 2003; Lai et al., 2010). Furthermore, high genipin concentrations (500 mM) are required in these analytical conditions (Dimida et al., 2015). It is also known from the literature that genipin binding to amino group leads to the formation of blue colored solutions (Dimida et al., 2015).

In this first part of the project, CTL was selected as a polysaccharide with amine groups soluble at neutral pH due to its chemical and physical properties (D'Amelio et al., 2013).

In order to propose a mechanism for genipin binding to amino groups, we first studied the behavior of genipin alone, using UV-Vis spectroscopy and CD as analytical tools. Genipin was dissolved in PBS (pH 7.4), measurements were performed at the beginning and after 6 hours of incubation at 37 °C.

UV-Vis spectral analysis shows the presence of a peak at 240 nm (Figure 11a). At the same wavelength, the spectrum of CD also shows a positive peak (Figure 11b), which depends on the concentration of genipin (Figure 11c).

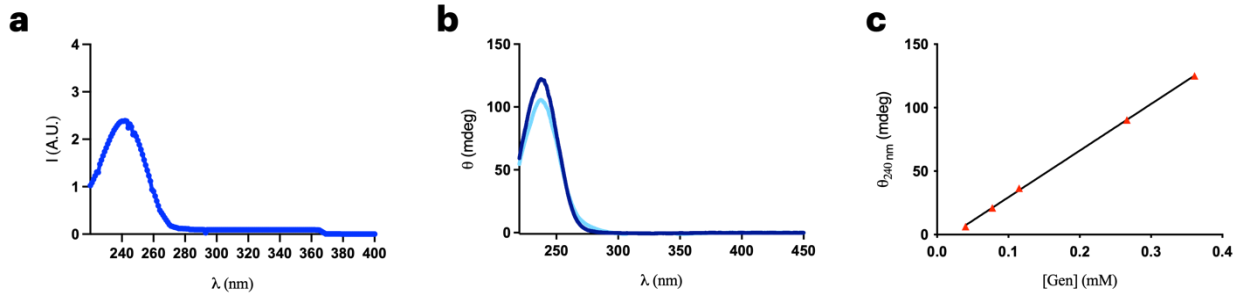

Figure 11. Genipin incubated with PBS (pH 7.4) at 37° C at time 0 (blue) and after 6 hours (light blue). a) UV-Vis spectrum of genipin in the range 240-400 nm. b) CD spectrum of genipin in the range 240 – 450 nm. C) Calibration curve for genipin in PBS at 37° C reported as ellipticity of the CD signal at 240 nm *vs* genipin concentration at time 0.

When genipin is incubated at 37 °C and in the presence of oxygen for 6 hours, the CD spectrum also shows the presence of two bands: a positive peak at 265 nm (Figure 12a) and a negative peak at 330 nm (Figure 12b).

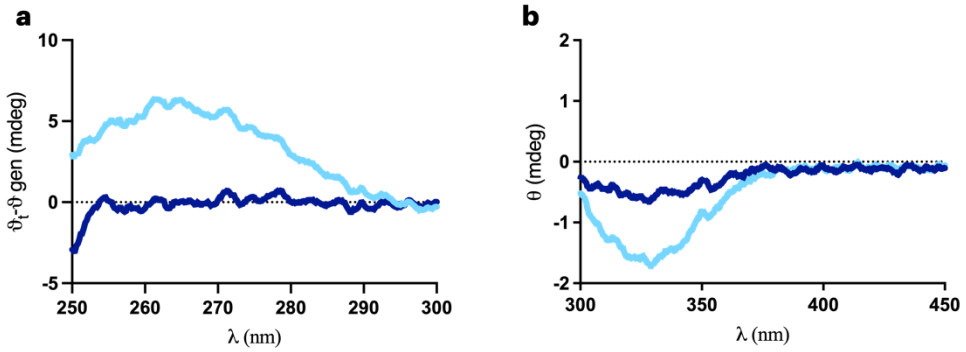

Figure 12. Genipin incubated with PBS (pH 7.4) at 37 °C a) Magnification in the range 250 – 300 nm. The light blue curve represents the differences between the CD spectrum at time *t* and the spectrum of the sole genipin at the concentration calculated from the CD signal at 240 nm. b) Magnification in the range of 300 – 450 nm at time 0 (blue) and after 6 hours (light blue).

When genipin is used alone, the blue color in the solution did not develop even after 24 hours of incubation (data not shown).

From these results, combined computational analysis (Pizzolitto et al., 2020) and considering the 8 possible stereoisomers of genipin reported in the literature (Di Tommaso et al., 2013), we propose a first reaction scheme for the behavior of genipin alone at neutral pH (Scheme 1). In this first scheme, we propose that the presence of oxygen leads to an oxidation of genipin into compound **GII**, which shows the presence of two chiral centers, as shown by CD signal.

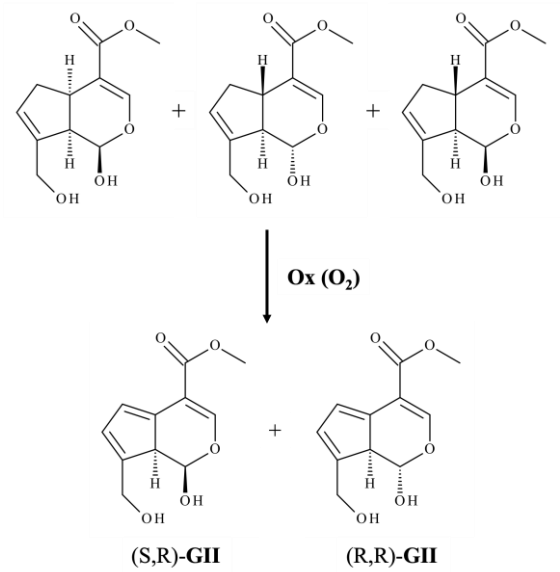

Scheme 1. Proposed reaction for genipin alone incubated at 37 °C in PBS (pH 7.4)

Scheme 1 provides the basis for describing the reaction between genipin and molecules containing amine groups. There are several reaction schemes in the literature based on the analysis of UV-vis spectra (Butler et al., 2003)(Touyama et al., 1994) (Di Tommaso et al., 2014) Unfortunately, the interpretation of these spectra is contradictory from one work to another. To clarify on the different interpretations, we combine UV-vis measurements with CD measurements. Since the signal from CD is based on the chirality of the molecules, we also analyzed the behavior of two other small molecules in contact with genipin: glucosamine (chiral amine) and ethylamine (achiral amine). CD measurements on these two molecules show that both have a positive peak at 280 nm, but only glucosamine also has the positive peak at 380 nm (Figure 13). The behavior of genipin treated with ethylamine and the presence of a peak at 380 nm have already been reported in literature using UV-Vis (Di Tommaso et al., 2014), so the CD signals are from a molecule that does not have a chiral center in the genipin derived moiety or that is present in a racemic mixture.

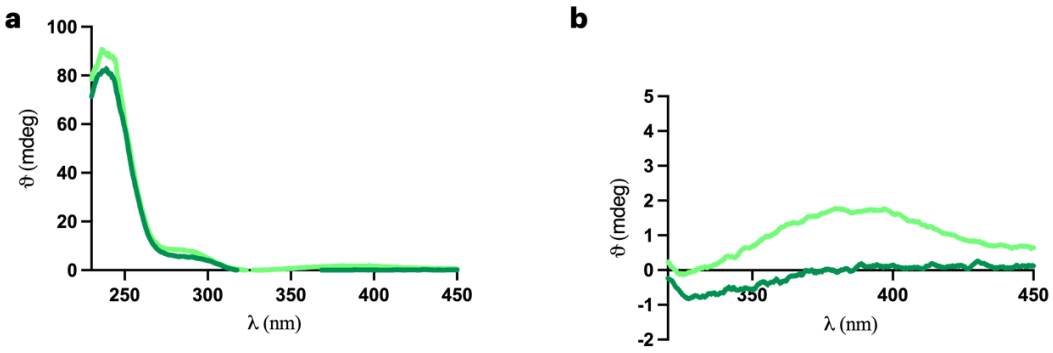

Figure 13. a) CD spectrum of genipin (0.37 mM) incubated with glucosamine (light green curve) and ethylamine (green curve), respectively, for 2 h at 37 °C in PBS (pH 7.4). In both cases, the concentration of amino groups was 1 mM. b) Magnification of the range 320 – 450 nm.

UV-Vis analysis of genipin treated with glucosamine. When the incubation time is increased, the signal of genipin (240 nm) increases and the peaks at around 280 nm and 600 nm become prominent (Figure 14a). In addition, the peak at 380 nm is visible at the beginning, but in a later incubation stage it becomes impossible to distinguish it from the tails of the peaks at around 280 nm and 600 nm (Figure 14b).

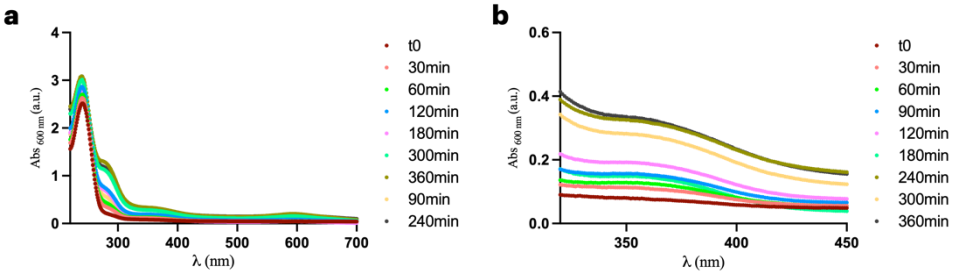

Figure 14. a) UV-Vis spectrum of glucosamine treated with genipin at 37 °C recorded at different time point. b) Magnification of the spectrum in the range 320 – 450 nm.

UV analysis also shows that the signal related to the formation of a blue product is time-dependent (Figure 15).

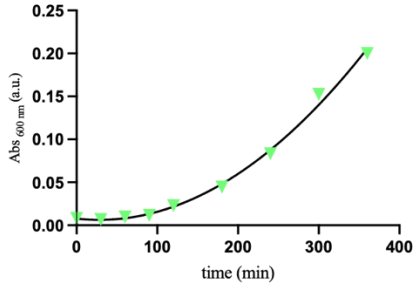

Figure 15. Time dependence of the UV-Vis signal recorded at 600 nm.

The CD spectrum (Figure 16a) for the binding of genipin to glucosamine was analyzed both in the presence and absence of oxygen. The peak at 240 nm decreases with time, indicating the decrease of free genipin due to its binding to glucosamine (Figure 16b).

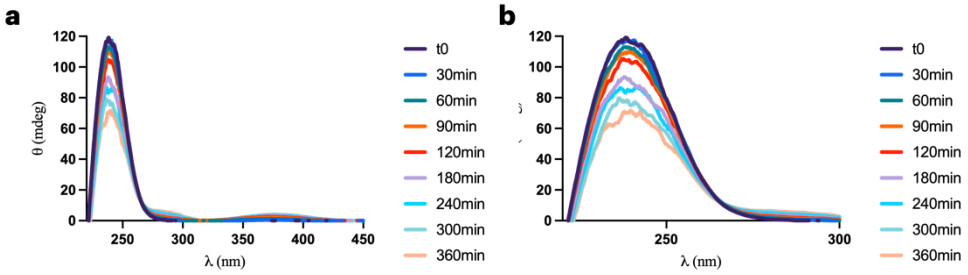

Figure 16. a) CD spectrum of glucosamine treated with genipin at 37 °C recorded at different time point in the presence of oxygen. b) Magnification of the spectrum in the range 220 – 300 nm.

The 280 nm signal (Figure 17), on the other hand, shows an oxygen-dependent behavior. In the presence of oxygen, it exhibits a positive signal, indicating the formation of a chiral compound in solution. Furthermore, this signal shows a sigmoidal increase over the incubation period. Finally, this signal disappears when the reaction takes place in the absence of oxygen.

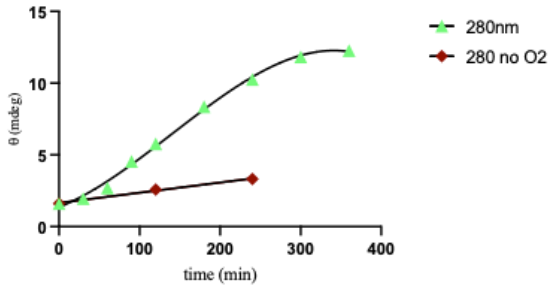

Figure 17. Time dependence of CD signal of glucosamine treated with genipin at 37 °C recorded at 280 nm in the presence of oxygen (green triangle) or in oxygen-depleted conditions (red rhombus)

At 380 nm (Figure 18), on the other hand, a positive signal is present in the presence of oxygen. However, this signal shows a non-monotonic trend over time: during the first 90 minutes the signal increases, but afterwards it decreases significantly. This behavior can be safely correlated with the temporal increase of the UV-VIS signal at 600 nm: negligible during the first 90 minutes and rapidly increasing thereafter. Under oxygen-depleted conditions, the peak at 380 nm leads to a linear increase in the first 4 hours.

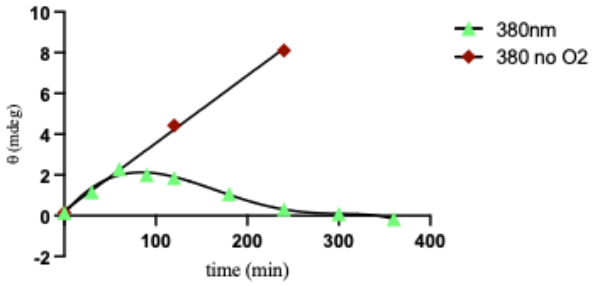

Figure 18. Time dependence of CD signal of glucosamine treated with genipin at 37 °C recorded at 380 nm in the presence of oxygen (green triangle) or in oxygen-depleted conditions (red rhombus)

Finally, no signal is detected on CD associated with the development of blue color (600 nm signal) under any of the conditions analyzed. Furthermore, no blue color is developed under oxygen depleted conditions (data no show).

Based on these considerations and following Scheme 1, we can therefore propose two possible reaction pathways between the genipin and the amino groups (Scheme 2).

In the first case, the reaction leads to the formation of a compound that we have called **G-N**, without the needed of oxygen. The evolution of this compound is explained by a computational analysis and takes into account the different stereoisomers of the genipin (Pizzolitto et al., 2020). We propose two possible mechanisms for the association of two **G-N** molecules in the presence of oxygen:

- In the first case, we have suggested an oxidation of two **G-N** molecules, in the presence of oxygen, with the formation of **2(G-N)$_{ox}$**.
- In the second case, the oxidation of **G-N** is accompanied by a dehydration to give the adduct **2(G-N)$_{dox}$**.

Both resulting compounds showed a computed UV-Vis spectrum comparable to the peak at 600 nm and a complete absence of chiral center (Pizzolitto et al., 2020)

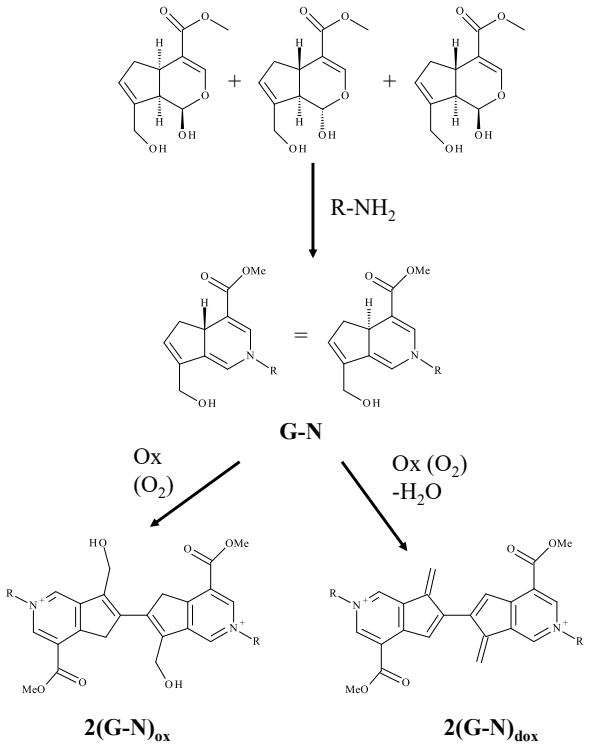

Scheme 2. Proposed reaction scheme for genipin incubated with primary amines at 37 °C in PBS (pH 7.4), Pathway 1.

A second pathway instead involves the reaction of genipin with primary amines in the presence of oxygen, leading to the formation of a **G-N II** compound. Computational analysis of this compound shows the absence of UV-Vis peaks at around 280 nm and 430 nm (Pizzolitto et al., 2020) and no positive peaks in the CD are expected. Further reaction leads to the formation of a molecule with chiral carbon atoms, but without much delocalization of electrons, as no blue color follows the formation of the CD band at 280 nm. The presence of a cyclopentadine unit on **G-N II** could be indicative of a Dies-Alder reaction in according to the literature (Otto and Engberts, 2000; Pirrung, 2006; Xu et al., 2006). This reaction could involve another **G-N II** leading to the formation of **2(G-N II)**, which shows a computer UV-Vis peak and a CD band around 280 nm (Pizzolitto et al., 2020)

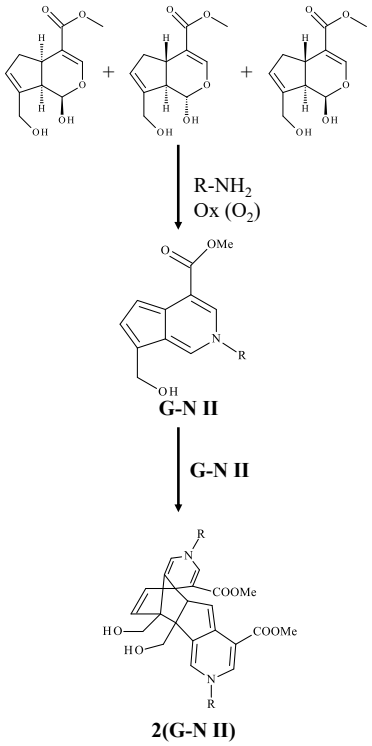

Scheme 3. Proposed reaction scheme for genipin incubated with primary amines at 37 °C in PBS at pH 7.4, Pathway 2.

When the reaction is carried out without oxygen, the pathways to form **G-II** and **2(G-N)** are prevented. Indeed, the 280 nm band for the CD spectrum and the 600 nm band for the UV-Vis spectrum are missing. As a result, only the **G-N** component is formed and leads to the formation of the CD spectrum at 380 nm when glucosamine is used as a molecule with primary amines (Figure 13).

Looking specifically at the reaction between genipin and CTL, the two proposed reaction models (Scheme 2 and Scheme 3) can occur in the presence of oxygen. This is confirmed by the fact that the peaks (280 nm and 380 nm) appear over time and at the same time the concentration of genipin (peak at 240 nm) decreases (Figure 19)

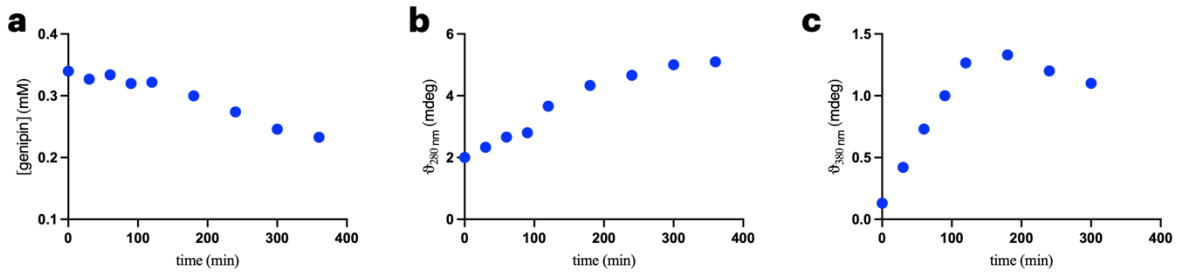

Figure 19. a) Decrease of genipin concentration as measured from the ellipticity at 240 nm and increase of the ellipticity at 280 nm (b) and at 380 nm (c) for CTL. The concentration of primary amino groups was 1 mM and the incubation was performed in the presence of oxygen at 37 °C in PBS with pH 7.4.

According to the Scheme 3, two genipin molecules must bind two distinct chains of CTL to allow a Diels-Alder reaction and the formation of compound **2(G-N II)**. The initial rate ν was evaluated as the following equation:

$$v_{280nm} = \frac{d[280nm]}{dt} \propto \frac{d(\theta_{280nm})}{dt}$$

where [280nm] represent the molar concentration of the specie providing the CD signal at 280 nm, while θ_{280nm} represent the ellipticity at 280 nm. The kinetics leading to peak formation at 280 nm is a second order kinetics for the genipin and CTL concentration (Figure 20):

$$v_{280nm} \propto [Genipin]^2[CTL]^2$$

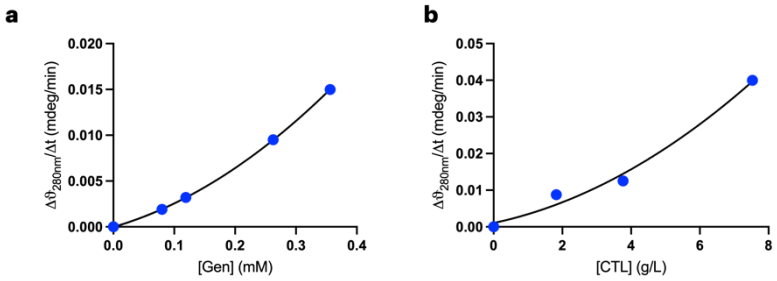

Figure 20. A) Dependence of the initial rate of development of peaks at 280 nm from genipin concentration. CTL concentration was equal to 3.75 g/L. B) Dependence of the initial rate of development of peaks at 280 nm from CTL concentration. Genipin concentration was equal to 0.37 mM. In both cases the black line represents the best-fit of the experimental data according to a parabolic equation $y = ax^2 + bx$ (R2 > 0.985). In both cases, samples were incubated in the presence of oxygen at 37 °C in PBS at pH 7.4.

The measurement of the relative viscosity also confirms the above information (Figure 21), whereby the viscosity increases simultaneously with the peak formation at 280 nm, but no blue color is present.

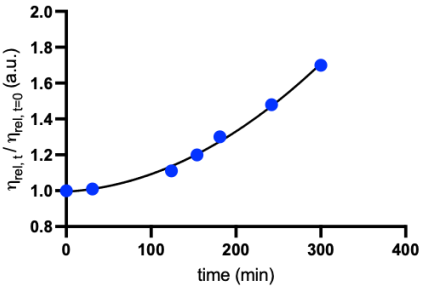

Figure 21: Time dependence of the ratio between the relative viscosity at time t and the initial relative viscosity for CTL (3.75 g/L) incubated with genipin at concentration of 0.13 mM (red) at 37 °C in PBS at pH 7.4. Lines are drawn to guide the eye.

For the peak at 380 nm, the initial rate ν was evaluated as the following equation:

$$v_{380nm} = \frac{d[380nm]}{dt} \propto \frac{d(\theta_{380nm})}{dt}$$

However, the CD kinetics for the 380 nm peak is a first order (Figure 22): the CD signal is not closely related to the immediate cross-linking of the polymer, but to the formation of **G-N** in Scheme 2.

$$v_{380nm} \propto [Genipin][CTL]$$

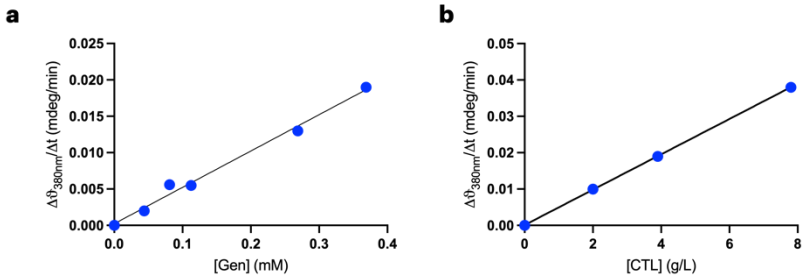

Figure 22. A) Dependence of the initial rate of development of peaks at 380 nm from genipin concentration. CTL concentration was equal to 3.75 g/L. B) Dependence of the initial rate of development of peaks at 380 nm from CTL concentration. Genipin concentration was equal to 0.37 mM. In both cases the black line represents the best-fit of the experimental data according to a linear equation $y = ax$ (R2 > 0.99). In both cases, samples were incubated in the presence of oxygen at 37 °C in PBS at pH 7.4.

Indeed, in the presence of oxygen, part of **G-N** transforms into **2(G-N)$_{ox}$** and **2(G-N)$_{dox}$**, forming a blue color and additional cross-links in the CTL network. However, topological limitations prevent, to some extent, cross-reactions between two **G-N** residues on the polymer. As a result, the UV-vis signal at about 600 nm is less intense than that recorded for glucosamine with the same amount of primary amines (Figure 23).

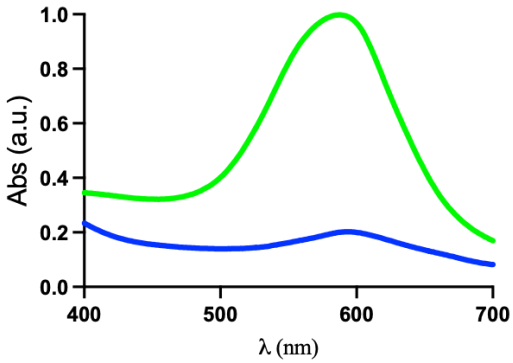

Figure 23. UV-Vis spectrum of genipin treated with glucosamine (light green) and CTL (blue) for 6 h. In both cases, the concentration of primary amino groups was 1 mM. The incubation was performed in the presence of oxygen at 37 °C and in PBS (pH 7.4).

When CTL is incubated with genipin for 24 hours without oxygen, the blue color developed is even less because the cross reaction between **G-N** compounds is affected by the absence of the oxidant. When the sample is exposed to the oxygen again, the topological limitation due to the non-negligible amount of **2(G-N II)** reticulations further limits the amount of cross reaction among **G-N** groups. In fact, the UV-Vis signal at 600 nm does not increase over time when the sample is re-exposed to oxygen after 24 hours (Figure 24).

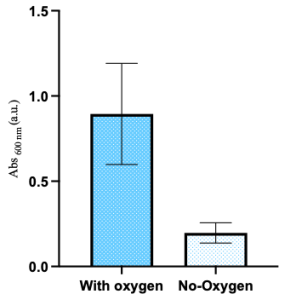

Figure 24. Absorbance measured at 600 nm for CTL (3.75 g/L) incubated with genipin (0.13 mM) for 24 h in the presence of oxygen and in oxygen-depleted conditions for 24 h. In all cases, the incubation was performed at 37 °C in PBS at pH 7.4.

3.1.4. Main conclusions

Genipin is often used in combination with chitosan for the production of various biomaterials. It is frequently reported in the literature that genipin interacts with primary amines. Unfortunately, the mechanism is still debated and all hypothesis were made under acid conditions. In this section, a novel approach to identify the binding mechanism is proposed using CD, UV-Vis, intrinsic viscosity analysis and computational analysis. The second novelty of this work is that it was possible to work

at neutral pH (pH 7.4) thanks to the use of CTL. New features were discussed for both the autoreaction of genipin, its binding to primary amines and the role of oxygen.

A central role was assigned to compound **G-N,** of which two types of oxidation reactions and their kinetics in the presence of oxygen were studied. Both reactions, when CTL was used to bind genipin, lead to the formation of a network. The first pathway is involved in the formation of the typical blue color of the solution. In the second case, oxidation leads to a Dies-Alder reaction, resulting in the **2(G-N II)** compounds. This latter reaction explains the marked increase in the relative viscosity of CTL before the blue coloration of the solution.

3.2. CHAPTER 2: Temporary/permanent dual cross-links hydrogels as 2D substrates to study mesenchymal stem cell osteogenic differentiation.

3.2.1. Aim of the work

Dual cross-links hydrogels with adjustable degree of immediate stress dissipation based on a lactose-modified chitosan (CTL), with boric acid as transient and genipin as permanent crosslinkers, have been developed and described here as novel 2D platforms for mechanobiology studies. In particular, the osteogenic commitment of mesenchymal stem cells from adipose tissue (hMSC-AT) seeded atop these hydrogels was evaluated in response to the different mechanics of the substrates.

3.2.2. Materials and methods.

3.2.2.1. Materials.

Hydrochloride form of lactose-modified chitosan, CTL (CAS Registry Number 2173421-37-7) was kindly provided by biopoLife s.r.l. (Trieste, Italy). The chemical composition of CTL was determined by ^{1}H NMR spectroscopy and resulted: fraction of deacetylated units (F_D) 0.21, fraction of lactose-modified units (F_L) 0.63, and fraction of acetylated units (F_A) 0.16. The calculated molar mass of CTL repeating unit ($MW_{r.u.}$) resulted 403 g/mol. The physical properties of CTL were determined by viscometry: the intrinsic viscosity, [η], of CTL was measured at T = 25 °C by means of a CT 1150 Schott Geräte automatic measuring apparatus and a Schott capillary viscometer. A buffer solution, composed by 20 mM AcOH/AcNa, pH 4.5, and 100 mM NaCl filtered through a 0.22 μm Millipore cellulose filter (VWR International), was used as solvent. The resulting [η] was 344 mL/g. Given the molar mass of chitosan used in the synthesis process (325 000 g/mol) and its repeating unit (168 g/mol), the molar mass of CTL was estimated to be at around 800 000 g/mol.

Boric acid, mannitol, sodium hydroxide, sodium chloride, magnesium chloride, Triton X-100, Tris buffer, Phosphate Buffered Saline (PBS - 137 mM NaCl, 2.7 mM KCl, 8 mM Na_2HPO_4 and 2 mM KH_2PO_4), dexamethasone, bovine serum albumin (BSA - molecular mass 66 430 g/mol), fibronectin bovine plasma, poly-L-lysine solution, AlamarBlue reagent, silver nitrate, sodium thiophosphate, Tween-20, Fast Blue BB salt Hemi (ZnCl) salt, Naphtol AS-X phosphate, Oil Red O, hematoxylin, formaldehyde, Normal Goat Serum (NGS), Tri Reagent, p-nitrophenylphosphate and Bradford reagent were all purchased from Sigma-Aldrich Chemical Co. (USA). Human Osteocalcin Instant ELISA Kit were purchased from Affymetrix eBioscience (USA). L-ascorbic acid and ß-glycerophosphate were from Fluka Biochemika. Hydrochloric acid and Propan-2-ol was from Carlo

Erba (Italy). Genipin (purity 98%) was from Challenge Bioproducts Co., Ltd. (Taiwan). DMEM (Dulbecco's Modified Eagle's Medium) High Glucose, Fetal Bovine Serum (FBS), streptomycin, penicillin and trypsin were from EuroClone (Italy). Mesenchymal Stem Cell Growth Medium was from PromoCell.

All reagents and chemicals were of high purity grade and deionized (Milli-Q) water was used as solvent in all experiments.

3.2.2.2. Preparation of CTL hydrogels.

To obtain dual cross-links hydrogels, two solutions were prepared: a CTL solution (referred to as *solution A*) and a cross-linking solution (referred to as *solution B*), the composition of which varied depending on the type of hydrogel. To prepare solution A, CTL (150 mg) was dissolved in 3.5 mL of deionized water and the pH was adjusted to 7.4 by adding aliquots of NaOH (1 M and 5M). Finally, 400 µL of PBS 10X and deionized water were added to give a final volume of 4 mL. Solution B consisted of a mixture of boric acid (80 mM) and mannitol (160 mM) prepared in PBS 1X and pH 7.4, and a genipin solution (15.6 mM) prepared in PBS 1X, pH 7.4.The final concentration of CTL was 3% w/v in all experiments, while the concentrations of boric acid and mannitol were in the range of 2-8 mM and 4-16 mM, respectively. The final concentration of genipin was chosen so that the molar ratio between the glucosamine units of CTL (D) and genipin (G), $R_{D/G}$: hydrogels with a $R_{D/G}$ of 10, was achieved with a genipin concentration of 1.56 mM. A typical gel preparation was performed as follows: 4 mL of solution A was mixed with 1 mL of cross-linking solution B using a Luer-Lock syringe system, resulting in an even mixture of the solutions. The finished mixture was poured into the well plates and incubated at T = 37 °C for 24 hours. The following table (Table 2) summarizes the composition of the various hydrogels analyzed and gives the nomenclature by which they are named in the following section.

		Solution A	**Solution B**		
Sample	**R $_{D/G}$**	**CTL (3.75%)**	**Boric Acid (80 mM) - Mannitol (160 mM)**	**Genipin (15.6 mM)**	**PBS 1X**
B8 - G1.56	10	4 mL	500 µL	500 µL	-
B2 - G1.56		4 mL	125 µL	500 µL	375 µl
B0 - G1.56		4 mL	-	500 µL	500 µL

Table 2. Experimental conditions used for the preparation of Dual cross-links hydrogels.

3.2.2.3. Stability test

In order to investigate the structural stability of the hydrogels as a function of time, a swelling test was carried out. The hydrogels were synthesized as previously described. 3 mL of the gel mixture was poured into 6-well plates and incubated at T = 37 °C. After complete gelation, small cylinders were punched out of the hydrogels (Ø = 10 mm, h = 2,5 mm) and weighted (t = 0). Later, the samples were transferred to well plates, immersed in DMEM High Glucose (1:4 V/V) and stored at T = 37 °C. Samples were removed from the incubation medium, blotted with filter paper to remove excess medium and weighed at different time points. The experimental data are expressed as the percentage increase in mass with respect to the initial weight according to the formula:

$$Medium\ uptake\ (\%) = \frac{W_t - W_0}{W_0} \times 100$$

where W_0 is the weight of hydrogels at time zero and W_t is the weight of the same sample at selected time.

3.2.2.4. Mechanical characterization

To study the mechanical properties, hydrogels were synthesized according to a previously established protocol (3 mL gel mixture in 6-well plates). Prior to mechanical testing, samples were cut into regular small cylinders (Ø = 21 mm, h = 2 - 2.8 mm) using a disposable biopsy punch.

Rheological tests were performed with a HAAKE MARS III rheometer (Thermo Scientific) operating in oscillatory shear conditions. The samples were tested using a shagreened titanium plate with plate/plate geometry (HPP20: Ø = 20 mm). All rheological tests were performed at T = 37 °C. A glass bell (solvent trap) covering the measuring device was used to improve thermal control and avoid water-evaporation from the hydrogel. To prevent both wall-slippage and excessive gel squeezing, which could lead to a change in the properties of the polymer network, the gap between the plates was adjusted for each sample by executing a series of short stress sweep tests (frequency, ν = 1 Hz; stress, τ = from 1 to 5 Pa) characterized by a decrease in the gap. The gap chosen was the one that maximized the value of the storage modulus (G′).

The following tests were performed for each sample:

- **Frequency sweep test** was used to determine the mechanical spectra of the samples. The storage (G′) and loss (G″) moduli of the systems were recorded in the frequency range of 0.01 – 100 Hz, keeping the stress constant (τ = 4 Pa).

- To analyze the extension of the linear viscoelastic regime, **long stress sweep test** was performed with a constant frequency (ν = 1 Hz) in the stress range of 0.1 and 1000 Pa.
- **Creep-recovery test** was used to calculate the degree of plasticity of the samples. A constant stress (τ = 100 Pa) was applied for 600 s while the strain (γ) was measured in response to the stress; then the stress was removed in recovery tests and the strain was monitored until it reached equilibrium. Plasticity was defined as the ratio of the irreversible strain after the recovery tests to the maximum strain at the end of the creep tests(Nam et al., 2016).
- **Stress-relaxation** in which a constant strain (γ = 1%) was applied for 600 s and the time-dependent decrease in stress in response to the strain was measured.

The Young's moduli of the hydrogels were measured by performing compression tests using a Universal Testing Machine (Multites 2.5-*i*) coupled with a 100 N load cell. The compression speed was set on 5 mm/min and samples were compressed until 15% strain. The Young's modulus was calculated by measuring the slope of the stress-strain curve (first 1-5% of strain).

3.2.2.5. Preparation of CTL hydrogels for biological experiments

For the biological test, the hydrogels were prepared under sterile conditions: beckers and spatulas were heat-sterilized, syringes were UV-sterilized and the solutions (i.e., deionized water, PBS, NaOH 1 M, cross-linking solution) were filtered with 0.2 µm Millipore filters. After mixing, 500 µL of the gel mixture was poured into sterile 24-well plates, UV-sterilized for 20 min and incubated at T = 37 °C for 24 hours. After complete gelation, followed by another UV- sterilization passage for 20 minutes, the substrate surfaces were coated with 250 µL fibronectin to promote cell anchorage(Stanton et al., 2019). The concentration of fibronectin was 20 µg/mL (dissolved in PBS 1X). After 24 hours of incubation in a humidified atmosphere of 5% CO_2 at T = 37 °C, the hydrogels were carefully washed twice with PBS 1X before cell seeding.

3.2.2.6. Cell culture and seeding

Human osteosarcoma cells (MG-63) and human adipose mesenchymal stem cells (hMSC-AT cells, PromoCell) were used as cell models for the *in vitro* experiments. Human osteosarcoma cells (MG-63) were cultured in DMEM High Glucose supplemented with 10% v/v heat-inactivated (FBS), 1% penicillin/streptomycin in a humidified atmosphere of 5% CO_2 at T = 37 °C.

Human adipose-derived mesenchymal stem cells were cultured in Mesenchymal Stem Cell Growth Medium, in a humidified atmosphere of 5% CO_2 at T = 37 °C. Both cell culture media were changed every 2-3 days.

Once cells reached approximately 80% confluence, they were harvested and seeded at a density of 7 000 cells/cm^2 for viability tests and 15 000 cell/cm^2 for differentiation analysis on fibronectin-coated hydrogels. The concentration of the cells was determined using the Bürker chamber. The cells used in these experiments were between passage 3-5.

For differentiation analysis, the hMSC-AT cells were first seeded with Mesenchymal Stem Cell Medium over the hydrogels. After 24 hours, the culture media were discarded and replaced with DMEM High Glucose supplemented with 50 µg/mL L-ascorbic acid, 10 mM ß-glycerophosphate and 0.1 µM dexamethasone (Chaudhuri et al., 2016). The differentiation medium was changed every 2-3 days.

3.2.2.7. Alamar blue assay

Cell viability and growth rate were determined as a function of time using the AlamarBlue assay according to the manufacturer's protocol. After cell adhesion, the culture medium was discarded, cells were rinsed once with PBS 1X and incubated with 250 µL/well of AlamarBlue reagent (1:30 V/V in complete DMEM High Glucose) for 4h at T = 37 °C under dark conditions. At the end of this period, 120 µL of supernatant was transferred to a black 96-well plate and the fluorescence was measured using a FLUOStar Omega-BMG Labtech spectrofluorometer (λ_{ex} = 544 nm, λ_{em} = 590 nm). Metabolic activity was measured by evaluating the chemical reduction of AlamarBlue reagent by the cells at the time point studied. Adherent cells cultured on plastic served as a positive control and DMEM High Glucose was used as a blank.

3.2.2.8. Analysis of stem cell differentiation towards a bone-like phenotype.

Various techniques have been used to assess the differentiation of hMSC-AT towards a bone-like phenotype. For all experiments adherent cells cultured on plastic was used as a positive control (data not shown).

- **Quantification of the activity of the enzyme Alkaline Phosphatase (ALP)**. Cells were harvested after 7 and 14 days of incubation in the differentiation medium. After trypsinization (10 min), cells were collected into 1.5 mL Eppendorf tubes, rinsed with PBS 1X (1 mL) and lysed by adding 100 µL of Lysis Buffer (100 mM Tris-HCl, 0.2% V/V Triton X-100, pH 9.8). Samples were then incubated at T = -80 °C for 30 minutes, at T = 60 °C for 10 minutes, and then collected by centrifugation at 13 000 *g* for 5 minutes. 40 µL of the resulting lysate was mixed with 40 µL of Reaction Buffer (100 mM Tris-HCl, 1 mM $MgCl_2$, 6 mM p-nitrophenylphoshate, pH 9.8) in an optically clear 96-well plate and incubated for 60 minutes at T = 37 °C under dark conditions. The reaction was stopped by adding 2 µL of NaOH (5 M) and the absorbance of the samples was

measured at λ = 420 nm using a FLUOStar Omega-BMG Labtech spectrofluorometer. The enzymatic activity of ALP was normalized for total protein content as the ratio between the absorbance at λ = 420 nm and at λ = 600 nm. The amount of protein content in the cellular extract was determined using the Bradford assay. For this purpose, 5 µL of the samples were added to 250 µL of the Bradford Reagent into an optically clear 96-well plate. After incubating the samples for 5 minutes at room temperature, the absorbance was measured using a FLUO Star Omega-BMG Labtech spectrofluorometer at λ = 600 nm. DMEM-HG was used as a blank.

- **Fast Blue staining** was used to analyze the cells for alkaline phosphatase after 14 days of culture. For this analysis cells were detached from the hydrogels by trypsinization and seeded on coverslips coated with poly-L-lysine. Cells were next equilibrated in alkaline buffer (100 mM Tris-HCl, 100 mM NaCl, 0.1% Tween-20, 50 mM $MgCl_2$, pH 8.2) for 15 min and stained in 500 µg/mL napthol-AS-MX phosphate and 500 µg/mL Fast Blue BB Salt Hem (ZnCl)salt in alkaline buffer for 60 min. The samples are then washed in alkaline buffer and in PBS. Cells are counterstained with hematoxylin for 2 min. Images were taken with a Zeiss Aziophot Microscope (Carl Zeiss, Germany) equipped with a Pentax digital camera and using a 20x objective lens. Data are given as percentage of ALP positive cells in relation to total cells.
- **Von Kossa Staining** was used to detect calcium deposits. This staining was performed on the cells on the hydrogels after 14 days of incubation in osteogenic medium. The cells were fixed with 4% V/V formaldehyde in PBS 1X for 10 min and then equilibrated in distilled water. Then the samples were incubated with 1% silver nitrate solution and irradiated with UV-light for 40 min. After washing in distilled water, the cells were incubated with 5% sodium thiosulphate solution for 5 min and finally washed with distilled water. Images were taken with a Zeiss Aziophot Microscope (Carl Zeiss, Germany) equipped with a Pentax digital camera and using a 4x objective lens.
- **Gene expression analysis:** the relative expression of selected osteogenic (RUNX2, OCN, ALPL, COL1A1) was determined by quantitative Real Time PCR (qPCR). hMSC-AT were cultured on hydrogels at a density of 15 000 cells/cm^2 and RNA was extracted after 0, 7, 14 and 21 days of culture using TRI-Reagent (Sigma, USA) according to the manufacturer's instructions. The sequences of the primers used for the qPCRs are listed in following table (Table 3).

Gene	Size	Forward (F) / Reverse (R)	Sequence 5' – 3'
ALPL	68 bp	F	GACCCTTGACCCCCACAA
		R	GCTCGTACTGCATGTCCCCT
OCN	71 bp	F	CGAAGCCCAGCGGTGC
		R	CACTACCTCGCTGCCCTCC
RUNX2	81 bp	F	AGCAAGGTTCAACGATCTGAGAT
		R	TTTGTGAAGACGGTTATGGTCAA
COL1A1	139 bp	F	CCCTGGAAAGAATGGAGATGAT
		R	ACTGAAACCTCTGTGTCCCTTCA

Table 3. Sequence of real-Time PCR primers.

For cDNA synthesis, 500 ng of total RNA was retranscribed using M-MLV reverse transcriptase (Thermo Fisher Scientific, Waltham, MA, USA) and hexameric random primers or poly-(T)20 primers (Merck- Sigma-Aldrich, St. Louis, MO, USA). Specific primer pairs were designed for analysis of gene expression levels using SYBR Green qPCR (Bio-Rad Laboratories, Redmond, WA, USA). Expression of the house-keeping gene RPLP0 was used to normalize gene expression of the targets. qPCR amplifications were performed using a CFX96 Real-Time PCR detection system (Bio-Rad Laboratories, Redmond, WA, USA) and the relative expression levels were calculated using the 2^-ΔΔCT method.

3.2.2.9. Morphological analysis

Cells were seeded at a density of 7000 cells/cm2 on hydrogels of different composition and cultured for 14 days. The cells were fixed on days 5 and 14 with formaldehyde 4% V/V in PBS for 10 minutes at room temperature. Then the hydrogels were washed 3× with PBS and permeabilized with Triton X-100 0.2% V/V in PBS for 15 minutes at room temperature. The hydrogels were then washed with PBS and incubated with BSA 4% w/V + normal goat serum 5% V/V in PBS (blocking solution) for 1 h at T = 37 ◦C. The blocking solution was then removed and the samples washed with PBS. For visualization of the nuclei, the cells were counterstained with Hoechst (33258) 1:100 in PBS. Finally, the hydrogels were washed twice and stored in PBS. Images were taken using a Nikon Eclipse Ti-E epifluorescence live imaging microscope with a 20x objective. The area and diameter of the cells were calculated from the captured images using Fiji- ImageJ software.

3.2.2.10. Statistical analysis

Statistical analysis and graph elaboration were performed using GraphPad Prism 9 (GraphPad Software, San Diego, CA). One-way ANOVA (analysis of variance) followed by Dunnett's or Tukey's multiple comparison *post hoc* tests were performed to evaluate differences among groups and the control. An unpaired Mann-Whitney two-tailed *t*-test was also performed to evaluate significant differences between two groups. Differences were considered significant for p values < 0.05.

3.2.3. Results and discussion

3.2.3.1. Dual cross-link CTL based hydrogels

The first objective of this chapter was to prepare a series of hydrogels that have the same stiffness and similar viscoelastic behavior but differ significantly in terms of viscoplastic response. To this end, a series of hydrogels with two different cross-links was first synthesized. The starting point was a purely elastic hydrogel consisting of a lactose-modified chitosan covalently crosslinked with genipin. These hydrogels have been prepared starting from the results on the binding between CTL and genipin obtained in Chapter 1. The introduction of dynamic cross-linking into this structure helped us to obtain gels with the same stiffness but different viscosity contribution. It has already been reported from our group that hydrogels cross-linked only with genipin behave as elastic networks, while the double cross-linked hydrogels show particular viscoelastic properties (Pasquale Sacco et al., 2020b). Based on these findings, the genipin concentration was kept constant between samples, but the molar ration of glucosamine-to-genipin was increased ($R_{D/G}$ = 10). To modify the viscoplastic response of the substrates when stress/deformations are applied over time, the concentration of the temporary crosslinker (boric acid-mannitol) was varied between samples. The two crosslinkers used bind the CTL in two different ways. Boric acid binds the lateral diols of the CTL and caused an immediate increase in the viscosity of the sample. The network formed is transient, with the boric acid acting like a weak "sticker" that binds and dissolves the polymer in a highly dynamic manner. The presence of mannitol in the mixture allows the formation of a homogeneous and clear network, avoiding phase separation phenomena. Genipin, on the other hand, binds covalently to the primary amino groups of CTL with a slower binding kinetics and in a temperature-dependent manner (Chapter 3.1).

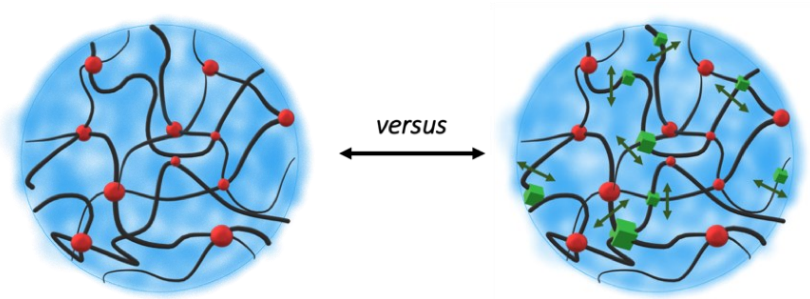

Figure 25. Sketch representation of the hypothetical internal network of the hydro- gel systems investigated in this study. In the case of exclusively permanent, genipin- based, cross-links (red dots), the network is expected to behave like an elastic material under load with negligible relaxation of the applied stress. After the introduction of temporary boric acid cross-links (green cubes), which are transient in nature, the hydrogel becomes viscoplastic; the higher the content of temporary cross-links, the higher the stress relaxation Original source from (Pizzolitto et al., 2023)

3.2.3.2. Gel stability and cellular response

The purpose of this chapter is to investigate how the mechanical properties of dual cross-links hydrogels affect the cellular response of mesenchymal cells seeded on their surface. For this reason, in a first step, the substrates described in the previous section were characterized in terms of their stability and their ability to allow cell growth on their surface for up to 21 days.

The stability of the hydrogels was studied at T = 37 °C as a function of time for 21 days by observing the swelling behavior after incubation of the samples in DMEM High Glucose. The uptake of the medium appeared to be limited for all hydrogels tested even after 21 days (medium uptake < 10%) (Figure 26).

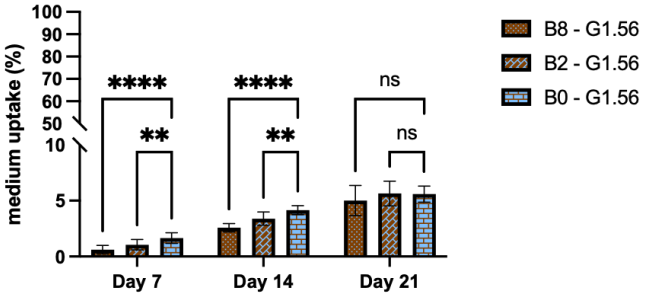

Figure 26. Stability test performed on dual cross-links hydrogels with different compositions after incubation in DMEM – High Glucose after different time points (7, 14, 21 days). Data are reported as mean ± s.d., n = 12 replicates analyzed for each experimental condition. Statistics: One-Way ANOVA followed by Dunnet's Multiple Comparison *post hoc* test; ns = not significant; ** = p <0.01; **** = p < 0.0001.

The ability of the substrate to promote cell anchorage, together with its non-cytotoxic nature, is an essential prerequisite for conducting biological studies. As described in the Materials and Methods section, hMSC-AT were seeded on hydrogels coated with fibronectin to enhance cell attachment. The proliferation rate of the cells was examined using the AlamarBlue assay after 4, 7 and 14 days of

culture. No significant differences were found between the samples with different cross-linkers concentrations (Figure 27).

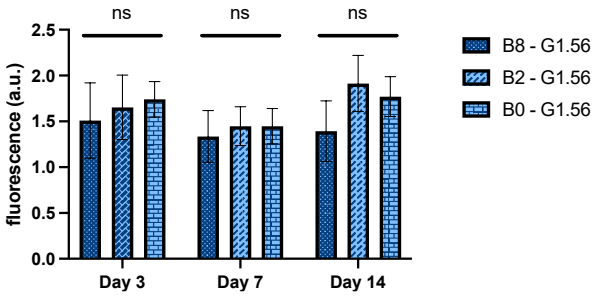

Figure 27. Alamar Blue analysis on hMSC-AT seeded on dual cross-links hydrogels with different composition and cultured after 3, 7 and 14 days in osteogenic medium. All data are reported as mean ± s.d., n = 6 replicates analyzed for each experimental condition.

This result is also important for the study of osteogenic differentiation, which is discussed in the following sections. Given the same proliferation in the three hydrogels considered, any differences in cell differentiation are exclusively due to the mechanical properties of the substrates.

3.2.3.3. Mechanical characterization

Rheological measurements were performed on the three hydrogels described above (b8-g1.56, b2-g1.56, b0-g1.56) to study their mechanical behavior.

Both G′ (storage modulus) and G″ (loss modulus) experimental data of mechanical spectra (frequency sweep tests – Figure 27) were analyzed using the generalized Maxwell model, which consists of a combination of Maxwell elements, composed of a sequence of springs and dashpots arranged in parallel (Turco 2011). The following equations were used to model the G′ (equations 1) and G″ (equations 2) as a function of pulsation (ω):

$$G' = G_e + \sum_{i=1}^{n} G_i \frac{(\lambda_i \omega)^2}{1 + (\lambda_i \omega)^2} \; ; \; G_i = \frac{\eta_i}{\lambda_i} \qquad (1)$$

$$G'' = \sum_{i=1}^{n} G_i \frac{\lambda_i \omega}{1 + (\lambda_i \omega)^2} \qquad (2)$$

where n is the number of Maxwell elements considered, G_i, η_i, and λ_i represent the spring constant, the dashpot viscosity, and the relaxation time of the i^{th} Maxwell element, respectively. G_e is the spring

constant of the last Maxwell element which is supposed to be purely elastic. The use of three Maxwell element is sufficient to accurately fit experimental data for b8-g1.56, b2-g1.56, b0-g1.56.

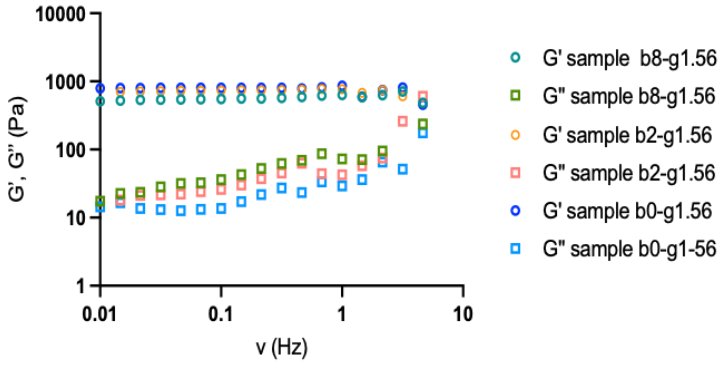

Figure 27. Sample-case of mechanical spectra with the dependence of storage (G') and loss (G'') moduli from frequency for b8-g1.56, b2-g1.56, b0-g1.56.

The three samples analyzed show the same purely elastic response in terms of G*e* (Figure 28a) and Young's modulus (Figure 28b).

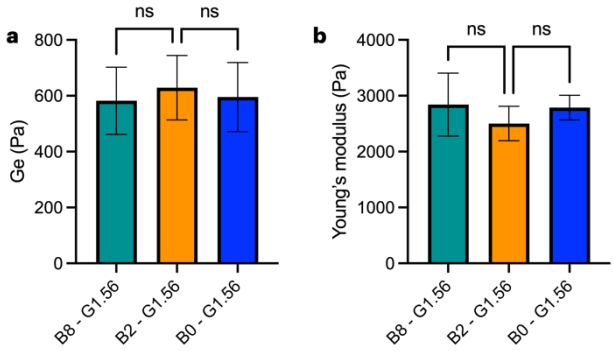

Figure 28. A) Purely elastic spring constant G*e* calculated from the fitting of the experimental mechanical spectra using the equations described above. Data are reported as mean ± s.d. of at least of 5 replicates. B) Young's moduli calculated under uniaxial compression. Data are reported as mean ± s.d. , n= 7 replicates

This approach allows the calculation of the shear modulus, G, using the following equations:

$$G = G_e + \sum_{i=1}^{n} G_i$$

There are small differences between the samples in terms of shear modulus (Figure 29). The addition of boric acid causes an increase in the elastically active segments due to the diol binding in the polysaccharide chain. Furthermore, all hydrogels considered have a shear modulus below to 3 kPa.

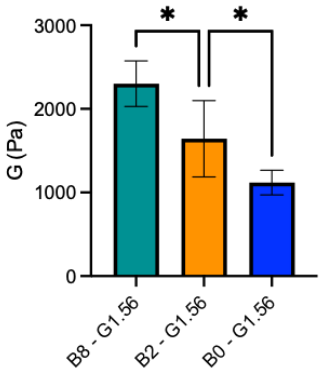

Figure 29. Shear modulus calculated by means of Equations reported above; data are reported as mean ± s.d., *n* = at least 5 hydrogels analyzed for each experimental condition.

Since these hydrogels are soft, we do not expect that the observed differences in G will affect the behavior of the cells. Recently, it was shown that the initial elastic modulus of the substrate has no influence on the myoblast activity in soft substrates (shear modulus lower than about 12 kPa)(Bauer et al., 2017).

Equations 1 and 2 can be used to determine the relaxation times λ which are influenced by the composition of the hydrogels (Figure 30). The introduction of boric acid, due to the transient cross-links with the diols in the CTL (Furlani et al., 2019b), gradually reduced the relaxation times (from $9.5*10^{-3}$ to $4.7*10^{-3}$ s). The effect of boric acid on the elastic components is more pronounced at the shortest relaxation time (Figure 30a), which determines the experimental profile of the mechanical spectrum at high frequencies. In this case, the rate of mechanical stimulation is similar or higher than the binding/unbinding rate of boric acid (Pasquale Sacco et al., 2020b). On the other hand, the effect of boric acid at the higher relaxation time λ3 (Figure 30c), is still found in b8.g1.56, but is significantly less pronounced.

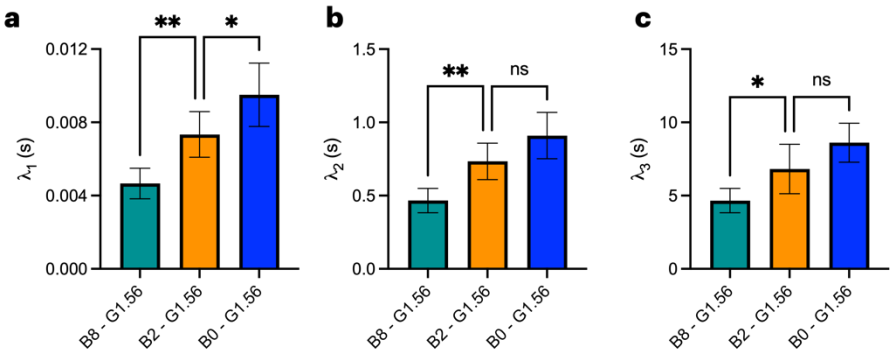

Figure 30. Relaxation time λ_1, λ_2 ,λ_3 calculated from the fitting of the experimental mechanical spectra using the equations described above. Data are reported as mean ± s.d. of at least of 5 replicates.

The figure bellow shows the contributions of the three-Maxwell elements to the total viscosity.

The viscosity of the first and second Maxwell-element is increased by the presence of boric acid in the systems, corresponding to the fastest relaxation time and the second most rapid. Thus, the presence of boric acid affects the relative molecular motions at medium to high frequency due to its rapid association and dissociation to the CTL diols (Pasquale Sacco et al., 2020b). The effect of boric acid is negligible for the third Maxwell element with longer relaxation time. In this last case, the molecular motions take place on a scale of ten seconds, which is much too slow to be affected by the transient binding of boric acid. Overall, the sum of all viscous terms shows no differences between the samples, as the most important contribution in numerical terms comes from the third Maxwell-element.

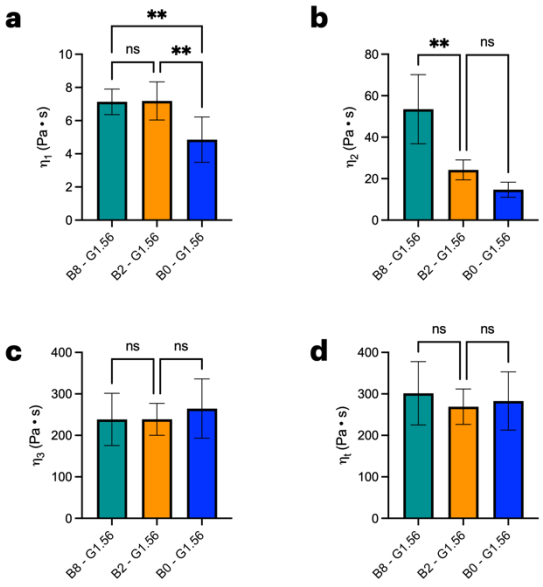

Figure XXX. Viscosity of the **a)** first ($\eta 1$, associated with $\lambda 1$), **b)** second ($\eta 2$, associated with $\lambda 2$), **c)** third ($\eta 3$, associated with $\lambda 3$) Maxwell elements obtained from the fitting of the mechanical spectra using equations. 1 and 2. **d)** Sum of the three values, $h_t = h1 + h2 + h3$. Data are reported as mean ± s.d. of at least 5 replicates.

Additional indications on the characteristics of the system come from the analysis of the long stress sweep. Both G' (storage modulus) and G" (loss modulus) were recorded at a frequency of 1 Hz, *i.e.* similar to the relaxation time of the second Maxwell element $\lambda 2$. The trend of G'' for b8-g1.56, b2-g1.56 and b0-g.1.56, which is consistent with the viscosity of the second Maxwell element, reveals a dependence of the viscous response on the boric acid content (Figure 31).

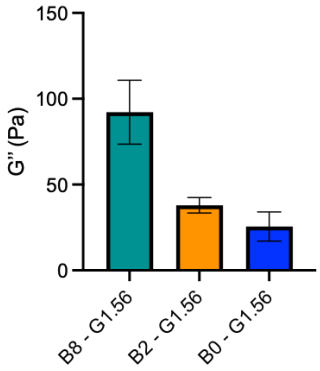

Figure 31. Loss modulus (G'') measured at 1 Hz. Data are reported as mean ± s.d., *n* = at least 10 hydrogels analyzed for each experimental condition

The presence of the temporary cross-links has no influences on the critical strain – *i.e.* the strain at which the linear stress-strain relationship is lost (Figure 32) (Sacco et al., 2020).

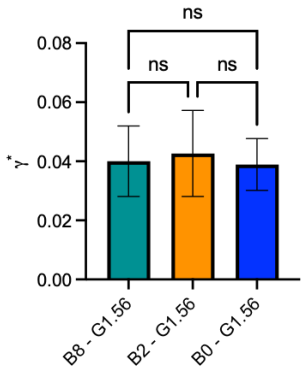

Figure 32. Critical strain, γ^*, obtained from long stress sweep measurements. Data are reported as mean ± s.d., *n* = at least 10 hydrogels analyzed for each experimental condition.

Stress relaxation and creep compliance analysis were also carried out on the three hydrogels. The stress-relaxation curves show the presence of temporary cross-links in the structure of the hydrogels containing boric acid. The almost instantaneous stress relaxation was caused by the presence of boric acid: the higher the boric acid concentration, the greater the immediate decrease in stress. This is attributed to the transient nature of the boric acid cross-links, as the immediate application of stress leads to the unzipping of the bound boric acid. For the sample with only genipin (b0-g1.56), the relaxation of the stress over the analyzed time period is limited, as expected for highly elastic structures (Figure 33).

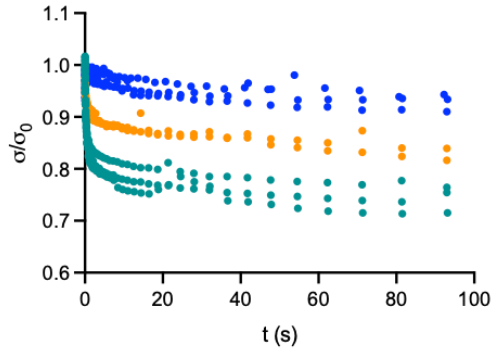

Figure 33. Relative variation of the stress relaxation ($\sigma/\sigma_{t=0}$) over time; for each sample, three replicates are reported

The same effect is observed for the analysis of the creep compliance curve. In this case, there are no differences between b2-g.156 and the sample without boric acid. However, for the sample with the higher amount of boric acid (b8-g1.56), an increase in strain after 600s is visible. It should be noted, however, that all the hydrogels return to almost their original size during the creep recovery phase, with plasticity (final permanent deformation) in the range of 8% to 14%. Again, the dynamic nature of the boric acid cross-link results in a rapid unbinding of the bond when the stress is applied, but also a rapid re-binding when it is removed (Figure 34).

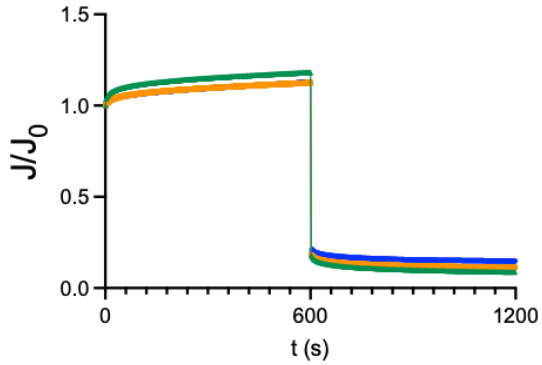

Figure 34. Relative variation of the compliance ($J/J_{t=0}$) over time; each curve is the average of at least 5 replicates.

3.2.3.4. Analysis of osteogenic commitment

While many studies have addressed the role of matrix stiffness in mediating osteogenic differentiation of mesenchymal stem cells (Huebsch et al., 2010; Trappmann et al., 2012), much less is known about how variations in substrate viscoplasticity may affect cell fate decisions. Since the osteogenic potential of hMSC-AT has been demonstrated in terms of extracellular matrix mineralization, osteocalcin expression and ALP production (Im et al., 2005), we investigated the influence of the content of temporary cross-links (boric acid) in the hydrogels on the osteogenic commitment of

hMSC-AT cultured under 2D conditions. Highly elastic hydrogels (*i.e.* those containing only genipin as cross-linkers) were used as a control.

Following the standard procedure for osteogenic differentiation of stem cells, a confluent monolayer of cells was treated with a cocktail of dexamethasone, ascorbic acid and beta-glycerophosphate (Chaudhuri et al., 2016; Langenbach and Handschel, 2013). hMSC-AT were plated on substrates with the same storage modulus G′ (~ 0.8 kPa) but different amounts of boric acid (from 2 mM to 8 mM). To improve cell adhesion and facilitate cell confluence, the gels were functionalized with fibronectin (Stanton et al., 2019).

Osteogenic differentiation was investigated using different techniques.

We started with the analysis of Runt-related transcription factor 2 (RUNX2), an early osteogenic regulator that plays a crucial role in osteoblastic differentiation and bone formation (Bruderer et al., 2014). Using gene expression analysis, we found that after 7 days of culture, there is a dependence between the concentration of boric acid and the expression of RUNX2 (Figure 35)

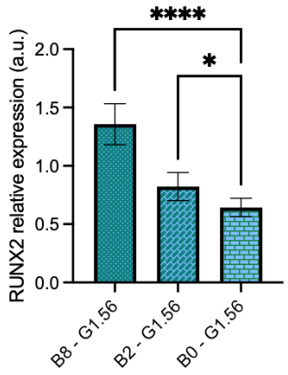

Figure 35. Relative gene expression quantification (arbitrary units, a.u.) of runt-related transcription factor 2 (RUNX2) in cells grown on B8-g.156, B2-g1.56 and B0-g1.56, respectively, after 7 days of incubation using osteogenic medium. Data are reported as mean ± s.d., n = 6–10 replicates analyzed for each experimental condition

Since RUNX2 is involved in regulating the expression of other early osteogenic markers such as type 1 collagen (COL 1) and alkaline phosphatase (ALP) (Bruderer et al., 2014), we also investigate the expression of these two markers.

Gene expression of COL 1 confirms the trend found for RUNX2 (Figure 36).

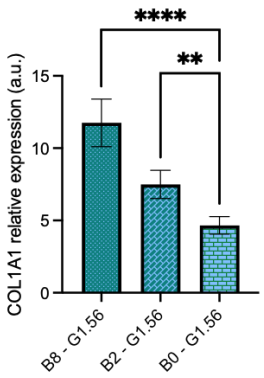

Figure 36. Relative gene expression quantification (arbitrary units, a.u.) of type I collagen (COL1A1) in cells grown on B8-g.156, B2-g1.56 and B0-g1.56, respectively, after 7 days of incubation using in osteogenic medium. Data are reported as mean ± s.d., *n* = 6–10 replicates analyzed for each experimental condition.

For ALP, we quantified the production of the enzyme over a period of fourteen-day (Figure 37). ALP shows a particular behavior during osteogenic differentiation (Huang et al., 2007) so its analysis at different time points helped us to get a clear picture of the process. After 4 days of culture, the cells expressed a very low level of ALP (basal production), regardless of the mechanics of the substrate. As described in the literature, immature osteoprogenitor cells do not yet express this marker (Huang et al., 2007). The second quantification was performed after 7 days and only in the hydrogels with a high concentration of boric acid we found a significant increase in ALP production. The influence of the substrate on differentiation becomes evident on day 14 of incubation with a clear dependence in ALP production on the composition of the hydrogel. While the hydrogels containing only genipin maintain a constant baseline production of ALP over the two weeks (~ 0.06 fluorescence a.u.), the production of ALP increases significantly in the more viscoplastic sample.

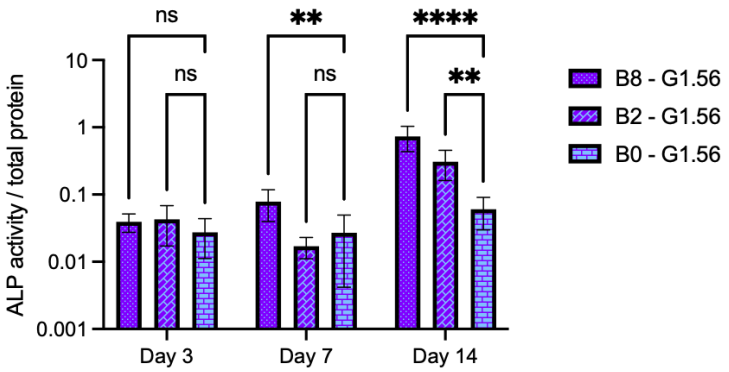

Figure 37. Quantification of alkaline phosphatase (ALP) enzyme activity after 3, 7 and 14 days of incubation in osteogenic medium. Data are reported as mean ± s.d., *n* = 6–12 replicates analyzed for each time point.

These results were confirmed qualitatively by Fast Blue staining and the calculation of ALP positive cells (Figure 38).

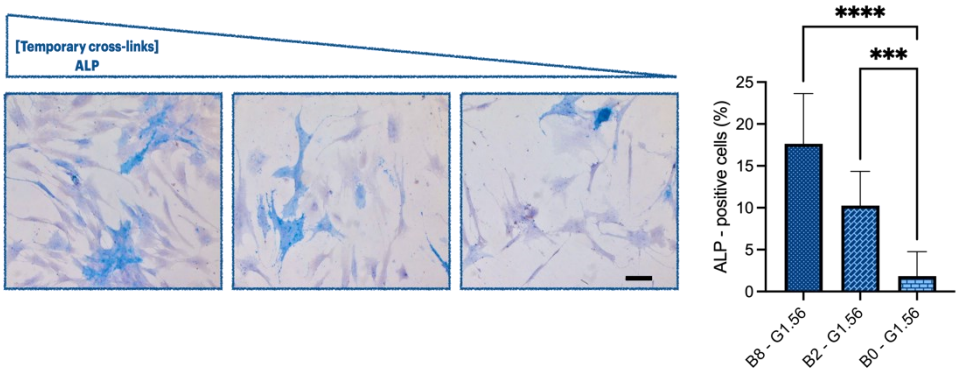

Figure 38. Representative images and quantification of positive cells to ALP detected by Fast blue staining, indicating the osteogenic differentiation of mesenchymal stem cells after 14 days of incubation in osteogenic medium; scale bar is 100 µm. Data are reported as mean ± s.d., *n* = 17–25 images analyzed for each experimental condition.

The final step of our analysis was to evaluate later events of osteogenic differentiation, such as the expression of the marker osteocalcin (OCN), which is regulated by RUNX2, and the production of mineralized matrix (calcium deposits). Again, after seven days of culture, the gene expression of OCN was about three times higher than in the sample with only genipin (Figure 39).

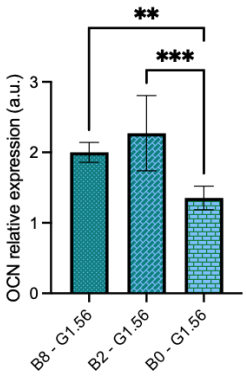

Figure 39. Relative gene expression quantification (arbitrary units, a.u.) of osteocalcin (OCN) after 7 days of incubation in osteogenic medium. Data are reported as mean ± s.d., *n* = 6–8 replicates analyzed for each experimental condition.

Finally, the qualitative analysis of the presence of a mineralized matrix (calcium deposits) also suggests that differentiation is influenced by the mechanics of the substrate as demonstrated by Von

Kossa staining. In particular, the mineralization process increased with the progressive addition of boric acid as a cross-linking agent (Figure 40).

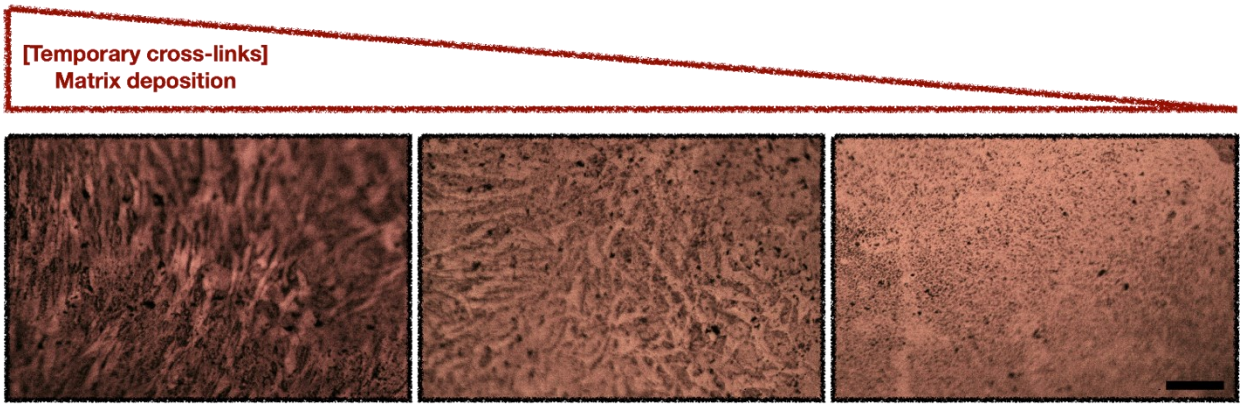

Figure 40. Representative images of calcium deposits detected by Von Kossa staining for hydrogels with different degree of plasticity after 14 days of incubation in osteogenic medium; scale bar is 50 μm.

Furthermore, we exclude that hMSC-AT differentiates into other lineages (adipogenic or chondrogenic). To check the adipogenic differentiation, we used Oil Red staining (Figure 41a), whereas for the chondrogenic phenotype we used qPCR-RT (Figure 41b).

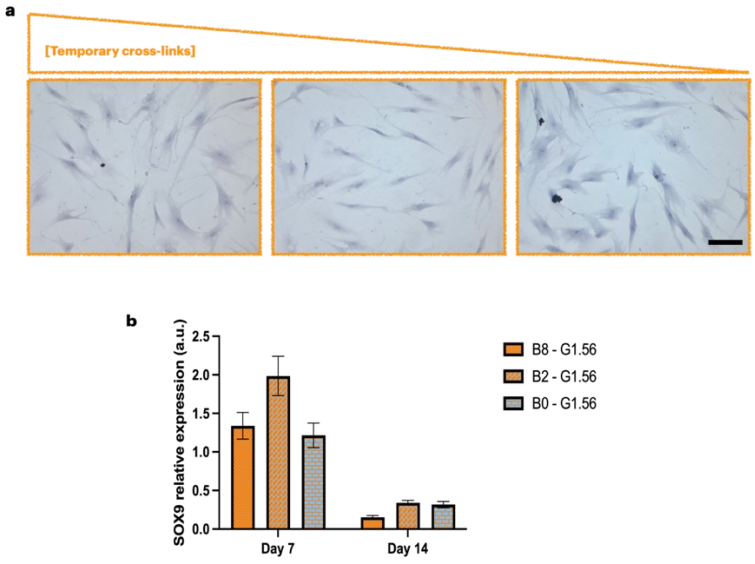

Figure 41. Analysis of the adipogenic and chondrogenic differentiation potential of hMSC-AT on hydrogels with different chemical composition. **(a)** Representative images of hMSC-AT, stained with Oil Red O and counterstained with haematoxylin, showing negligible adipogenic differentiation of mesenchymal stem cells after 14 days in osteogenic medium; scale is 100 μm. **(b)** Quantification of relative gene expression (arbitrary units, a.u.) of SOX9 after 7 and 14 days incubation in osteogenic medium. Data are given as mean s.d., n = 6 - 8 replicates analyzed for each experimental condition.

In summary, these results suggest that despite the fact that these hydrogels only drive cells towards an osteogenic phenotype, hMSC-AT cells are able to perceive some specific mechanical properties that facilitate and accelerate their osteogenic commitment. In particular, hMSC-AT increased their osteogenic commitment depending on the composition of the hydrogel in terms of the concentration of temporary cross-links. The presence of boric acid increases the viscosity at relatively fast relaxation times, suggesting that immediate dissipation of stress is a crucial material property controlling the fate of mesenchymal stem cells.

Viscoplasticity also influences cell spreading (Grolma et al., 2020). Since osteogenic differentiation is regulated by complex processes and also involves changes in the cytoskeleton (Fan et al., 2021), we also wanted to analyze whether the morphology of mesenchymal stem cells could be related to the degree of differentiation. For this series of experiments, the cells were seeded at low confluence on fibronectin-coated hydrogels and the morphology was examined using Nikon Eclipse Ti-E epifluorescence Live-imaging microscope. The area and diameter of the cells were calculated from the acquired images using Fiji-Images software.

Our analysis shows that both the spreading area and the diameter of the minor axis are larger in the samples with only genipin in the first days of culture, *i.e.* in the samples where the osteogenic commitment is lower. It seems that the cells in the early stages of incubation can spread more easily in a purely elastic substrate rather than start to differentiate.

Furthermore, previous *in vitro* studies have shown that MSCs become more elongated and have a lower proliferation rate when differentiating into osteoblasts (Docheva et al., 2008). Accordingly, a morphological analysis was performed to investigate cell spreading and minor axis diameter at two different time points (Figure 42).

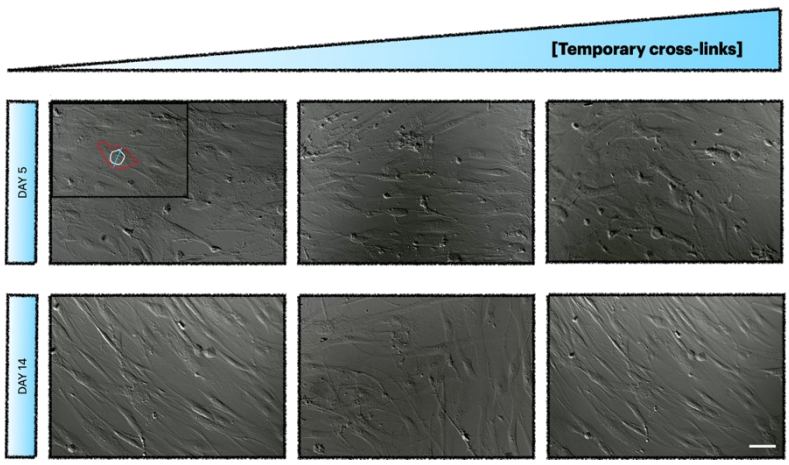

Figure 42. Representative images of mesenchymal stem cells plated atop B0-g1,56, B2 -g1.56and B8-g1.56, respectively, after 5 and 14 days of incubation in osteogenic medium. Zoom-in/inset red, cell area; yellow: nucleus; light blue: cell minor axis. Scale bar are 70 µm.

At day 5, a change in cell morphology was observed. In particular, the cells in the hydrogel with a high boric acid content have a smaller diameter than the cells in the other substrates. This diameter remains unchanged at day 14. However, the diameter of the cells in the hydrogels without temporary cross-links changes significantly. In the latter case, the cell diameter even decreases compared to day 5 (Figure 43).

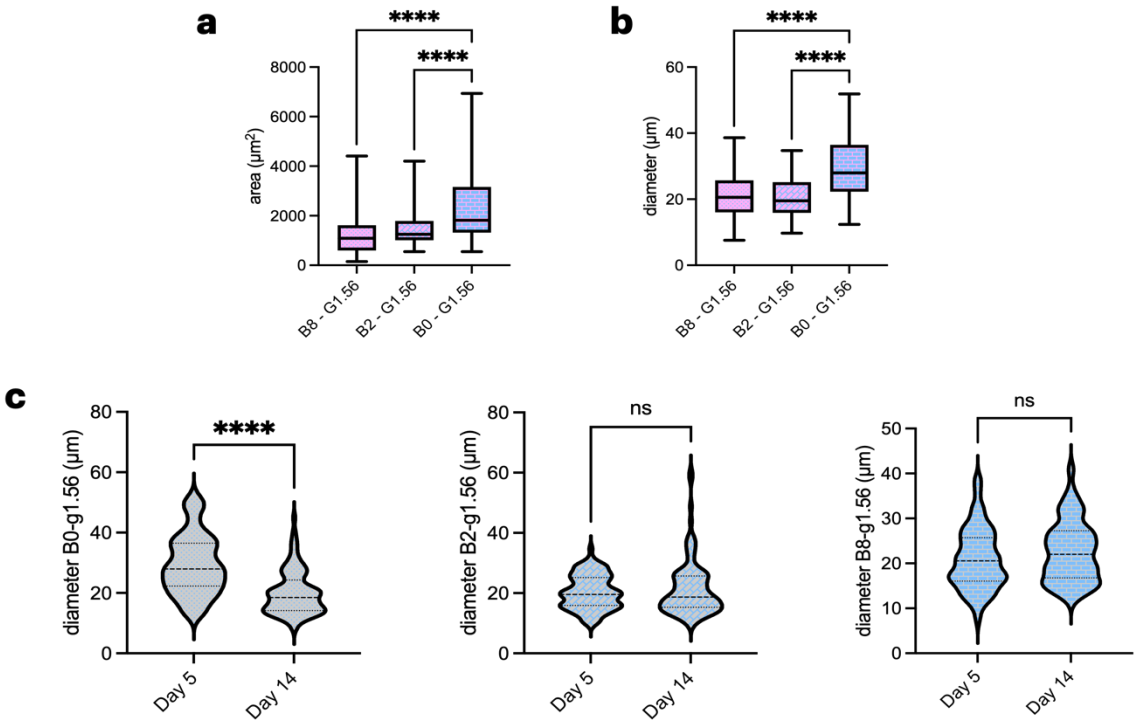

Figure 43. A Cell spreading area and (b) diameter of the minor axis for hydrogels with different composition after 5 days of incubation in osteogenic medium. Data are reported as mean ± s.d., n = 73–94 cells analyzed in (a) and n = 60–77 in (b). c) Time-comparison of minor axis diameter for hydrogels after 5 and 14 days of incubation in osteogenic medium (b0-g1.56 on the left, b2-g.156 in the centre, b8-g1.56 in the right)-. Data are reported as violin plots showing the median of values; n = 73 - 105 images analyzed in (a) and n = 94 - 104 in (b).

These results are consistent with the biological results and reconfirm the enhanced early osteogenic commitment in hydrogels with boric acid. In the other case, i.e. with only genipin as permanent cross-linker, osteogenic commitment seems to be slowed down. In the early days, the cells in the sample with only genipin prefer to spread rather than differentiate. Changes in the organization of the cytoskeleton are important for osteogenesis of stem cells (Stavenschi and Hoey, 2019). Only after two weeks the cells grown on the sample with only genipin are affected by a change in the cytoskeleton. This result suggests that they need more time to reach an osteoblastic phenotype. To confirm this hypothesis, we extend the incubation of the mesenchymal stem cells up to 21 days. As expected, we need to wait 21 days of culture under osteogenic conditions to find a significant

production of osteogenic markers. In particular analysis of ALP by qPCR-RT shows that the gene expression of ALP decreases in cells seeded on hydrogels containing boric acid, which is in line with the typical trend of this marker during osteogenic differentiation (Huang et al., 2007). In contrast, the production of ALP in the sample containing only genipin is constant for the first two weeks and only then starts to increase (Figure 44a). The same information is obtained when analyzing the trend of the early marker RUNX2 over time (Figure 44b) (Erickson and Payne, 2019).

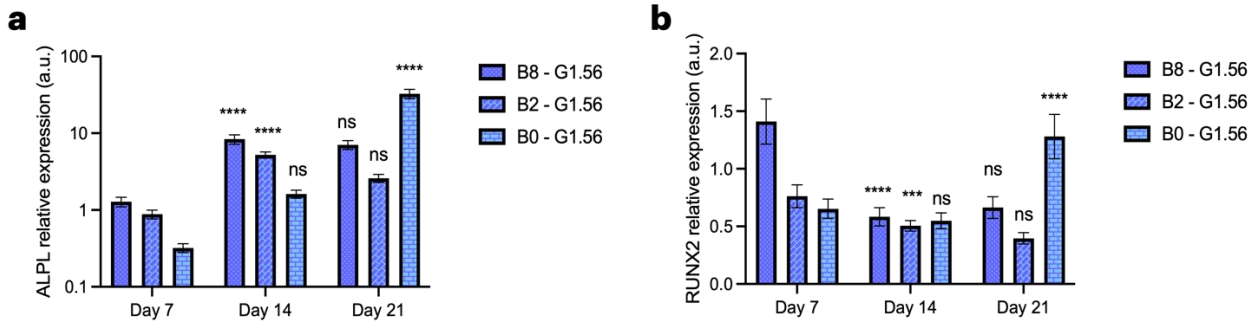

Figure 44. Relative gene expression quantification of a) ALP and (b) RUNX2 in cells grown on B0, B2, and B8 hydrogels, respectively. Data are reported as mean ± s.d., $n = 6$ replicates analyzed for each experimental condition

3.2.4. Main Conclusions

In this section, we have developed tunable viscoplastic hydrogels using a dual cross-link system based on the bioactive polymer CTL and assembled combining temporary (*i.e.*, boric acid) and permanent (*i.e.*, genipin) cross-linkers.

Initially, we found that these types of hydrogels are stable and promote cell growth on their surface for at least 21 days.

Detailed mechanical characterization showed that the rapid unbinding of the transient cross-links caused an immediate stress (energy) dissipation. The introduction of boric acid into the systems changes the purely elastic nature into a dissipative and viscoplastic one. In particular, by modulating the temporary cross-linker concentration, the viscous modulus of these hydrogels can be easily altered irrespective of the elastic modulus. The ability to fine-tune the mechanics of hydrogels provides an interesting scenario to use these materials as 2D substrates to investigate the effects of immediate stress dissipation of the substrate toward hMSC-AT osteogenic commitment. The analyses of MSCs differentiation revealed that, while all substrates guided cells towards an osteogenic phenotype, growth of cells on hydrogels with an immediate stress dissipation, *i.e.* a higher concentration of transient cross-linkers, accelerated this process. This is clearly evidenced by the higher expression of

bone marker and matrix mineralization. In contrast, osteogenic commitment is delayed in purely elastic hydrogels. In this case, the cells prefer to spread out before they start to differentiate.
All these results show that, in addition to stiffness and viscoelasticity, the content of temporary cross-linkers and the resulting immediate stress dissipation of the substrate also have a significant impact on the osteogenic commitment of MSCs. Our data provide an optimal starting point for future investigations in the field of mechanotransduction.

3.3. CHAPTER 3: CTL as matrix for the formation of cell-aggregates

3.3.1. Aim of the work

There is much interest in the use of scaffold-free culture strategies for cartilage regeneration. In this chapter, CTL is used as a bioactive polymer that can coordinate cell-aggregation. The role of CTL in contact with primary chondrocytes and hMSC-AT has been study in detailed. In addition, the ability of a sulfated lactose-modified chitosan to induced aggregation of hMSC-AT was also verified.

3.3.2. Materials and Methods

3.3.2.1. Materials

Hydrochloride form of lactose-modified chitosan, CTL (CAS Registry Number 2173421.37-7) with fractions of: N-acetyl-glucosamine (GlcNAc; "acetylated", A) (FA) = 0.16; glucosamine ($GlcNH_2$; "deacetylated", D) (FD) = 0.21; lactitol-substituted D unit (N-alkylated GlcLac; "lactitol", L) (FL) = 0.63 was kindly provided by Biopolife S.r.L. (Trieste, Italy) (Francesca Scognamiglio et al., 2020) and Sulfated lactose-modified chitosan with different degree of sulfation (Pizzolitto et al., 2022) were employed for chondrocytes and hMSC-AT aggregation. Phosphate-buffered-saline (PBS), Tryton X-100, Hyaluronidase from bovine testes type I-S, collagenase type II, toluidine blue, Alcian Blue, sodium hydroxide (NaOH), formaldehyde, bovine serum albumin (BSA), polyvinyl alcohol (MOWIOL ® 4-88), Normal Goat Serum and TRI Reagent, FITC, Transforming growth factor beta 1 (TGFβ1), dexamethasone, ITS Liquid Media Supplement (100x) were all purchased from Sigma Aldrich (USA). Dulbecco Modified Eagle Medium (DMEM), penicillin/streptomycin, trypsin EDTA 1X, fetal bovine serum (FBS) were all purchased from EuroClone s.p.a. Acetic acid glacial, acetic acid and ethanol were purchased from Carlo Erba. L-ascorbic acid and β-glycerophosphate were from Fluka Biochemika. Collagen II Monoclonal Antibody (2B1.5) (Catalog number #MA5-12789), Collagen I Monoclonal Antibody (COL-1) (Catalog number #MA1-26771), Goat anti-Mouse IgG (H+L) Highly Cross-Adsorbed Secondary Antibody, Alexa Fluor 594 (Catalog number #A-11032), Insulin-Transferrin-Selenium-Sodium pyruvate (ITS) were all from Thermo Fisher Scientific (U.S.A.). Hoechst was from Invitrogen (Bleiswijk, The Netherlands). Killik, O.C.T. was purchased from Bio-Optica (Milan, Italy). Mesenchymal Stem Cell Growth Medium was from PromoCell.
All reagents and chemicals were of high purity grade and deionized (Milli-Q) water was used as solvent in all experiments.

3.3.2.2. Isolation and expansion of pig articular chondrocytes

Primary chondrocytes were isolated from intact joints of adult pigs provided by a local slaughterhouse following a procedure previously described by Grandolfo *et al.*,(Grandolfo et al., 1993) After dislocation of the joints, the cartilage was washed with sterile PBS 1X. Thin slices of the articular cartilage were cut with a sterile scalpel and the cells were isolated by enzymatic digestion of the tissue. The cartilage slices were digested for 1 h in 15 mL of hyaluronidase solution (hyaluronidases 250 U/mL, penicillin 500 U/mL and streptomycin 500 U/mL in PBS 1X) at T = 37 °C in a humidified environment with 5% CO_2. Tissue digestion was completed by overnight incubation with 10 mL collagenase solution (collagenase type II 250 U/mL, penicillin500 U/mL and streptomycin 500 U/mL in PBS 1X) at 37 °C under vigorous shaking. Enzymes and digestion products were removed by running the mixture through a sieve. Finally, cells were washed with PBS 1X and with DMEM. Chondrocytes were seeded in flasks and cultured in DMEM High Glucose supplemented with FBS. Cells were incubated at 37 °C in a humidified environment with 5% CO_2 for at least one day and then used for biological assays.

3.3.2.3. Spheroids formation

To induce spheroid formation, the protocol described by Donati *et al.,* was used (Donati et al., 2005). Specifically, 400 µL of a 2% CTL or 400 µL of a 2% sulfated lactose-modified chitosan was distributed on the bottom of a 24-well plate and dried overnight. The coated wells were sterilized by UV irradiation for 30 minutes. The cells were then seeded at a final density of 6 x 10^4 cells/well and kept in culture for a maximum of 14 days.

For chondro-aggregates, the cell medium was supplemented with FBS 10%, penicillin/streptomycin 1%, ascorbic acid (50 µg/mL) and TGFβ1 (0.05 ng/mL).

For spheroids resulting from the aggregation of hMSC-AT Stem Cell Growth medium was supplemented with 100 µM ascorbic acid, 0.2 µM dexamethasone, 10 ng/mL TGFβ1 and ITS 1x in order to enhance chondrogenic differentiation.

Stem cell growth medium without any additional factors was used to analyze the ability of sulfated lactose-modified chitosan to induce cell aggregation.

As a control for induced spheroid formation in the absence of CTL, 400 µL of a 2% w/v agar solution in PBS 1X was poured onto the bottom of a 24-well plate. After 30 minutes mesenchymal stem cells and chondrocytes were seeded atop hydrogels at the same concentration as described above.

3.3.2.4. Viability assay (MTT and Alamar Blue Assay)

MTT and Alamar Blue assays were performed on chondro-aggregates and MSC-aggregates to assess their viability and proliferation rate during the 14-day culture.

For the MTT assay, spheroids were removed from the wells at the preselected time point, transferred to a vial, washed with PBS 1x and incubated with 300 µL MTT solution (0.5 mg/mL) for 4 hours at 37 °C in the dark. After incubation, the MTT solution was removed and 100 µL of DMSO was added to each vial to dissolve the formazan crystals. The absorbance of each sample was measured at 570 nm using a FLUOStar Omega-BMG Labtech spectrophotometer.

For the Alamar Blue, the spheroids were removed from the wells, transferred to a vial and centrifugated at 69 x *g* for 5 min. The supernatant was removed and the Alamar Blue solution (20% v/v in DMEM) was added. Each sample was incubated at 37 °C and 5% pCO_2 in the dark condition for 4 hours. After centrifugation, 200 µL of each sample was transferred to a black 96-well plate and fluorescence was measured using with a FLUOStarÒ Omega-BMG Labtech spectrophotometer (λ_{ex} = 544 nm; λ_{em} = 590 m; gain 500, gain 700).

3.3.2.5. LDH assay on chondro-aggregates and on hMSC-AT spheroids formed with sulphated-CTL

To assess the suffering of the chondro-aggregates, the release of lactose dehydrogenase (LDH) into the culture medium was measured using the "*In Vitro* Toxicology Assay Kit, Lactic Dehydrogenase bases" (SIGMA) according to the manufacturer's instructions. Briefly, at the same time point chosen for the MTT assay, before to collect aggregates for viability assay, the medium was used for LDH assay. 45 µL of the cell medium and chondro-aggregates lysates were added to the LDH mixture (30 µL LDH assay substrate, 30 µL LDH cofactor, 30 µL die solution) and incubated for 30 minutes in the dark. The enzymatic reaction was stopped by adding 1/10 HCl 1 N to each sample. The plate was read at 490 nm and 690 nm using a spectrophotometer (Tecan ®, Microplate reader). The percentage of LDH release was calculated by normalizing the absorbance of the sample with the absorbance of cellular lysis at each time point considered. Four replicates were considered for each time point.

3.3.2.6. Live/Dead

The viability of the aggregates was also analyzed qualitatively using a Live/Dead Assay Kit (SIGMA). For this analysis, 2 µL of solution A (containing Calcein-AM) and 1 µL of solution B (containing Propidium Iodide) were added to 1 mL of PBS 1X. Then 100 µL of the resulting mixture was added to the sample. Images were taken using Nikon Eclipse Ti-E epifluorescence live imaging

microscope equipped with a motorized stand and a Nikon DS-Qi2 camera and 10x objective, after incubating the samples for 15 minutes in the dark, at 37 °C and in a humidified environment.

3.3.2.7. External morphological analysis

The external morphological analysis of the spheroids was carried out using Scanning Electron Microscopy (SEM, Quanta 250, FEI, Oregon, USA). At a preselected time point, spheroids were washed with PBS 1X and fixed with 2.5% (w/V) glutaraldehyde in PBS 1x at room temperature for 1 hour. The fixative was removed by washing the spheroids with PBS 1x. The spheroids were dehydrated by successive immersions in ethanol (30 – 70 – 100%) and finally dried using a critical point dryer (HMDS). Each step was performed twice (20 minutes each), and between each step, samples were centrifugated at 69 x *g* for 5 minutes to collect nodules. Prior to SEM analysis, the dehydrated samples were gold-sputtered (Sputter Coater K550X, Emitech, Quorum Technologies Ltd, UK).

3.3.2.8. TEM and toluidine blue staining

The pellets of aggregates were fixed in 2.5% glutaraldehyde EM grade in 0,1M phosphate buffer, pH 7.3 and post-fixed in 1% osmium tetroxide. The samples were dehydrated through a graded series of ethanol and finally in propylene oxide and then embedded in epoxy resin (Durcupan ACM – Sigma). The ultrathin sections (60-80 nm) were placed on copper grids, stained with UranyLess EM Stain, lead citrate, and viewed with a transmission electron microscope (Philips EM 208 at 100 kV). Images were taken using a Quemesa bottom-mounted TEM CCD Camera (Olympus, Germany) provided with a TEM imaging platform (Radius software). All the other reagents were from Electron Microscopy Sciences, Hatfield, PA. The resin-embedded samples were also cut with an ultramicrotome to obtain semi-fine sections of 1 µm and then hot-stained with toluidine blue.

3.3.2.9. Preparation of sample for internal characterization

For internal histological analysis cells were pre-embedded into agarose 1.5% w/v. Gels were then fixed with 4% formaldehyde for 30 minutes, washed with PBS and incubated overnight in 30% sucrose at 4°C. Then gels were placed in a mix of 50% of a 30% sucrose and 50% OCT for 5 hours. Finally, gels were embedded in OCT and froze. The frozen gels were sectioned with a cryotome (LEICA CM3050 S.) to a thickness of 50 µm and stained following standard histological and immunohistochemical protocols.

3.3.2.10. Synthesis of FITC-labelled CTL and analysis of CTL distribution

Spheroids were prepared with 10% w/w fluorescein isothiocyanate (FITC)-labelled CTL to analyze polymer distribution both outside and inside the structure.

Fluorescein isothiocyanate (FITC)-labelled CTL was prepared following the protocol described by Sacco et al., (Pasquale Sacco et al., 2018a). Briefly, CTL (500 mg) was dissolved in 167 mL of deionized water under stirring overnight and 1,1 mL of FITC solution (0.5 mg/mL in sodium bicarbonate buffer, 50 mM) was added under stirring. The reaction mixture was stirred protected from light for 24 hours at room temperature. After that, the CTL-FITC solution was dialyzed (Spectrapore, MWCO 12'000) against: $NaHCO_3$ 50 mM, NaCl 100 mM and later dialyzed against deionized water until the conductance was below 3 µS/cm at 4 °C. Finally, the pH of the solution was adjusted to 4.5 and freeze-dried using ALPHA 1-2 LD plus freeze-dryer (CHRIST, Osterode am Harz, Germany).

For external analysis the spheroids were collected at selected time points and fixed with formaldehyde 4% v/v in PBS for 10 minutes at room temperature. They were then washed 3 times with PBS 1X and permeabilized with Triton 0.2% V/V in PBS 1X for 15 minutes at room temperature. Subsequently, they were washed with PBS and incubated with BSA 4% w/V + NGS 5% V/V in PBS (blocking solution) for 1 hour at T = 37 °C. The blocking solution was then removed and the samples washed with PBS 1X. To visualize the nuclei, the cells were counterstained with Hoechst 1:1000 in PBS. Images were acquired with a Nikon Eclipse Ti-E epifluorescence Live-imaging microscope using a 10x as objective.

The same protocol was used for internal characterization of the spheroids. In this case, the spheroids were prepared according to the protocol described in the section 3.3.2.9

3.3.2.11. Analysis of internalization of CTL by chondrocytes.

To assess the internalization of CTL into cells, chondrocytes were cultured in three different modalities. In the first, chondrocytes were cultured in a 2D system. Cells were seeded at the final density of 6 x 10^4 cells/well on 24-well plate and treated only with DMEM medium supplemented with ascorbic acid (50 µg/mL) and TGF β1 (0.05 ng/mL). In the second case the formation of spheroids was carried out by employing agar-coated wells, instead of CTL-coated ones. For the agar coating a solution of 2% w/V agar was prepared in PBS 1X, autoclaved; 400 µL of autoclaved agar solution were poured into a 24-well plate. After 30 minutes 6 x 10^4 cells/well were seeded in DMEM medium supplemented with ascorbic acid (50 µg/mL) and TGFβ1 (0.05 ng/mL). The non-adhesiveness of the agar prevented cell adhesion to the bottom of the well and allowed aggregates to form. In the last case, 2D-chondrocytes were treated with DMEM supplemented not only with ascorbic acid (50 µg/mL) and TGFβ1 (0.05 ng/mL), but also with CTL. For this purpose, a solution

of CTL (2% w/V), was added to DMEM to obtain a final concentration of CTL 0.5% w/V. For all the conditions, chondrocytes were cultured for 3 days, collected and processed for TEM analysis as described in section 3.3.2.8.

3.3.2.12. Spheroids adhesion and cell-migration

In order to analyze the ability of spheroids to adhere to a surface and subsequently to evaluate the ability of chondrocytes to migrate from the structure and to spread, spheroids were formed and cultured for different periods of time. At different time points, the nodules were moved in a 24-well without changing the culture media. The spheroids were allowed to adhere for up to 14 days and after 7 days the medium was change. The process of adhesion of the same spheroid was followed over time using a Nikon Eclipse Ti-E epifluorescence Live-imaging microscope.

3.3.2.13. Analysis of matrix production (histological, immunological and qPCR)

For internal immunohistochemical analysis, the chondro-aggregates were pre-embedded in agarose 1.5% w/V. The resulting gels were then fixed with 4% formaldehyde for 30 minutes, washed with PBS and incubated overnight in 30% sucrose at 4 °C. Then the gels were incubated in a mixture containing 50% sucrose 30% and 50% OCT for 5 hours. Finally, gels were embedded in OCT and incubated at -20 °C to freeze the sample (Chaudhuri et al., 2016). The frozen gels were sectioned with a cryotome (LEICA CM3050 S.) to obtain slices of a thickness of 50 µm. The presence of Type II and Type I collagen was determined using a standard immunohistochemistry procedure. Sections were washed with PBS 1X, permeabilized with 0.2% V/V Triton X-100 for 10 min at room temperature and then blocked with blocking buffer containing 4% w/V bovine serum albumin (BSA), 5% V/V Neutral Goat Serum (NGS) in PBS for 2 hours at room temperature. The solution was then removed, and the cut samples were washed with PBS. The following primary antibodies were used for immunostaining: Collagen II Monoclonal Antibody (1:100), Collagen I Monoclonal Antibody (1:1000). The primary antibodies were diluted in blocking buffer and incubated overnight at 4 °C. Samples were then washed with PBS and incubated with the secondary antibody, Alexa Fluor 594 (1:500). The chondrocytes nuclei were counterstained with Hoechst (1:1000). Images were taken using Nikon Eclipse Ti-E epifluorescence Live-imaging microscope.

h-MSC-Spheroids samples, at the established experimental times, were collected, washed with PBS 1X and fixed with paraformaldehyde 4% w/V in PBS 1X for 20 minutes at RT. The fixative was removed and a washing step was performed twice in PBS 1X. The spheroids were then included in an agarose gel. The agarose gel containing the spheroid was then employed for the histological analyses. Subsequently, samples were dehydrated through ascending alcohols series, and then

paraffin embedded. Next, samples were dewaxed (alcohols at progressively decreasing concentrations) and cut, by means of a rotary microtome, in sections 4 μm thick; sections were further processed for hematoxylin-eosin and Masson's Trichrome staining. After that, randomly selected sections for each experimental point were observed and acquired by of Leica DM 4000 light microscopy (Leica Cambridge Ltd., Cambridge, UK) equipped with a Leica DFC 320 camera (Leica Cambridge Ltd., Cambridge, UK). Leica Application Suite X (LASX) (Leica Cambridge Ltd., Cambridge, UK) image analysis software was employed for the image acquisition.

On h-MSC-Spheroids also Real Time PCR analysis was performed. At preselected time point total RNA was purified from cells by using Trifast reagent (Euroclone, Milan, Italy), according to manufacturer's protocol. The synthesis of RNA and the qRT-PCR was carried out following the protocol described in section 3.2.2.8. The sequences of the primers used for assess chondrogenic differentiation are listed in following table:

Gene	Size	Forward (F) / Reverse (R)	Sequence 5' – 3'
GAPDH		F	TCAAGGCTGAGAACGGGAAG
		R	CGCCCCACTTGATTTTGGAG
COL2A1		F	CCTGGCAAAGATGGTGAGACAG
		R	CCTGGTTTTCCACCTTCACCTG
COL10A1		F	CAAGGCACCATCTCCAGGAA
		R	AAAGGGTATTTGTGGCAGCATATT
COL1A1		F	CCCTGGAAAGAATGGAGATGAT
		R	ACTGAAACCTCTGTGTCCCTTCA

Table 4. Sequence of real-Time PCR primers.

3.3.3. Results and discussion

3.3.3.1. CTL as a temporary ECM for the formation of chondro-aggregates

Previous studies have reported that CTL induces aggregation of primary chondrocytes with the formation of large nodules in 12-24 hours (Donati et al., 2005). Based on these results, in this first part we focused on the influence of the polymer CTL on the formation of chondro-aggregates and analyzed in detail structure, morphology and formation process, in order to develop a scaffold-free cell system that could promote cartilage regeneration.

For the analysis of the morphology of the chondro-aggregates from day 1 to day 14, optical microscopy and SEM images were used (Figure 45). Both techniques showed that, the size of the aggregates increases with time. Twenty-four hours after seeding, the aggregates are composed of few cells with clearly defined edges and are very small (100 μm). After 14 days, however, the aggregate size is greater and close to 1 mm in most cases. However, as the size increases, the aggregates in the well gradually decrease in number. Moreover, after the third day, the aggregates no longer have well-defined bounders. In addition, the individual cells are no longer distinguishable, but appear to be embedded in a fibrous/granular matrix. Already from this initial morphological analysis, we can see that the process of aggregate formation in the presence of CTL differs from that reported in the literature. In fact, most of chondro-spheroids reach a size of 900-1000 μm in the first days of aggregation and the structure remains uniformly spherical and compact (Armoiry et al., 2019; Du et al., 2014; Kulish et al., 2008) and this behavior is also described in the literature for spheroids formed from other primary cells and mesenchymal stem cells (MSC) (Cesarz and Tamama, 2016; Zubillaga et al., 2020). Due to this characteristic, we referred to this structure with the term of aggregates.

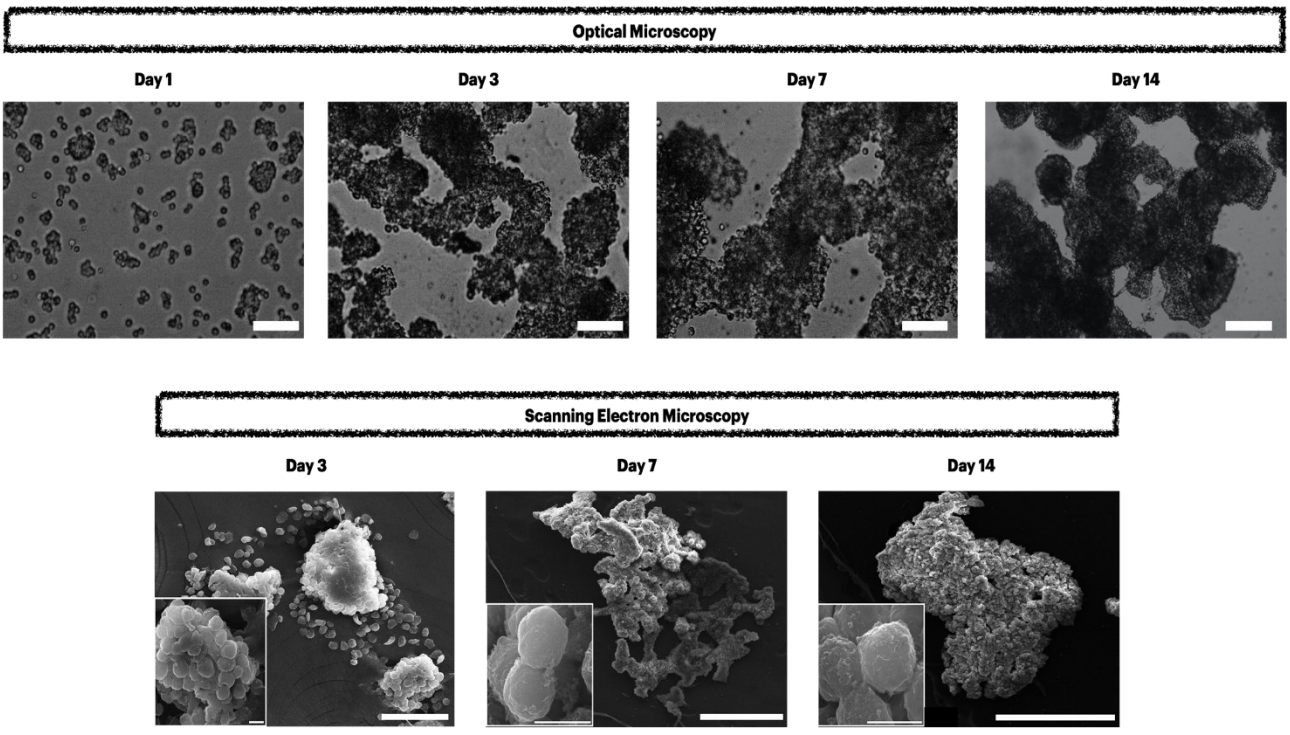

Figura 45. (a) Bright-field images of representative chondro-aggregates at different time points. From day 1 to day 7: scale bar 50 μm. Day 14: scale bar 100 μm. (b) SEM images of the chondro-aggregates. Day 3: scale bar 100 μm. Days 7 and 14: scale bars 500 μm. The inset highlights that chondrocytes are embedded in a filamentous matrix that increases over time. For the inset, the scale bar is 10 μm.

The following step aimed at determining, by means biochemical assays, if the increase in size in aggregates was due to a process of cell aggregation or proliferation. The viability of the chondrocytes

was investigated using MTT assay. The chondrocytes in the aggregates do not show proliferative rate (Figure 46), as already been reported by Marcon (Marcon et al., 2005). However, a slight reduction in cell proliferation is observed at day 11, followed by a slight increase in proliferation again on the 14th day. This process is probably caused by the suffering of the cells in the core of the aggregates at day 11, followed by a recovery of the MTT signal due to the mild replication activity of the chondrocytes located in the periphery of the aggregates. This behavior was also highlighted in the literature for spheroids formed by mesenchymal stem cells. As the diameter of the spheroid increases, the cells that form the inner core of these aggregates are in hypoxic and nutrient-poor conditions that impair the cells' ability to replicate (Cesarz and Tamama, 2016).

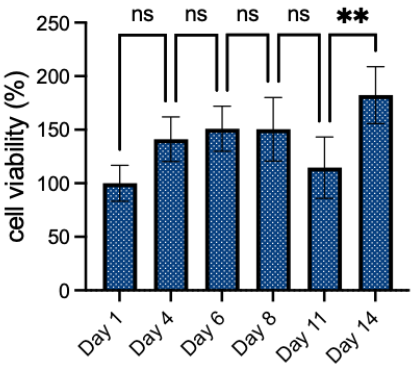

Figure 46. MTT assay. The percentage of cell viability at day 1 was set at 100%, and the relative viability was calculated for the other selected time points. Results ($N = 4$) are given as mean ± standard error.

The good vitality of the chondrocytes in a spheroid environment has also been confirmed by Live/Dead (Figure 47). The images show that most of the cells on the surface are green (*live cells*). As expected, the few dead cells (*red cells*) are inside the structure where the exchange of nutrient is hampered.

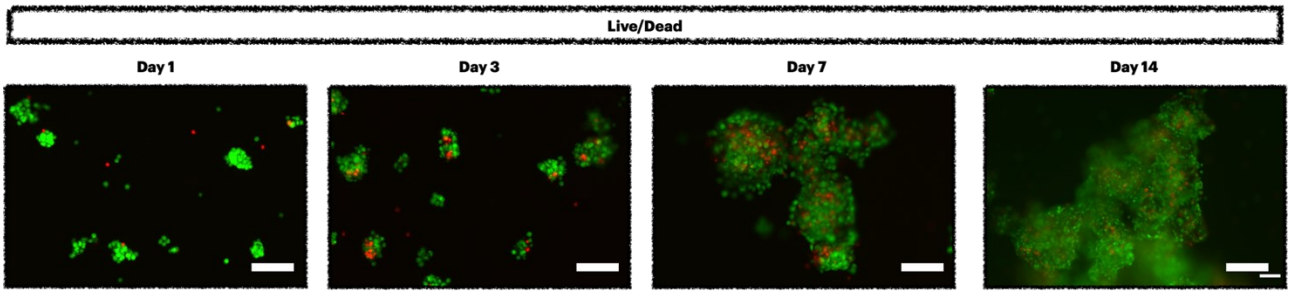

Figure 47. Live/dead cell imaging of chondro-aggregates at different time points. Chondrocytes were stained with two different fluorescent probes to demonstrate cell viability. Dead cells appear red, and living cells appear green.

In addition, the release of lactate dehydrogenase (LDH), an enzyme released by cells whose membranes are damaged due to necrosis or apoptosis, was constant during the 14-day culture (Figure 48), confirming that CTL based chondro-aggregates are a suitable system for the growth of chondrocytes.

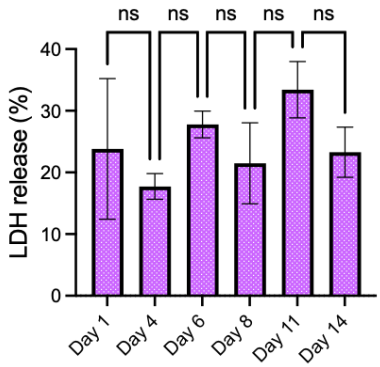

Figure 48. LDH assay on chondro-aggregates at different time points. The percentage of LDH release was calculated by normalizing the absorbance values of the samples to the absorbance of cellular lysis. For each series 4 replicates were tested, and results are reported as mean ± standard error.

Toluidine blue staining was used to obtain information on the arrangement of the chondrocytes in the interna structure (Figure 49). After three days small chondro-aggregates are present, the chondrocytes are organized in a homogeneous manner in the structure and the cells do not interact directly with each other. Additionally, Toluidine Blue Staining shows the presence of small but multiple positive tined granular structures in the cytoplasm of the cells (pink arrows in Figure 49). Over time, the size of the aggregates surprisingly increases and the arrangement of the chondrocytes within the structure begins to change, with a progressive process of nodule cavitation is observed. After 14 days a cellular crown can be seen surrounding a central area that is poor in chondrocytes but rich in an amorphous matrix.

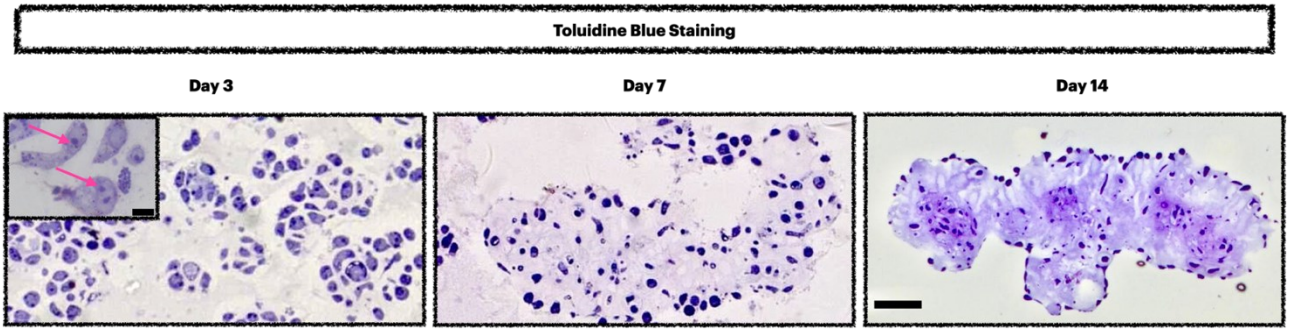

Figure 49. Optical images of the internal structure of chondro- aggregates stained with Toluidine Blue after 3 days (a), 7 days (b), and 14 days (c) of culture. Scale bar 100 μm.

It is important to note that the chondrocytes are not arranged in a compact structure, as can be seen in chondro-aggregates formed in the absence of CTL (Figure 50) and as reported in the literature (Lin et al., 2006).

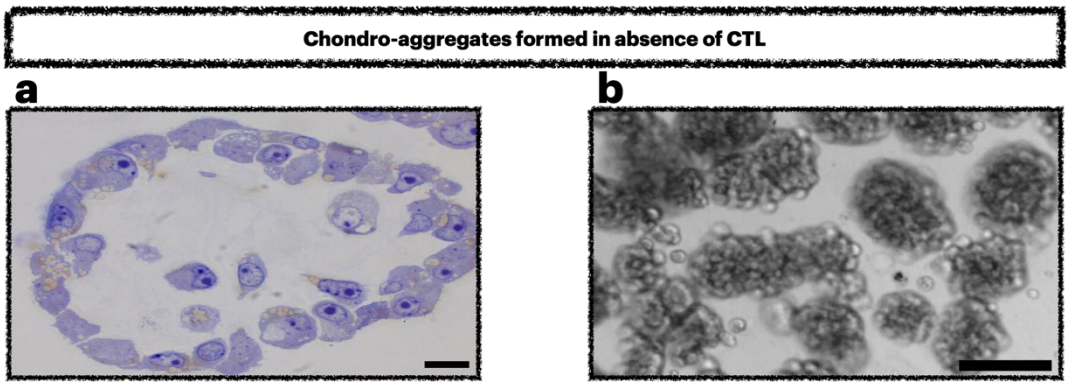

Figure 50. Representative images of chondrocytes cultured in spheroids (3D) in the absence of CTL (a) Toluidine blue staining on sectioned spheroids (scale bar 10 μm) (b) Optical microscopy (scale bar 100 μm)..

Additional information was obtained by using transmission electron microscopy (TEM) (Figure 51). Three days after spheroid formation, the intracellular morphology is characterized by a well-defined nucleus, many mitochondria, and an abundant rough endoplasmic reticulum (black arrows), which is clearly visible in the cytoplasm (Figure 51a). However, the most striking feature of the ultrastructural analysis is the presence of multiple electrodense vesicles not only at day 3 but also on day 7 (light blue arrows in Figure 51a-c). A more detailed analysis shows that these electrodense vesicles contain some intensely osmiophilic materials (Figure 51.b). Moreover, the vesicles are surrounded by several granules of glycogen (white asterisk in Figure 51.b). By the 7^{th} day, the presence of a newly synthetized filamentous extracellular matrix is clearly visible (Figure 51.c). An enlargement of these structures shows the classical banding structure typical of mature collagen fibers (Figure 51.d). Finally, the last time point analyzed (day 14) (Figure 51.e) shows that the presence of electrodense vesicles diminishes compared to the previous days and part of the endoplasmic reticulum is vacuolated, which indicate a degree of suffering.

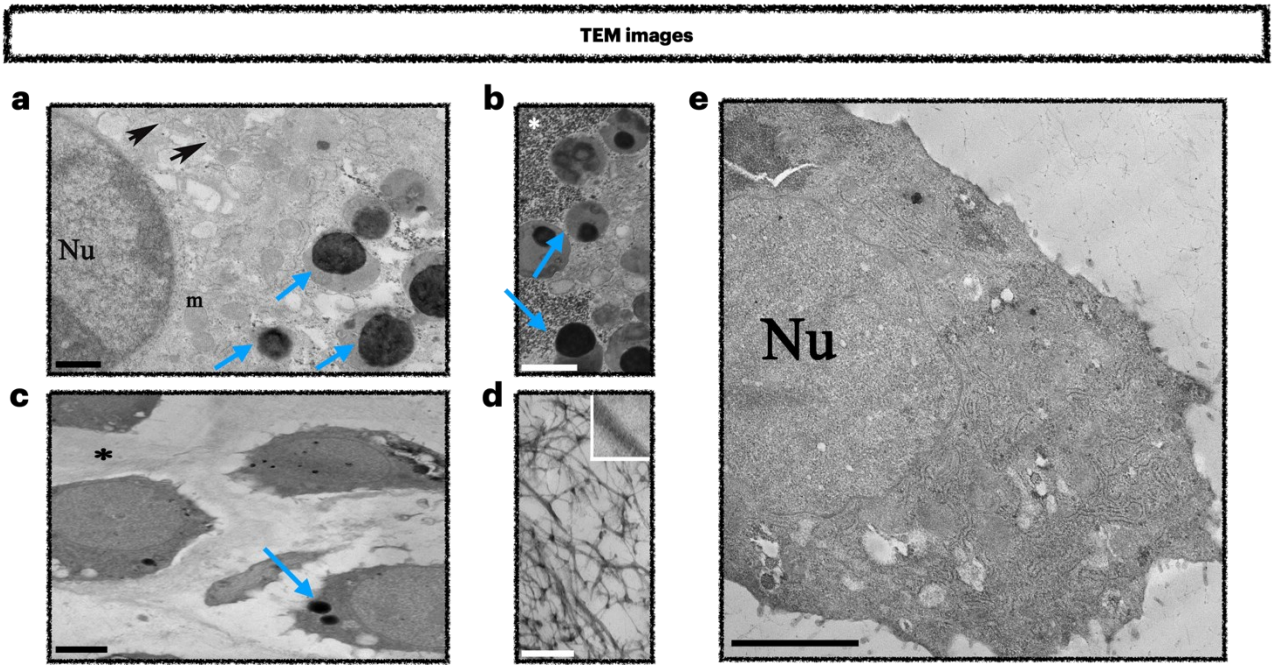

Figure 51. Transmission electron microscopic images at different time points. (a) Chondro-aggregates after 3 days of culture and (b) magnification of their cytoplasmic electrodense vesicles. (c) Chondro-aggregates after 7 days of culture and (h) magnification of their extracellular matrix fibers. (d) Chondro-aggregates after 14 days of culture. Nu, nucleus; m, mitochondria; black arrows, rough endoplasmic reticulum; white asterisk, glycogen granules; black asterisk, extracellular matrix; light blue arrows, electrodense vesicles containing the inclusion material that has a high affinity for osmium.

Donati et al., previously reported that the polymer was present in the structure (Donati et al., 2005). However, no indication on the presence of the CTL inside the structure or its hypothetical internalization by the chondrocytes is available at the present. By using a CTL labeled with FITC to form chondro-aggregates, we were able to confirm the presence of CTL in the structure, both externally and internally, during the entire period analyzed (Figure 52). After 3 days, we can see how the polymer is distributed uniformly among the cells. Surprisingly, this disposition was not maintained over the next few days. If we analyze the outside of spheroid from the on the 7th and 14th day, it is possible to notice that the fluorescence of the polymer is masked by the signal arising from the nuclei of chondrocytes. This finding is in line with the analysis of the inner part of the spheroid. After day 7 in culture, in correspondence with the formation of the central cavity, the CTL is mostly located inside the spheroids. Based on these findings, we conclude that the CTL acts as a structuring agent for the formation of the spheroid in the first days. Over time, the cells start to reorganize and segregating the polymer in the inner part of the structure.

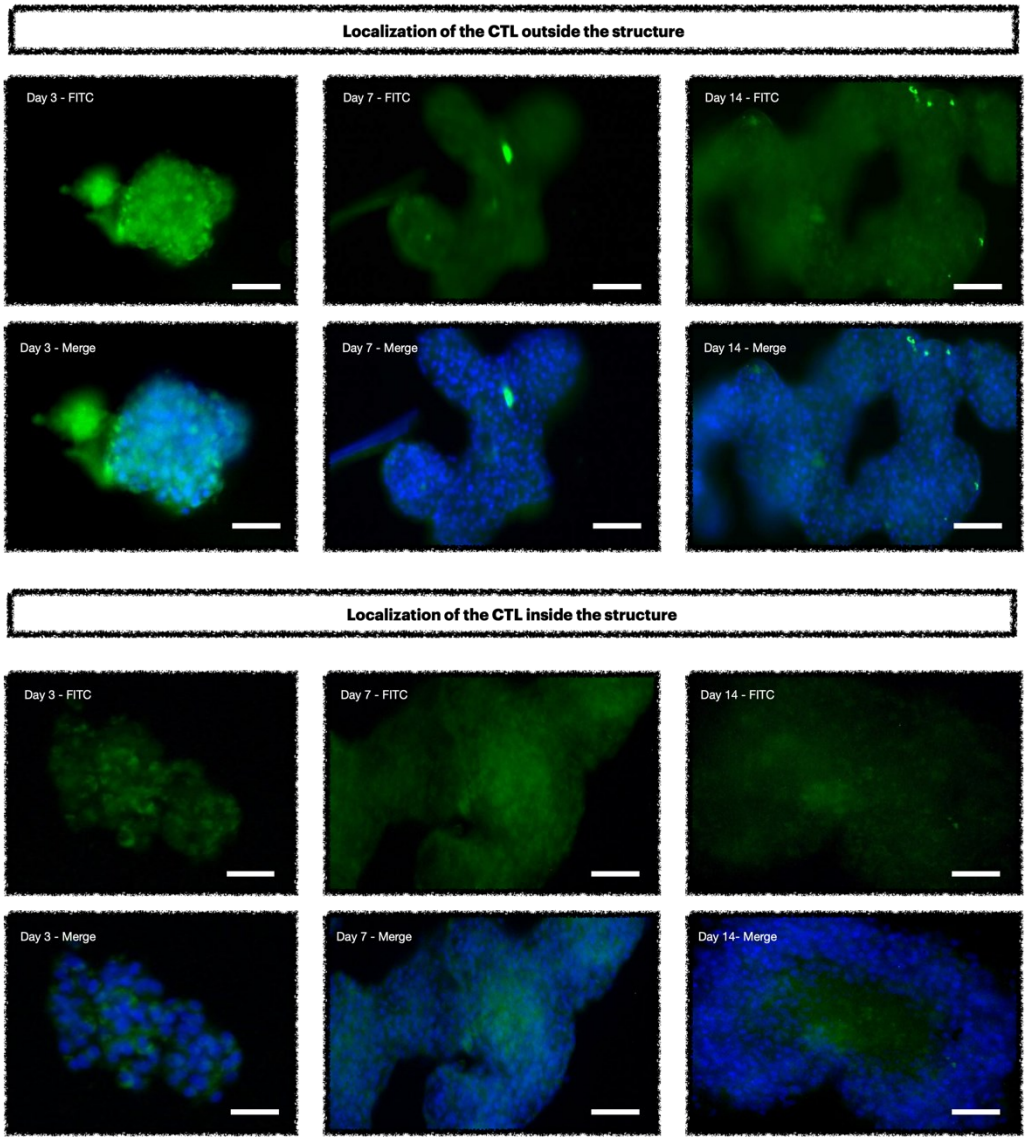

Figure 52. Localization of CTL in chondro-aggregates. Surface localization of CTL and internal localization of CTL at different time points. FITC-labeled CTL was used for polymer localization (green fluorescence); nuclei are stained with Hoechst (blue fluorescence). Scale bars 50 μm

The outer crown of the chondrocytes is held together by a newly formed matrix rich in type II collagen. Analysis of the chondro-aggregates sections showed that matrix production increases over the 14 days, especially on the outside of the structure (Figure 53).

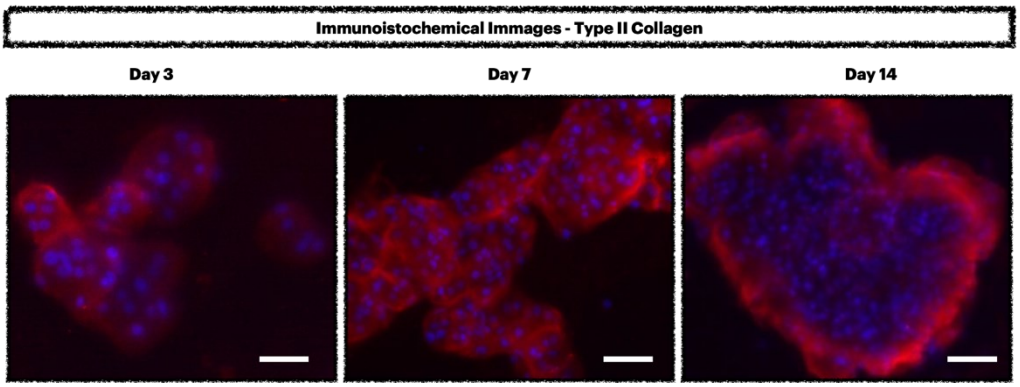

Figure 53. Immunohistochemical images of type II collagen deposition at different time points. Nuclei were stained with Hoechst (blue) (scale bar 50 μm).

It is also important to note that we found no evidence of the production of type I collagen, the most important marker of fribrocartilage tissue (Jiang et al., 2020), over the entire period studied (Figure 54).

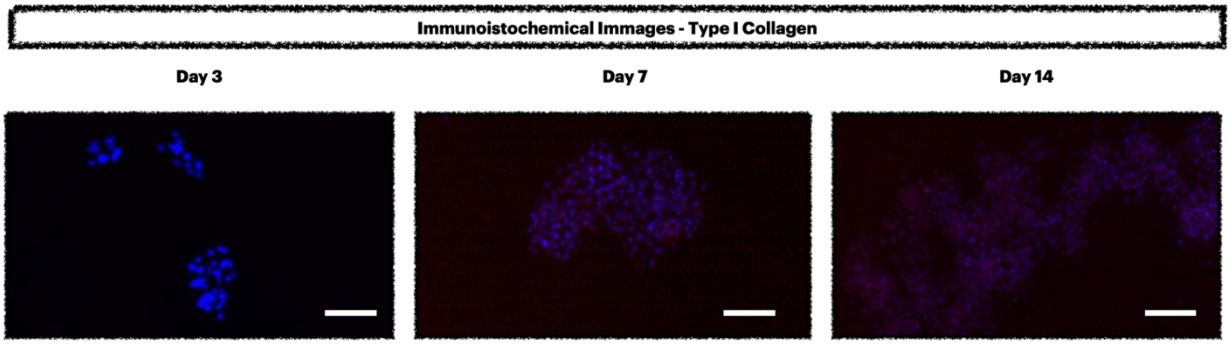

Figure 54. Immunohistochemical images of type I collagen deposition at different time points. Nuclei were stained with Hoechst (blue) (scale bar 50 μm).

A possible more specific interaction between the polymer and the chondrocytes was then investigated. As described before, electrodense vesicles and a toluidine blue-positive structure were observed in the first days of culture by TEM and optical analysis, respectively. Since CTL has a strong affinity for osmium (Brun et al., 2011), we speculated that these are vesicular structures containing CTL internalized through the cell membrane. To test this hypothesis, chondrocytes grown in different conditions were analyzed by electron microscopy and optical microscopy.

Chondrocytes grown by adhesion (2D) without the polymer were used as controls. As expected, no vesicles with electrodense material were detected (Figure 55).

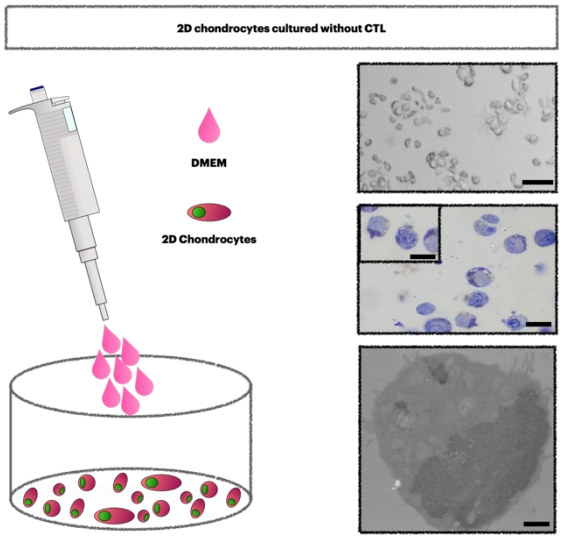

Figure 55. On the right: Schematic representation of the sample preparation for microscopy analysis. Chondrocytes were cultured in 2D conditions without CTL. On the left from the top to the bottom: light microscope images (scale bar 100 µm), toluidine blue staining (scale bar 10 µm) and TEM images (scale bar 1 µm)

Chondrocytes grown in a spheroidal system, but without CTL, were selected as a second control. In this case, a layer of agar was used to prevent cell adhesion. After three days, spheroids are formed, and TEM images show no electrodense vesicles (Figure 56).

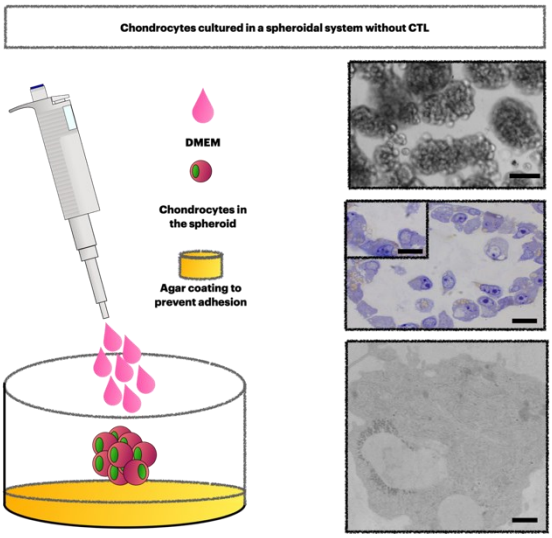

Figure 56. On the right: Schematic representation of the sample preparation for microscopy analysis. Chondrocytes were on agar coating without CTL to prevent adhesion and form spheroid. On the left from the top to the bottom: light microscope images (scale bar 100 µm), toluidine blue staining (scale bar 10 µm) and TEM images (scale bar 1 µm)

Finally, the chondrocytes were seeded in a 2D culture system and treated with a solution of 0.5% w/v CTL. This is the same CTL concentration that occurs if the whole polymer coating dissolves during

spheroid formation. In this case, electrodense vesicles similar to those in the spheroid samples formed with CTL are observed (pink arrows in Figure 57).

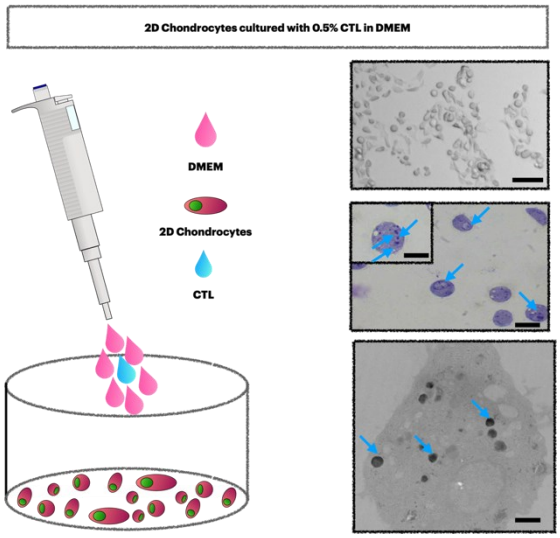

Figure 57. On the right: Schematic representation of the sample preparation for microscopy analysis. Chondrocytes were cultured in adhesion (2D) with 0.5% w/v of CTL dissolved in culture medium. On the left from the top to the bottom: light microscope images (scale bar 100 µm), toluidine blue staining (scale bar 10 µm) and TEM images (scale bar 1 µm)

These findings enable us to state that these electrodense vesicles are not present in chondrocytes cultured in a 2D or 3D system but occur only when the chondrocytes come in contact with CTL. The latter CTL not only serves as a temporary matrix to form the spheroid structure but is also internalized by the cells. The process of internalization only occurs during the first few days of culture and the polymer is subsequently metabolized by the chondrocytes themselves. As shown in Figure 51, the electrodense vesicles containing the polymer actually decreased after two weeks. The process of intracellular degradation of CTL is not yet known, but by analogy with what has been reported for chitosan (Du et al., 2014; Islam et al., 2019; Kulish et al., 2008), acid hydrolysis, oxidation and the action of non-specific enzymes such as lysozyme (Scognamiglio et al., 2020) and glycosidases are probably involved. In the future, it would be very interesting to study in detail the mechanism of internalization of polymers by chondrocytes and to assess a possible role of glycosidases. Indeed, some studies have discussed the role of hexosaminidase as the predominant glycosidases in the degradation of GAGs in cartilage degeneration processes (Pásztói et al., 2009; Shikhman et al., 2000). Research into inhibitors of this enzyme may be a good strategy to prevent and treat cartilage degeneration (Liu et al., 2001).

The final analysis performed on this system was to assess the ability of chondrocytes to migrate out from the chondro-aggregates structure and adhere to the cell culture wells. To this end a cell migration assay was performed. This test simulated the ability of the cells composing the chondro-aggregates to colonize the cartilage defect and potentially allow tissue regeneration (Anderer and Libera, 2002). Chondro-aggregates were formed as already described and after 1, 3, 7 and 10 days their formation were moved on a non-coated well plate (Figure 58). The optical images show that the presence of the polymer had no effect on the ability of the chondro-aggregates to adhere and on the ability of the chondrocytes to migrate. However, the test showed different behaviors depending on the timing of transfer to the uncoated well after formation. In particular, if the chondro-aggregates are moved after one or three days of culture, they can easily adhere to the surface, regardless of the size of the aggregate. The situation is different for chondro-aggregates that have been moved after 7 or 10 days. In these latter cases the chondro-aggregates have a much larger structure and the process of adhesion to a permissive surface is impaired, with only a few aggregates are able to adhere. As we have seen previously chondro-aggregates have a tendency to aggregate with each other. Aggregation involves the formation of numerous cell-cell, cell-matrix and cell-polymer interactions. The chondrocytes then become bound into a compact structure and the cell release from this structure is compromised.

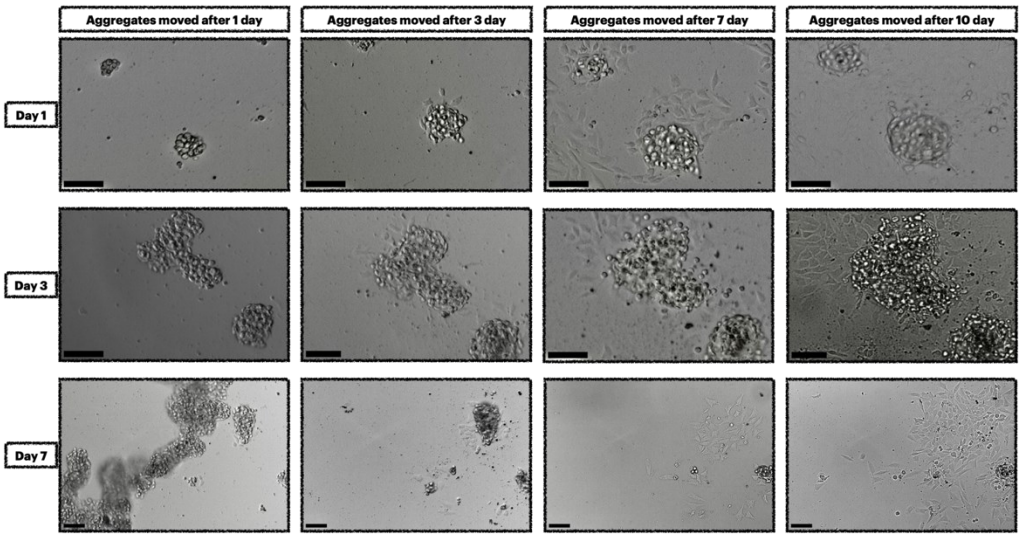

Figure 58. Spreading assay on the adherent surface. Representative bright-field images of chondro-aggregates seeded on adherent substrates followed by cell spreading over 10 days of culture. Chondro-aggregates were transferred 1 (a), 3 (b), and 7 (c) days after assembly on well plates coated with CTL (scale bars 100 μm).

3.3.3.2. Influence of the CTL on the aggregation and chondrogenic differentiation of hMSC-AT spheroids.

The bioactive properties of CTL towards chondrocytes are discussed in detailed in the literature and in the introduction of this Thesis (Donati et al., 2005; Marsich et al., 2008; Salamanna et al., 2019). Following these findings, the next step was to investigate the influence of the polymer CTL on the aggregation and chondrogenic differentiation of hMSC-AT. The protocol used to formed CTL-based aggregates is the same as the one used for the formation of chondro-aggregates. The aggregates formed in the presence of CTL are compared with spheroids formed on non-adhesive agar-coated wells to simulate the spheroids described in the literature, where cellular interactions predominate (Białkowska et al., 2020). For both culture conditions, mesenchymal stem cells from adipose tissue (hMSC-AT) were treated with a chondrogenic medium.

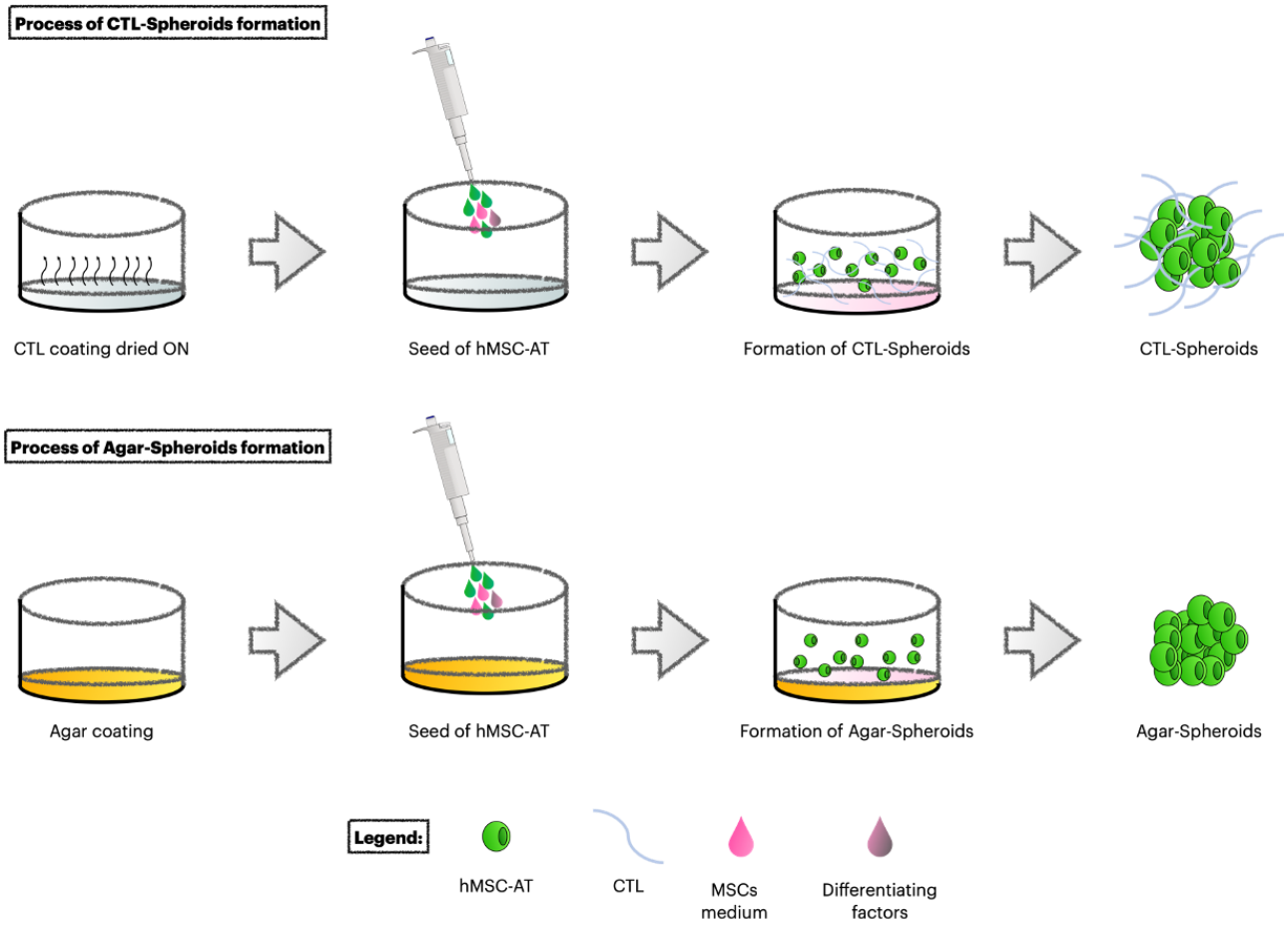

Figure 59. Process of CTL and Agar-Spheroids formation.

The first step was to analyze the morphology using optical microscope images. From the beginning, we can observe a morphology that is different from that of the chondro-aggregates. Indeed, using mesenchymal stem cells, we obtained aggregates with clear boundaries and a spherical shape at all

the time point analyzed (Figure 60). In reference to this feature, the term spheroid will be used for these structures from now on.

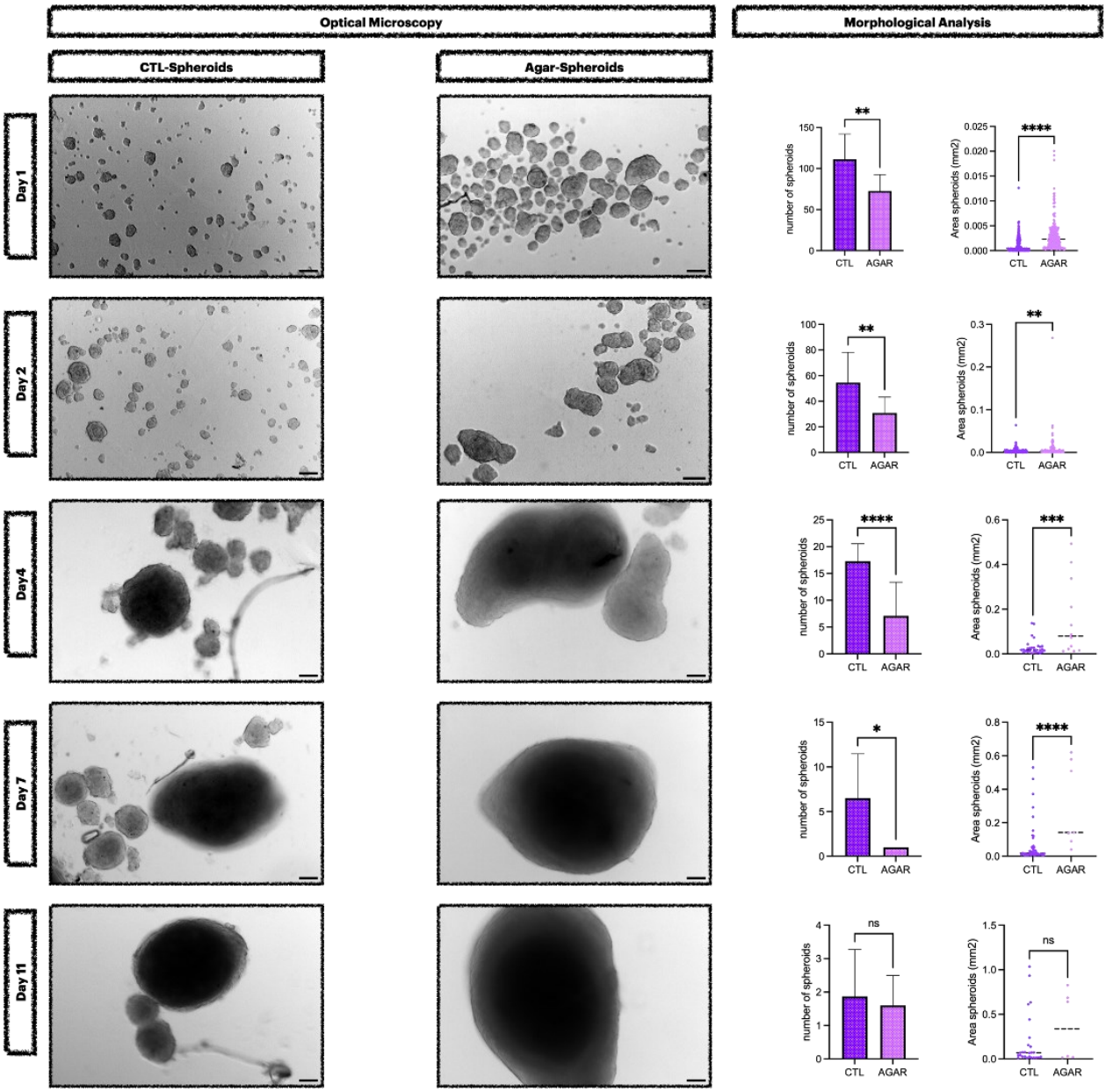

Figure 60. On the left Bright-field images of representative CTL-spheroids and Agar-Spheroids at different time points. Scale bar 100 µm. On the right morphological analysis of CTL-spheroids and Agar-Spheroids. The different types of spheroids were compared in term of number of spheroid and dimensions.

A more detailed analysis shows that, the number of spheroids in the well decreases with time in both culture conditions. Simultaneously, these spheroids increase in size. As with the chondro-aggregates, the increase in size seems to be due to an aggregation process of pre-existing spheroids. While the general behavior of the spheroids over time is the same in both systems, there are some important differences. In the first days of culture (day 1 and day 2), the spheroids that form on the CTL coating appear to be more numerous and, in terms of size, these spheroids are much smaller. From day 7

onwards, in the agar coated wells it is already possible to notice the presence of a single spheroids, whereas in the case of CTL it is necessary to wait for day 11. Moreover, it is only from this point onward that the dimensions of the two types of aggregates become comparable. These data are interesting because they lead to the hypothesis of two different mechanisms of cell aggregation. The agar coating makes the surface no adhesive so cells are forced to immediately aggregate. In this instance, cell-cell interaction will prevail. In the case of the CTL the polymer not only prevents the adhesion of the cells to the bottom of the wells, but also coordinates the aggregation of the cells. It is reasonable to think that immediately after seeding the polymer creates a steric hindrance between the cells, preventing them from aggregating into large aggregates. The cells will not only interact with each other but also with the CTL. After the polymer has been reworked, the aggregates can fuse together. This assumption can be partially confirmed by analyzing the arrangement of the polymer in the structure. Using a FITC-labeled CTL, it was found that the polymer is evenly distributed among the cells only during the first few days. At the other times analyzed the polymer seems located inside the structures, since the fluorescence of the polymer is hidden by the position of the fluorescence of the cell nuclei (Figure 61).

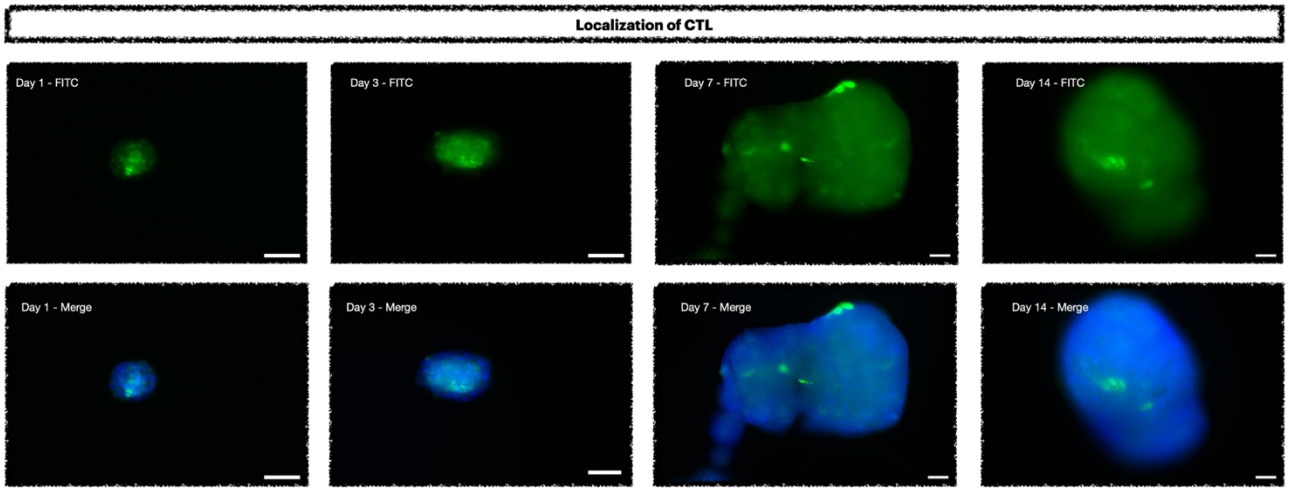

Figure 61. Localization of CTL in CTL-Spheroids. FITC-labeled CTL was used for polymer localization (green fluorescence); nuclei are stained with Hoechst (blue fluorescence). Scale bars 100 μm

Similar to the chondrocytes aggregates, the viability of the spheroids was also assessed. The Alamar Blue assays shows that the viability signals for CTL-Spheroids is higher than the signal of spheroids formed on agar coating. Furthermore, the vitality of agar samples decreases from the first few days, whereas CTL shows a slight proliferation in the same timeframe (Figure 62).

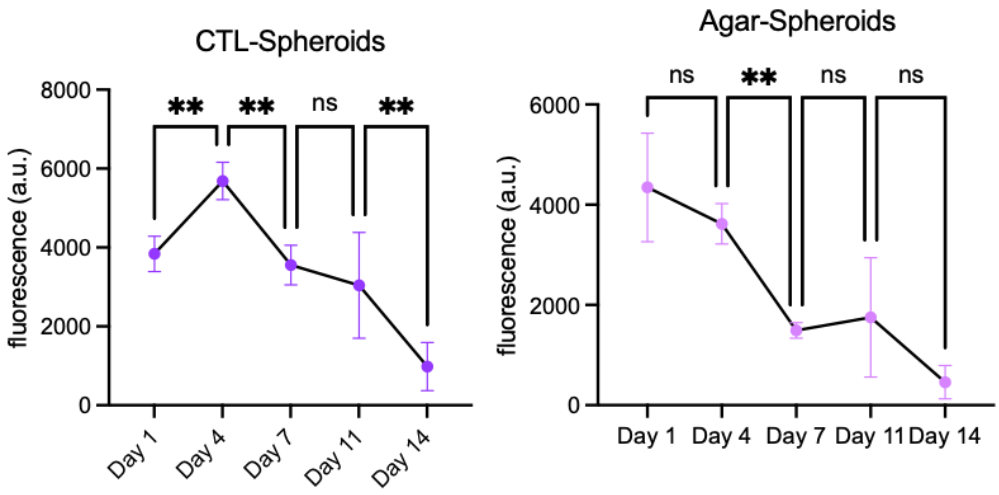

Figure 62. Alamar Blue Assay of CTL-spheroids on the right and on Agar-Spheroids on the left.

Qualitative analysis of viability performed with Live/Dead Assay confirm the biochemical assay (Figure 63). Agar-spheroids exhibits the necrotic core from the fourth day of culture, and this is consistent with the previous morphological analysis. In the first day of culture, spheroids formed on agar-coating are larger than those formed on CTL-coating. A larger and more compact structure can interfere with the exchange of nutrients and oxygen, resulting in premature cell death in the core of the spheroids. In the case of CTL, a looser structure can be expected due to the presence of the polymer between the cells. Hypoxia and necrosis in the core of spheroids are critical phenomena described in the literature, especially for tumor spheroids (Barisam et al., 2018) and depend on the diameter of the spheroid.

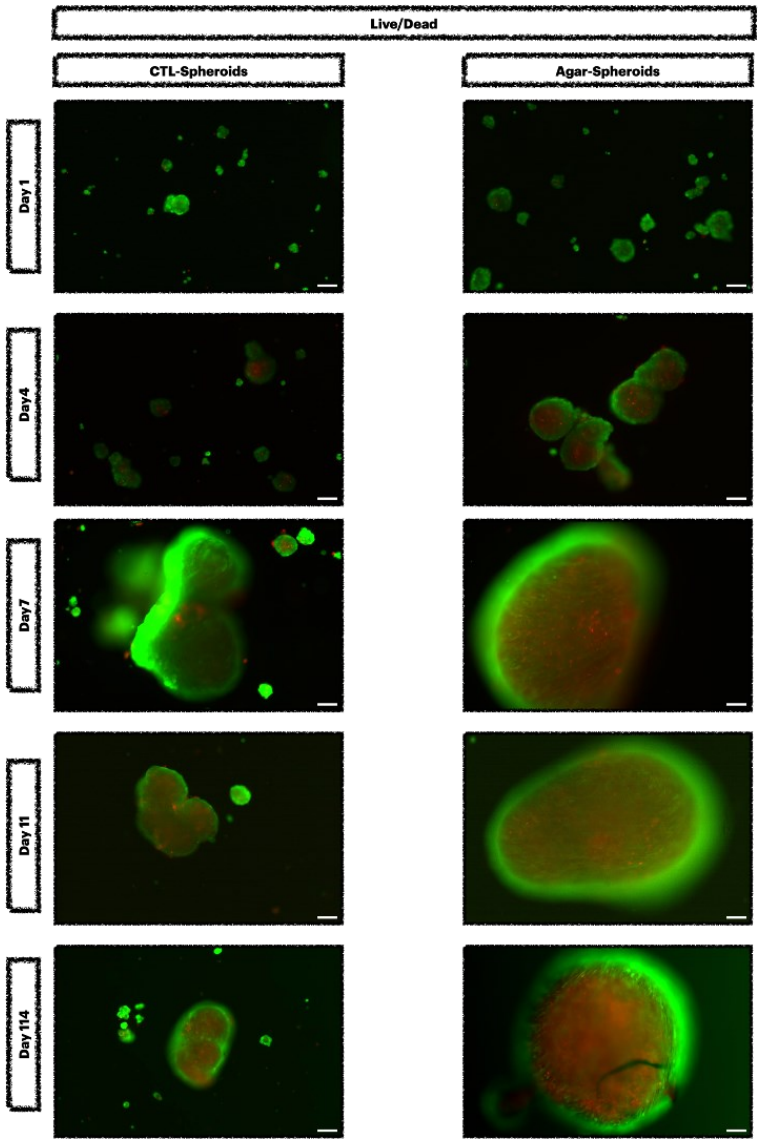

Figure 63. Live/dead cell imaging of CT-Spheroids and Agar-Spheroids at different time points. Cells were stained with two different fluorescent probes to demonstrate cell viability. Dead cells appear red, and living cells appear green.

Confirmation of the different arrangement of cells in the spheroids is obtained by internal analysis. Hematoxylin and Eosin staining on semi-fine section shows that a looser structure is evident in the CTL-spheroids at all time point analyzed (Figure 64). The observed structure is more open, less dense and has a lower number of cells than the structure observed for Agar-spheroids. In addition, an amorphous matrix is visible in the core. This amorphous matrix could be related to the presence of CTL given its ability to bind this type of dyes. This hypothesis is in line with the above discussion. Indeed, the immunohistochemical images with FITC-labelled CTL show that the polymer is predominantly present inside the spheroids. Furthermore, the lower number of cells present in CTL-spheroids might be related to the smaller size of this type of aggregates.

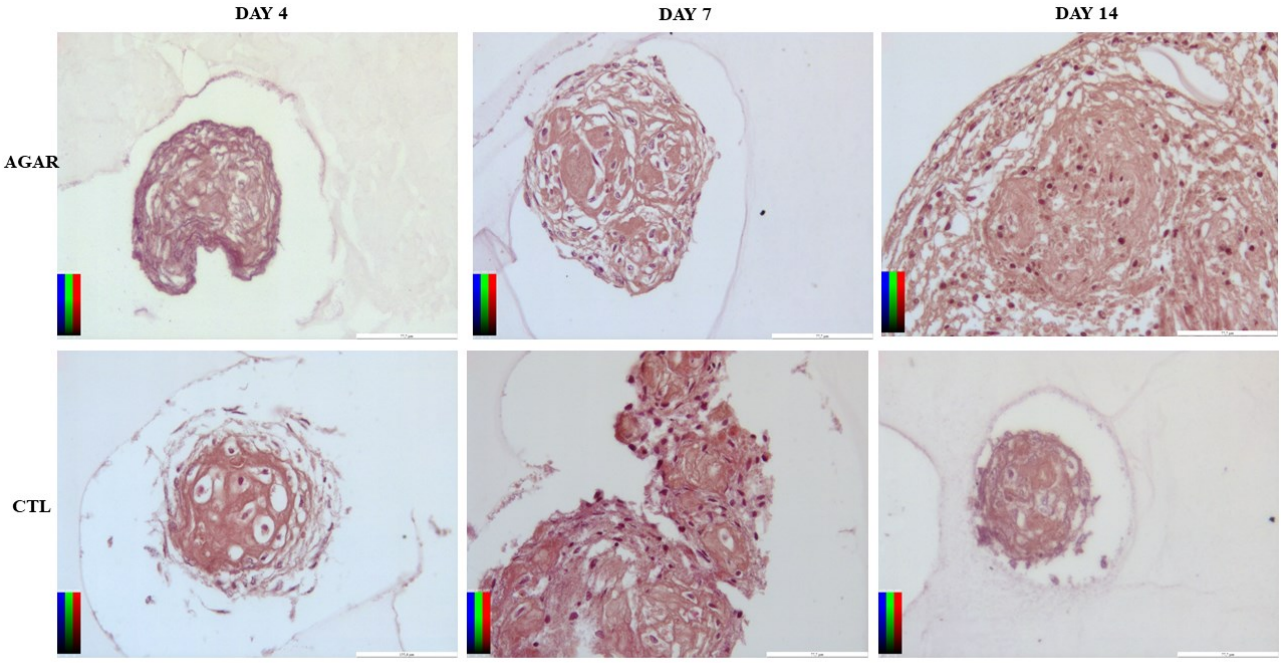

Figure 64. Hematoxylin/Eosin staining on Agar-Spheroids and CTL-Spheroids after 4,7 and 14 days of culture. Scale bar 77 µm.

The final step in our analysis aims at assessing the chondrogenic differentiation of the hMSC-AT. qRT-PCR was used to evaluate the expression of chondrogenic markers such as type II collagen (Figure 65). The latter signals is much higher in the CTL-spheroids than in the Agar ones in the first days of culture. The higher expression of type II collagen persists also for longer incubation times. For agar-spheroids, a significant increase in type II collagen expression occurs only after 14 days of culture.

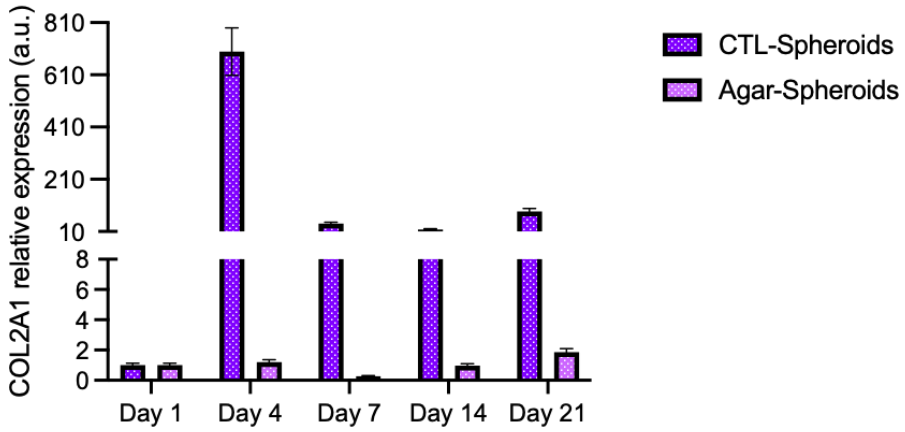

Figure 65. Relative gene expression quantification of COL2A1 in CTL and Agar-Spheroids. Data are reported as mean ± s.d., $n = 4$ replicates analyzed for each experimental condition.

However, it is possible to notice that values of gene expression decrease between day 4 and day 7 in the CTL-spheroids. In contrast, the values in the Agar-spheroids increase steadily over time. To exclude that this decrease is not due to chondrocytes de-differentiation and chondrocytes hypertrophy, the expression of type I collagen or type X collagen was tested (Jiang et al., 2020; Kim et al., 2022). The expression of both markers does not increase during the period of analysis (Figure 66).

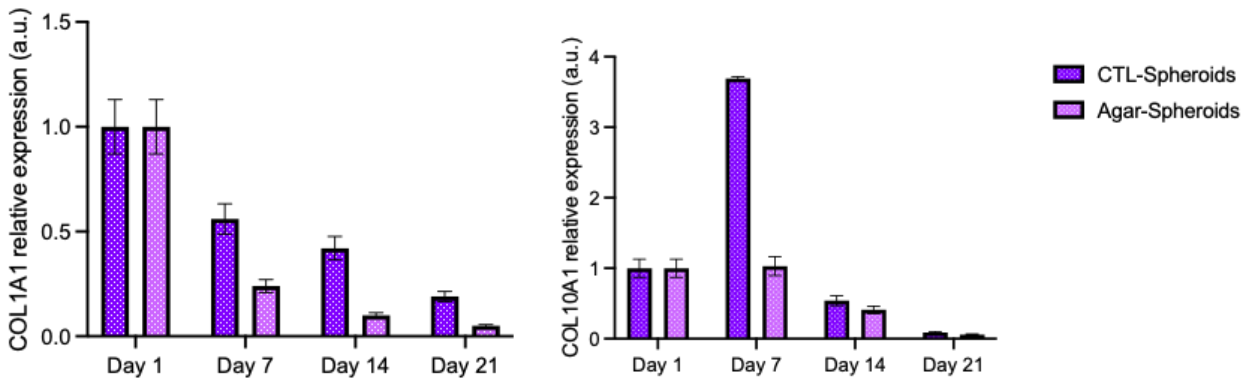

Figure 66. Relative gene expression quantification of COL1A1 and COL10A1 in CTL and Agar-Spheroids. Data are reported as mean ± s.d., $n = 4$ replicates analyzed for each experimental condition.

It is reasonable to assume that, despite the decrease in type II collagen expression, cells formed CTL-spheroids still produce type II collagen. In fact, for CTL-spheroids, after the decrease of expression from day 4 to day 7, the gene expression values for type II collagen increases again for longer time point. Moreover, these values are higher than those of Agar-spheroids. For Agar-spheroids, type II collagen production increases slowly within 21 days. The different expression trend may be related to the different behavior of the two types of spheroids.

Using conventional spheroids formation methods, the results is a very compact structure, with strong cell-cell interaction, producing radial/circumferential forces that lead to tight compaction of cells (Lee et al., 2019). The result is a structure in which the exchange of the nutrient and the oxygen diffusion decrease from the surface to the core. Furthermore, the reduced diffusion of signal molecules inhibits the control of cellular functions within the spheroids leading to a necrotic core (Coyle et al., 2019; Däster et al., 2017). These data are consistent with those described in the literature on Agar-spheroids. Hematoxylin and Eosin staining and morphological analysis pointed out a more compact structure with high dimension from the early time point analyzed. These characteristics result in a lower viability and in the formation of a necrotic core from day 4. Computational analysis and mechanical model carried out on tumor-spheroids show that the structures formed by high dimensions spheroids could be divided in three sub-zone, depending on the availability of oxygen and nutrient: a necrotic core, a quiescent or hypoxic zone and an external proliferating zone (Barisam et al., 2018; Xu et al.,

2016). A similar situation could also be found in spheroids with mesenchymal stem cells. For Agar-spheroids, only a few cells from the beginning have access to nutrients and to differentiating factors. Cells which can differentiate into chondrocytes phenotype will be very few and will result in a very poor type II collagen expression.

In contrast, as reported in the literature, a smaller diameter and a looser structures improve oxygen and nutrient exchange (Barisam et al., 2018). CTL-spheroids are smaller and in the first days have a higher viability than Agar-spheroids. This different structural feature might partly explain the high expression level of type II collagen during the first days of culture. A potential structural bioactivity of CTL towards spheroids of MSCs can be proposed. The ability of CTL to induce the aggregation of cells, and also to lead interaction between cells and the polymer, allow the formation of a looser structures with a high exchange of oxygen and nutrient. From day 7 the reduction of the signal of type II collagen is probably due to the aggregation of more spheroids, with the consequent formation of the necrotic core. As this point, in fact, the behaviors of the CTL spheroids is very similar to those of Agar-spheroids. However, a biochemical bioactivity of the CTL towards the chondrogenic differentiation of MSCs cannot be ruled out. Studies should be carried out to analyze in detail the mechanism of cell-CTL interaction. In this context, the involvement of specific cell receptors that are activated by this interaction and that may be involved in chondrogenic differentiation should also be analyzed.

As with chondrocytes-aggregates, the involvement of CTL in the formation of the spheroids is important for their application in the field of cartilage regeneration. The high expression of type II collagen already after four days of culture allows the spheroids to be transferred into the patients already at this time, when the ability of the spheroids to adhere to adhesive surfaces is very good. If you were to wait for the usual periods for chondrogenic differentiation, this ability would be compromised. In fact, large spheroids cannot adhere to the surface and colonize the cartilage defect (Figure 67).

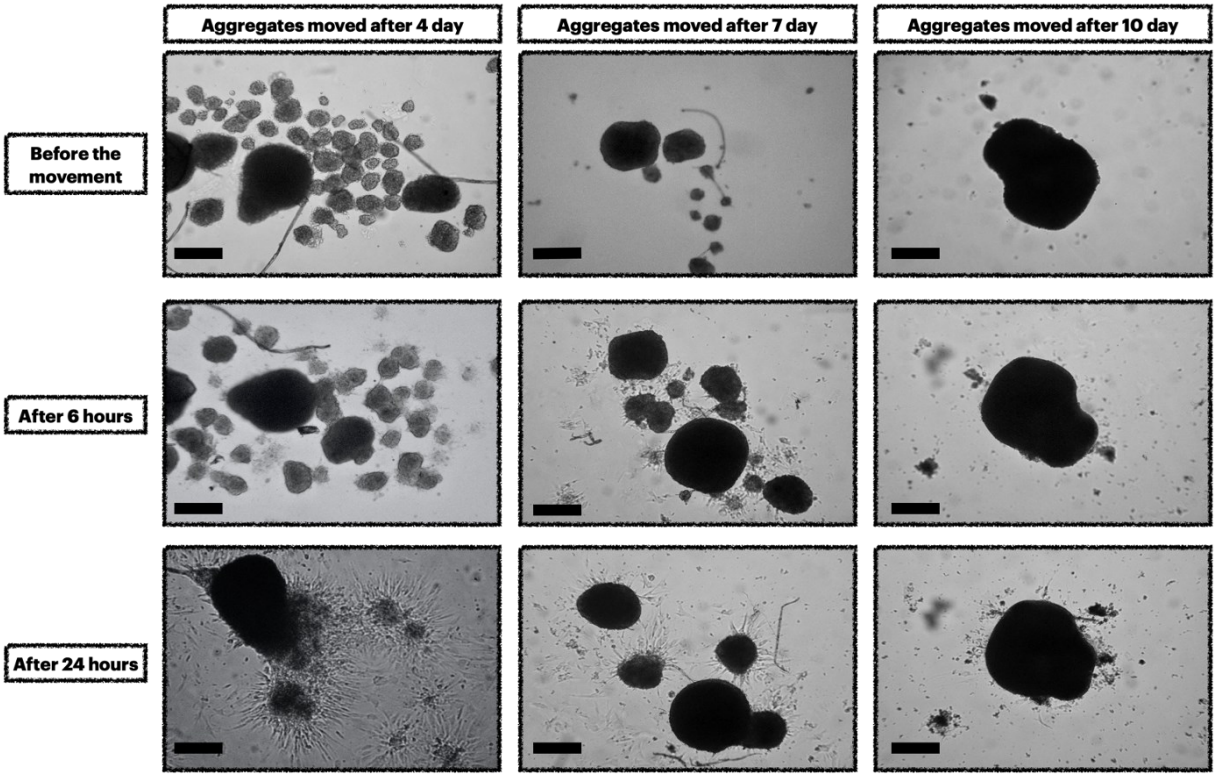

Figure 67. Spreading assay on the adherent surface. Representative bright-field images of CTL-Spheroids seeded on adherent substrates followed by cell spreading over 24 hours of culture. CTL-Spheroids were transferred 4, 7 and 10 days after assembly on well plates coated with CTL (scale bars 50 μm).

3.3.3.3. Ability of sulphated-CTL to coordinate aggregation of hMSC-AT

The last part of this chapter deals with the use of two sulphated-modified CTL for the formation of MSCs spheroids. Spheroids formed in the presence of sulphated-modified CTL are compared with spheroids formed with a standard CTL. The two sulphated-CTL have slightly different characteristics between themselves and with respect to the original CTL. Briefly, Sulphated-CTL-1 has a higher degree of sulfation but a lower degradation; on the other hand, Suphated-CTL-2 has a higher degradation. Moreover, both sulphated polymers are cleaved with respect to the polymer backbone of the original CTL (Pizzolitto et al., 2022).

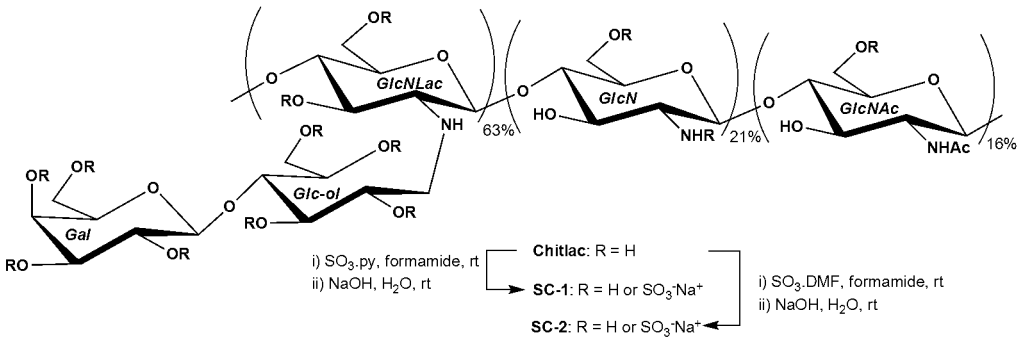

Figure 68. Conversion of CTL into sulfated derivatives SC-1 (Sulphated CTL-1) and SC-2 (Sulphated CTL-2).

At first, LDH assay was used to assess the biocompatibility of Sulphated-CTL. The results showed no considerable differences in terms of LDH release, considering cells cultured treated with 0.5% w/VSulphated CTL and the negative control (untreated cells). On the contrary, cells treated with Triton X-100 (positive control of cell toxicity) showed an increase in percentage of LDH enzyme released in cellular medium (Figure 69).

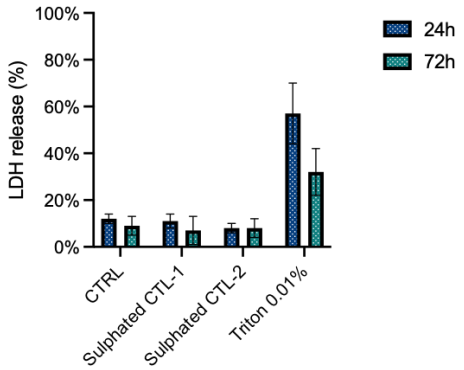

Figure 69. *In vitro* Biocompatibility (LDH Assay) on osteoblast (MG-63) treated with 0.5% Sulphated CTL-1 and Sulphated CTL-2 at 24 hours (blue bars) and 72 hours (green bars) after treatment.

The ability of Sulphated-CTL to induce cell aggregation was then tested using the same protocol. The morphological analysis shows that also Sulphated-CTL are able to induce aggregation of MSCs after 24 hours, but differences with CTL emerge. In general terms, more numerous but smaller spheroids are formed by the Sulphated-CTL samples. It is interesting to note that on day 1, there are also differences in the area of the two Sulphated-CTL. Specifically, Sulphated-CTL-2 induces the formation of smaller spheroids than those obtained with Sulphated-CTL-1. In addition, in sample with Sulphated-CTL-2 it is still possible to observe the presence of isolated cells. These cells do not take part to the formation of the aggregates and are able to adhere and spread independently from the presence of the polymer. After three days of culture the differences between the two Sulphated-CTL become more evident. In the case of Sulphated-CTL-1, the behavior is similar to those of CTL with the merging of preformed aggregates. For Sulphated-CTL-2, at variance, it is no longer possible to observe spheroids in suspension, but the few that still exist have adhered to the bottom of the well (Figure 70).

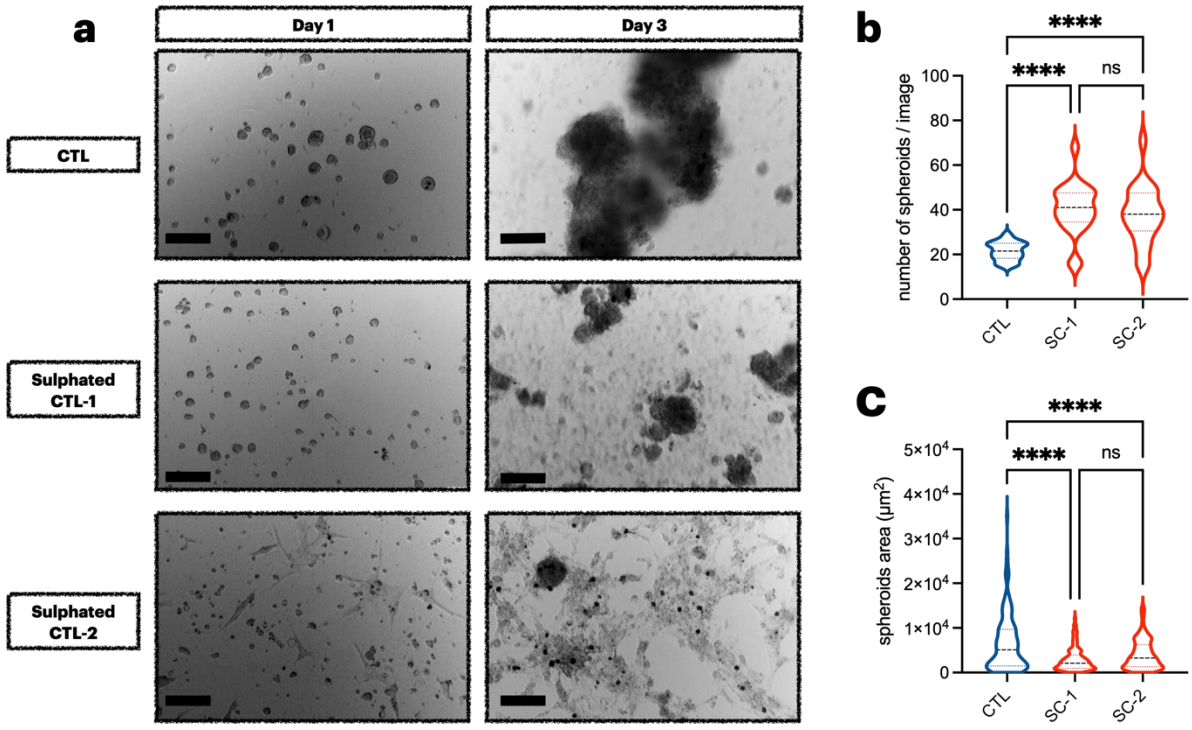

Figure 70. Optical Images of hMSC-AT spheroids at different investigated time points. Scale bars are 150 µm (a). Number of spheroids per image (b) and spheroids area (c) after 1 day of incubation in cell culture medium. Data are reported as violin plots showing the median of values (n = 13–15 images analyzed in b and n = 145–150 spheroids analyzed in c). Statistics: ns, not significant; ****, $p < 0.0001$; One way Anova followed by Tukey's multiple comparisons test.

These results demonstrate once again that the backbone of the CTL is involved in the formation of aggregates. The use of a CTL with a decreased molecular weight high, as for the Sulphated-CTL-2, hampers the aggregation process, leading to adhesion of spheroids to the surface and spreading of single cells. Moreover, the smaller dimensions of the spheroids obtained using Sulphated-CTL-1 certainly lead to advantages in terms of viability and nutrient exchange during the period useful for cartilage differentiation of MSCs.

Beside the individual results, however, the use of a sulphated CTL for spheroid formation can lead to numerous advantages in the field of cartilage, and more broadly tissue regeneration.

4. CONCLUDING REMARKS and FUTURE PERSPECTIVES

The search for biomaterials capable of mimicking the heterogeneity and complexity of the ECM remains a challenge. By exploiting CTL's chemical, physical and mechanical characteristics as well as its biological properties, the main results achieved in the filed from this work are summarized below.

- In the first section of the thesis, the reaction mechanisms between CTL and genipin was studied in detail using UV-Vis spectroscopy and CD. The proposed reaction is particularly innovative because the experiments were carried out at neutral pH thanks to the properties of CTL.
- In the second section, CTL was reticulated via both temporary (boric acid) and permanent (genipin) crosslinkers. The resulting hydrogels exhibit particular mechanical properties in terms of immediate stress dissipation. The osteogenic commitment of hMSC-AT seeded atop these hydrogels was investigated, and a correlation between the immediate stress dissipation and the expression of typical osteogenic marker was found. These results are significant for the field of mechanobiology, as they confirm that stiffness is not the only mechanical parameter controlling osteogenic differentiation.
- Finally, in the last part of the project, the bioactive properties of CTL were used to develop an innovative scaffold-free strategy. We showed that CTL coordinates the aggregation of different cell cultures (chondrocytes, hMSC-AT) and interact very closely with them. Furthermore, when comparing the spheroids formed with CTL with the classical spheroids described in the literature, the former are looser, which facilitates the exchange of nutrients inside the structure and anticipates the expression of type II collagen. Finally, we found that the chain degradation of the CTL impairs, to some extent, the ability to form spheroids, once again highlighting the active role of this polymer in coordinating of cell aggregation.

Overall, the results reported above indicate that CTL is a good candidate for the fabrication of 2D substrates and 3D structures that are useful as ECM models to gain fundamental insights into cell biology. The ability to modulate the mechanical response of hydrogels based on CTL represents a promising starting point to study the cellular response, also in relation to other phenotypes, with potential repercussion in different TE field. Furthermore, the close interaction that emerged between the CTL and the cells in the last part of the project is a good starting point for a more detailed investigation of its bioactive properties, especially in the field of cartilage and bone regeneration.

REFERENCES

Al-Halaseh, L.K., Al-Jawabri, N.A., Tarawneh, S.K., Al-Qdah, W.K., Abu-Hajleh, M.N., Al-Samydai, A.M., Ahmed, M.A., 2022. A review of the cosmetic use and potentially therapeutic importance of hyaluronic acid. J. Appl. Pharm. Sci. 12, 34–41. https://doi.org/10.7324/JAPS.2022.120703

Albanna, M., Binder, K.W., Murphy, S. V, Kim, J., Qasem, S.A., Zhao, W., Tan, J., El-Amin, I.B., Dice, D.D., Marco, J., Green, J., Xu, T., Skardal, A., Holmes, J.H., Jackson, J.D., Atala, A., Yoo, J.J., 2019. In Situ Bioprinting of Autologous Skin Cells Accelerates Wound Healing of Extensive Excisional Full-Thickness Wounds. Sci. Rep. 9, 1856. https://doi.org/10.1038/s41598-018-38366-w

Anderer, U., Libera, J., 2002. In vitro engineering of human autogenous cartilage. J. Bone Miner. Res. 17, 1420–1429. https://doi.org/10.1359/jbmr.2002.17.8.1420

Andersen, T., Auk-Emblem, P., Dornish, M., 2015. 3D Cell Culture in Alginate Hydrogels. Microarrays (Basel, Switzerland) 4, 133–161. https://doi.org/10.3390/microarrays4020133

Andersen, T., Strand, B.L., Formo, K., Alsberg, E., & Christensen, B.E., 2012. Chapter 9 Alginates as biomaterials in tissue engineering, in: Royal Society of Chemistry London. pp. 227–258.

Antman-Passig, M., Levy, S., Gartenberg, C., Schori, H., Shefi, O., 2017. Mechanically Oriented 3D Collagen Hydrogel for Directing Neurite Growth, Tissue Engineering - Part A. https://doi.org/10.1089/ten.tea.2016.0185

Armoiry, X., Cummins, E., Connock, M., Metcalfe, A., Royle, P., Johnston, R., Rodrigues, J., Waugh, N., Mistry, H., 2019. Autologous Chondrocyte Implantation with Chondrosphere for Treating Articular Cartilage Defects in the Knee: An Evidence Review Group Perspective of a NICE Single Technology Appraisal. Pharmacoeconomics 37, 879–886. https://doi.org/10.1007/s40273-018-0737-z

Barisam, M., Saidi, M.S., Kashaninejad, N., Nguyen, N.T., 2018. Prediction of necrotic core and hypoxic zone of multicellular spheroids in a microbioreactor with a U-shaped barrier. Micromachines 9, 1–19. https://doi.org/10.3390/mi9030094

Bauer, A., Gu, L., Kwee, B., Li, W.A., Dellacherie, M., Celiz, A.D., Mooney, D.J., 2017. Hydrogel substrate stress-relaxation regulates the spreading and proliferation of mouse myoblasts. Acta Biomater. 62, 82–90. https://doi.org/10.1016/j.actbio.2017.08.041

Beloussov, L. V., Grabovsky, V.I., 2006. Morphomechanics: Goals, basic experiments and models. Int. J. Dev. Biol. 50, 81–92. https://doi.org/10.1387/ijdb.052056lb

Bhosale, A.M., Richardson, J.B., 2008. Articular cartilage : structure , injuries and review of management 77–95. https://doi.org/10.1093/bmb/ldn025

Białkowska, K., Komorowski, P., Bryszewska, M., Miłowska, K., 2020. Spheroids as a type of three-dimensional cell cultures—examples of methods of preparation and the most important application. Int. J. Mol. Sci. 21, 1–17. https://doi.org/10.3390/ijms21176225

Borkenhagen, M., Clémence, J.F., Sigrist, H., Aebischer, P., 1998. Three-dimensional extracellular matrix engineering in the nervous system. J. Biomed. Mater. Res. 40, 392–400. https://doi.org/10.1002/(sici)1097-4636(19980603)40:3<392::aid-jbm8>3.0.co;2-c

Borzacchiello, A., Russo, L., Malle, B.M., Schwach-Abdellaoui, K., Ambrosio, L., 2015. Hyaluronic acid based hydrogels for regenerative medicine applications. Biomed Res. Int. 2015. https://doi.org/10.1155/2015/871218

Bruderer, M., Richards, R.G., Alini, M., Stoddart, M.J., 2014. Role and regulation of runx2 in osteogenesis.

Eur. Cells Mater. 28, 269–286. https://doi.org/10.22203/eCM.v028a19

Brun, F., Accardo, A., Marchini, M., Ortolani, F., Turco, G., Paoletti, S., 2011. Texture analysis of TEM micrographs of alginate gels for cell microencapsulation. Microsc. Res. Tech. 74, 58–66. https://doi.org/10.1002/jemt.20874

Buckwalter, J.A., 1998. Articular cartilage: Injuries and potential for healing. J. Orthop. Sports Phys. Ther. 28, 192–202. https://doi.org/10.2519/jospt.1998.28.4.192

Buckwalter, J.A., 1983. Articular cartilage. Instr. Course Lect. 32, 349–370.

Buckwalter, J.A., Mankin, H.J., 1998. Articular cartilage: tissue design and chondrocyte-matrix interactions. Instr. Course Lect. 47, 477–486.

Burdick, J.A., Prestwich, G.D., 2011. Hyaluronic acid hydrogels for biomedical applications. Adv. Mater. 23, H41-56. https://doi.org/10.1002/adma.201003963

Butler, M.F., Ng, Y.-F., Pudney, P.D.A., 2003. Mechanism and kinetics of the crosslinking reaction between biopolymers containing primary amine groups and genipin. J. Polym. Sci. Part A Polym. Chem. 41, 3941–3953. https://doi.org/10.1002/pola.10960

Cameron, A.R., Frith, J.E., Cooper-White, J.J., 2011. The influence of substrate creep on mesenchymal stem cell behaviour and phenotype. Biomaterials 32, 5979–5993. https://doi.org/10.1016/j.biomaterials.2011.04.003

Cesarz, Z., Tamama, K., 2016. Spheroid Culture of Mesenchymal Stem Cells. Stem Cells Int. 2016. https://doi.org/10.1155/2016/9176357

Chalimidi, K.R., Kumar, Y., Kini, U.A., 2015. Efficacy of Collagen Particles in Chronic Non Healing Ulcers. J. Clin. Diagn. Res. 9, PC01-3. https://doi.org/10.7860/JCDR/2015/11782.6001

Charrier, E.E., Pogoda, K., Wells, R.G., Janmey, P.A., 2018. Control of cell morphology and differentiation by substrates with independently tunable elasticity and viscous dissipation. Nat. Commun. 9, 1–13. https://doi.org/10.1038/s41467-018-02906-9

Chaudhuri, O., Cooper-White, J., Janmey, P.A., Mooney, D.J., Shenoy, V.B. file:///Volumes/Chiar. L. /Dottorato/paper meccano/Lee 2017. pd., 2020. Effects of extracellular matrix viscoelasticity on cellular behaviour. Nature 584, 535–546. https://doi.org/10.1038/s41586-020-2612-2

Chaudhuri, O., Gu, L., Darnell, M., Klumpers, D., Bencherif, S.A., Weaver, J.C., Huebsch, N., Mooney, D.J., 2015. Substrate stress relaxation regulates cell spreading. Nat. Commun. 6, 1–7. https://doi.org/10.1038/ncomms7365

Chaudhuri, O., Gu, L., Klumpers, D., Darnell, M., Sidi, A., Weaver, J.C., Huebsch, N., Lee, H., Lippens, E., Duda, G.N., Mooney, D.J., 2016. Hydrogels with tunable stress relaxation regulate stem cell fate and activity 15, 326–334. https://doi.org/10.1038/nmat4489.Hydrogels

Chen, A., Gupte, C., Akhtar, K., Smith, P., Cobb, J., 2012. The Global Economic Cost of Osteoarthritis: How the UK Compares. Arthritis 2012, 1–6. https://doi.org/10.1155/2012/698709

Chen, F.S., Frenkel, S.R., Di Cesare, P.E., 1999. Repair of articular cartilage defects: part I. Basic Science of cartilage healing. Am. J. Orthop. (Belle Mead. NJ). 28, 31–33.

Chiono, V., Pulieri, E., Vozzi, G., Ciardelli, G., Ahluwalia, A., Giusti, P., 2008. Genipin-crosslinked chitosan/gelatin blends for biomedical applications. J. Mater. Sci. Mater. Med. 19, 889–898. https://doi.org/10.1007/s10856-007-3212-5

Choi, J.R., Yong, K.W., Choi, J.Y., 2018. Effects of mechanical loading on human mesenchymal stem cells for cartilage tissue engineering. J. Cell. Physiol. 233, 1913–1928. https://doi.org/10.1002/jcp.26018

Cok, M., Sacco, P., Porrelli, D., Travan, A., Borgogna, M., Marsich, E., Paoletti, S., Donati, I., 2018. Mimicking mechanical response of natural tissues. Strain hardening induced by transient reticulation in lactose-modified chitosan (chitlac). Int. J. Biol. Macromol. 106, 656–660. https://doi.org/10.1016/j.ijbiomac.2017.08.059

Correa, D., Lietman, S.A., 2017. Articular cartilage repair: Current needs, methods and research directions. Semin. Cell Dev. Biol. 62, 67–77. https://doi.org/10.1016/j.semcdb.2016.07.013

Coyle, R., Yao, J., Richards, D., Mei, Y., 2019. The Effects of Metabolic Substrate Availability on Human Adipose-Derived Stem Cell Spheroid Survival. Tissue Eng. - Part A 25, 620–631. https://doi.org/10.1089/ten.tea.2018.0163

D'Amelio, N., Esteban, C., Coslovi, A., Feruglio, L., Uggeri, F., Villegas, M., Benegas, J., Paoletti, S., Donati, I., 2013. Insight into the molecular properties of chitlac, a chitosan derivative for tissue engineering. J. Phys. Chem. B 117, 13578–13587. https://doi.org/10.1021/jp4067263

Däster, S., Amatruda, N., Calabrese, D., Ivanek, R., Turrini, E., Droeser, R.A., Zajac, P., Fimognari, C., Spagnoli, G.C., Iezzi, G., Mele, V., Muraro, M.G., 2017. Induction of hypoxia and necrosis in multicellular tumor spheroids is associated with resistance to chemotherapy treatment. Oncotarget 8, 1725–1736. https://doi.org/10.18632/oncotarget.13857

Davidson, M.D., Song, K.H., Lee, M.-H., Llewellyn, J., Du, Y., Baker, B.M., Wells, R.G., Burdick, J.A., 2019. Engineered Fibrous Networks To Investigate the Influence of Fiber Mechanics on Myofibroblast Differentiation. ACS Biomater. Sci. Eng. 5, 3899–3908. https://doi.org/10.1021/acsbiomaterials.8b01276

Di Tommaso, S., David, H., Gomar, J., Leroy, F., Adamo, C., 2014. From iridoids to dyes: a theoretical study on genipin reactivity. RSC Adv. 4, 11029–11038.

Di Tommaso, S., David, P., Picolet, K., Gabant, M., David, H., Morançais, J.-L., Gomar, J., Leroy, F., Adamo, C., 2013. Structure of genipin in solution: a combined experimental and theoretical study. RSC Adv. 3, 13764–13771. https://doi.org/10.1039/C3RA42147C

Dimida, S., Barca, A., Cancelli, N., De Benedictis, V., Raucci, M.G., Demitri, C., 2017. Effects of genipin concentration on cross-linked chitosan scaffolds for bone tissue engineering: Structural characterization and evidence of biocompatibility features. Int. J. Polym. Sci. 2017. https://doi.org/10.1155/2017/8410750

Dimida, S., Demitri, C., De Benedictis, V.M., Scalera, F., Gervaso, F., Sannino, A., 2015. Genipin-cross-linked chitosan-based hydrogels: Reaction kinetics and structure-related characteristics. J. Appl. Polym. Sci. 132. https://doi.org/10.1002/app.42256

Discher, D.E., Mooney, D.J., Zandstra, P.W., 2009. Growth factors, matrices, and forces combine and control stem cells. Science (80-.). 324, 1673–1677. https://doi.org/10.1126/science.1171643

Docheva, D., Padula, D., Popov, C., Mutschler, W., Clausen-Schaumann, H., Schieker, M., 2008. Researching into the cellular shape, volume and elasticity of mesenchymal stem cells, osteoblasts and osteosarcoma cells by atomic force microscopy: Stem Cells. J. Cell. Mol. Med. 12, 537–552. https://doi.org/10.1111/j.1582-4934.2007.00138.x

Doillon, C.J., 1988. Porous collagen sponge wound dressings: in vivo and in vitro studies. J. Biomater. Appl. 2, 562–578. https://doi.org/10.1177/088532828700200404

Donati, I., Borgogna, M., Turello, E., Casàro, A., Paoletti, S., 2007a. Tuning supramolecular structuring at

the nanoscale level: Nonstoichiometric soluble complexes in dilute mixed solutions of alginate and lactose-modified chitosan (Chitlac). Biomacromolecules 8, 1471–1479. https://doi.org/10.1021/bm0610828

Donati, I., Feresini, M., Travan, A., Marsich, E., Lapasin, R., Paoletti, S., 2011. Polysaccharide-based polyanion--polycation--polyanion ternary systems. A preliminary analysis of interpolyelectrolyte interactions in dilute solutions. Biomacromolecules 12, 4044–4056. https://doi.org/10.1021/bm201046p

Donati, I., Haug, I.J., Scarpa, T., Borgogna, M., Draget, K.I., Skjåk-Bræk, G., Paoletti, S., 2007b. Synergistic effects in semidilute mixed solutions of alginate and lactose-modified chitosan (chitlac). Biomacromolecules 8, 957–962. https://doi.org/10.1021/bm060856h

Donati, I., Paoletti, S., 2009. Material Properties of Alginates. https://doi.org/10.1007/978-3-540-92679-5_1

Donati, I., Stredanska, S., Silvestrini, G., Vetere, A., Marcon, P., Marsich, E., Mozetic, P., Gamini, A., Paoletti, S., Vittur, F., 2005. The aggregation of pig articular chondrocyte and synthesis of extracellular matrix by a lactose-modified chitosan. Biomaterials 26, 987–998. https://doi.org/10.1016/j.biomaterials.2004.04.015

Dosio, F., Arpicco, S., Stella, B., Fattal, E., 2016. Hyaluronic acid for anticancer drug and nucleic acid delivery. Adv. Drug Deliv. Rev. 97, 204–236. https://doi.org/10.1016/j.addr.2015.11.011

Du, H., Yang, X., Zhai, G., 2014. Design of chitosan-based nanoformulations for efficient intracellular release of active compounds. Nanomedicine 9, 723–740. https://doi.org/10.2217/nnm.14.8

Dupont, S., Morsut, L., Aragona, M., Enzo, E., Giulitti, S., Cordenonsi, M., Zanconato, F., Le Digabel, J., Forcato, M., Bicciato, S., Elvassore, N., Piccolo, S., 2011. Role of YAP/TAZ in mechanotransduction. Nature 474, 179–184. https://doi.org/10.1038/nature10137

Engler, A.J., Sen, S., Sweeney, H.L., Discher, D.E., 2006. Matrix Elasticity Directs Stem Cell Lineage Specification. Cell 126, 677–689. https://doi.org/10.1016/j.cell.2006.06.044

Erickson, C.B., Payne, K.A., 2019. Inductive signals and progenitor fates during osteogenesis, Encyclopedia of Tissue Engineering and Regenerative Medicine. Elsevier Inc. https://doi.org/10.1016/B978-0-12-801238-3.65483-1

Esteban, C., Donati, I., Pantano, S., Villegas, M., Benegas, J., Paoletti, S., 2018. Dissecting the conformational determinants of chitosan and chitlac oligomers. Biopolymers 109, e23221. https://doi.org/10.1002/bip.23221

Fan, T., Qu, R., Jiang, X., Yang, Y., Sun, B., Huang, X., Zhou, Z., Ouyang, J., Zhong, S., Dai, J., 2021. Spatial organization and crosstalk of vimentin and actin stress fibers regulate the osteogenic differentiation of human adipose-derived stem cells. FASEB J. 35, 1–16. https://doi.org/10.1096/fj.202000378RR

Fujikawa, S., Yokota, T., Koga, K., Kumada, J. ichi, 1987. The continuous hydrolysis of geniposide to genipin using immobilized β-glucosidase on calcium alginate gel. Biotechnol. Lett. 9, 697–702. https://doi.org/10.1007/BF01024600

Furlani, F., Sacco, P., Cok, M., De Marzo, G., Marsich, E., Paoletti, S., Donati, I., 2019a. Biomimetic, Multiresponsive, and Self-Healing Lactose-Modified Chitosan (CTL)-Based Gels Formed via Competitor-Assisted Mechanism. ACS Biomater. Sci. Eng. 5539–5547. https://doi.org/10.1021/acsbiomaterials.9b01256

Furlani, F., Sacco, P., Scognamiglio, F., Asaro, F., Travan, A., Borgogna, M., Marsich, E., Cok, M., Paoletti, S., Donati, I., 2019b. Nucleation, reorganization and disassembly of an active network from lactose-modified chitosan mimicking biological matrices. Carbohydr. Polym. 208, 451–456.

https://doi.org/10.1016/j.carbpol.2018.12.096

Gao, Y., Liu, S., Huang, J., Guo, W., Chen, J., Zhang, L., Zhao, B., Peng, J., Wang, A., Wang, Y., Xu, W., Lu, S., Yuan, M., Guo, Q., 2014. The ECM-cell interaction of cartilage extracellular matrix on chondrocytes. Biomed Res. Int. 2014. https://doi.org/10.1155/2014/648459

Geckil, H., Xu, F., Zhang, X., Moon, S., Demirci, U., 2010. Engineering hydrogels as extracellular matrix mimics Review. Nanomedicine 5, 469–484.

Georgopoulou, A., Papadogiannis, F., Batsali, A., Marakis, J., Alpantaki, K., Eliopoulos, A.G., Pontikoglou, C., Chatzinikolaidou, M., 2018. Chitosan/gelatin scaffolds support bone regeneration. J. Mater. Sci. Mater. Med. 29. https://doi.org/10.1007/s10856-018-6064-2

Gérentes, P., Vachoud, L., Doury, J., Domard, A., 2002. Study of a chitin-based gel as injectable material in periodontal surgery. Biomaterials 23, 1295–1302. https://doi.org/10.1016/S0142-9612(01)00247-2

Gong, J.P., 2010. Why are double network hydrogels so tough? Soft Matter 6, 2583–2590. https://doi.org/10.1039/b924290b

Graham, S., Marina, P.F., Blencowe, A., 2019. Thermoresponsive polysaccharides and their thermoreversible physical hydrogel networks. Carbohydr. Polym. 207, 143–159. https://doi.org/10.1016/j.carbpol.2018.11.053

Grandolfo, M., D'Andrea, P., Paoletti, S., Martina, M., Silvestrini, G., Bonucci, E., Vittur, F., 1993. Culture and differentiation of chondrocytes entrapped in alginate gels. Calcif. Tissue Int. 52, 42–48. https://doi.org/10.1007/BF00675625

Grevenstein, D., Mamilos, A., Schmitt, V.H., Niedermair, T., Wagner, W., Kirkpatrick, C.J., Brochhausen, C., 2021. Excellent histological results in terms of articular cartilage regeneration after spheroid-based autologous chondrocyte implantation (ACI). Knee Surgery, Sport. Traumatol. Arthrosc. 29, 417–421. https://doi.org/10.1007/s00167-020-05976-9

Grolma, J.M., Weinand, P., Moone, D.J., 2020. Extracellular matrix plasticity as a driver of cell spreading. Proc. Natl. Acad. Sci. U. S. A. 117, 25999–26007. https://doi.org/10.1073/pnas.2008801117

Han, F., Wang, J., Ding, L., Hu, Y., Li, W., Yuan, Z., Guo, Q., Zhu, C., Yu, L., Wang, H., Zhao, Z., Jia, L., Li, J., Yu, Y., Zhang, W., Chu, G., Chen, S., Li, B., 2020. Tissue Engineering and Regenerative Medicine: Achievements, Future, and Sustainability in Asia. Front. Bioeng. Biotechnol. 8, 1–35. https://doi.org/10.3389/fbioe.2020.00083

Heimbuck, Abitha M, Priddy-Arrington, T.R., Padgett, M.L., Llamas, C.B., Barnett, H.H., Bunnell, B.A., Caldorera-Moore, M.E., 2019. Development of Responsive Chitosan–Genipin Hydrogels for the Treatment of Wounds. ACS Appl. Bio Mater. 2, 2879–2888. https://doi.org/10.1021/acsabm.9b00266

Heimbuck, Abitha M., Priddy-Arrington, T.R., Sawyer, B.J., Caldorera-Moore, M.E., 2019. Effects of post-processing methods on chitosan-genipin hydrogel properties. Mater. Sci. Eng. C 98, 612–618. https://doi.org/10.1016/j.msec.2018.12.119

Hesse, E., Hefferan, T.E., Tarara, J.E., Haasper, C., Meller, R., Krettek, C., Lu, L., Yaszemski, M.J., 2010. Collagen type I hydrogel allows migration, proliferation, and osteogenic differentiation of rat bone marrow stromal cells. J. Biomed. Mater. Res. A 94, 442–449. https://doi.org/10.1002/jbm.a.32696

Hiligsmann, M., Cooper, C., Guillemin, F., Hochberg, M.C., Tugwell, P., Arden, N., Berenbaum, F., Boers, M., Boonen, A., Branco, J.C., Maria-Luisa, B., Bruyère, O., Gasparik, A., Kanis, J.A., Kvien, T.K., Martel-Pelletier, J., Pelletier, J.P., Pinedo-Villanueva, R., Pinto, D., Reiter-Niesert, S., Rizzoli, R., Rovati, L.C., Severens, J.L., Silverman, S., Reginster, J.Y., 2014. A reference case for economic evaluations in osteoarthritis: An expert consensus article from the European Society for Clinical and

Economic Aspects of Osteoporosis and Osteoarthritis (ESCEO). Semin. Arthritis Rheum. 44, 271–282. https://doi.org/10.1016/j.semarthrit.2014.06.005

Huang, B.J., Hu, J.C., Athanasiou, K.A., 2016. Cell-based tissue engineering strategies used in the clinical repair of articular cartilage. Biomaterials 98, 1–22. https://doi.org/10.1016/j.biomaterials.2016.04.018

Huang, W., Yang, S., Shao, J., Li, Y.P., 2007. Signaling and transcriptional regulation in osteoblast commitment and differentiation. Front. Biosci. 12, 3068–3092. https://doi.org/10.2741/2296

Huang, Y., Lapitsky, Y., 2012. Salt-assisted mechanistic analysis of chitosan/tripolyphosphate micro- and nanogel formation. Biomacromolecules 13, 3868–3876. https://doi.org/10.1021/bm3014236

Huang, Y.C., Chen, C.T., Chen, S.C., Lai, P.H., Liang, H.C., Chang, Y., Yu, L.C., Sung, H.W., 2005. A natural compound (Ginsenoside Re) isolated from Panax ginseng as a novel angiogenic agent for tissue regeneration. Pharm. Res. 22, 636–646. https://doi.org/10.1007/s11095-005-2500-3

Huebsch, N., Arany, P.R., Mao, A.S., Shvartsman, D., Ali, O.A., Bencherif, S.A., Rivera-Feliciano, J., Mooney, D.J., 2010. Harnessing traction-mediated manipulation of the cell/matrix interface to control stem-cell fate. Nat. Mater. 9, 518–526. https://doi.org/10.1038/nmat2732

Hulme, C.H., Perry, J., McCarthy, H.S., Wright, K.T., Snow, M., Mennan, C., Roberts, S., 2021. Cell therapy for cartilage repair. Emerg. Top. Life Sci. 5, 575–589. https://doi.org/10.1042/ETLS20210015

Im, G. Il, Shin, Y.W., Lee, K.B., 2005. Do adipose tissue-derived mesenchymal stem cells have the same osteogenic and chondrogenic potential as bone marrow-derived cells? Osteoarthr. Cartil. 13, 845–853. https://doi.org/10.1016/j.joca.2005.05.005

Ingber, D., 2009. Mechanobiology and diseases of mechanotransduction Mechanobiology and diseases of mechanotransduction 3890. https://doi.org/10.1080/07853890310016333

Ingber, D.E., 2006. Cellular mechanotransduction: putting all the pieces together again. FASEB J. 20, 811–827. https://doi.org/10.1096/fj.05-5424rev

Islam, N., Dmour, I., Taha, M.O., 2019. Degradability of chitosan micro/nanoparticles for pulmonary drug delivery. Heliyon 5, e01684. https://doi.org/10.1016/j.heliyon.2019.e01684

Jeon, O., Powell, C., Ahmed, S.M., Alsberg, E., 2010. Biodegradable, photocrosslinked alginate hydrogels with independently tailorable physical properties and cell adhesivity. Tissue Eng. Part A 16, 2915–2925. https://doi.org/10.1089/ten.TEA.2010.0096

Jiang, S., Guo, W., Tian, G., Luo, X., Peng, L., Liu, S., Sui, X., Guo, Q., Li, X., 2020. Clinical Application Status of Articular Cartilage Regeneration Techniques: Tissue-Engineered Cartilage Brings New Hope. Stem Cells Int. 2020. https://doi.org/10.1155/2020/5690252

Jiang, Y., Chen, J., Deng, C., Suuronen, E.J., Zhong, Z., 2014. Click hydrogels, microgels and nanogels: Emerging platforms for drug delivery and tissue engineering. Biomaterials 35, 4969–4985. https://doi.org/10.1016/j.biomaterials.2014.03.001

Johnstone, B., Alini, M., Cucchiarini, M., Dodge, G.R., Eglin, D., Guilak, F., Madry, H., Mata, A., Mauck, R.L., Semino, C.E., Stoddart, M.J., 2013. Tissue engineering for articular cartilage repair--the state of the art. Eur. Cell. Mater. 25, 248–267. https://doi.org/10.22203/ecm.v025a18

Khong, T.T., Aarstad, O.A., Skjåk-Bræk, G., Draget, K.I., Vårum, K.M., 2013. Gelling concept combining chitosan and alginate-proof of principle. Biomacromolecules 14, 2765–2771. https://doi.org/10.1021/bm400610b

Kim, H.K., Shim, W.S., Kim, S.E., Lee, K.-H., Kang, E., Kim, J.-H., Kim, K., Kwon, I.C., Lee, D.S., 2009.

Injectable in situ-forming pH/thermo-sensitive hydrogel for bone tissue engineering. Tissue Eng. Part A 15, 923–933. https://doi.org/10.1089/ten.tea.2007.0407

Kim, J., Tomida, K., Matsumoto, T., Adachi, T., 2022. Spheroid culture for chondrocytes triggers the initial stage of endochondral ossification. Biotechnol. Bioeng. 119, 3311–3318. https://doi.org/10.1002/bit.28203

Kogan, G., Šoltés, L., Stern, R., Gemeiner, P., 2007. Hyaluronic acid: A natural biopolymer with a broad range of biomedical and industrial applications. Biotechnol. Lett. 29, 17–25. https://doi.org/10.1007/s10529-006-9219-z

Kong, M., Chen, X.G., Xing, K., Park, H.J., 2010. Antimicrobial properties of chitosan and mode of action: a state of the art review. Int. J. Food Microbiol. 144, 51–63. https://doi.org/10.1016/j.ijfoodmicro.2010.09.012

Koo, H.-J., Song, Y.S., Kim, H.-J., Lee, Y.-H., Hong, S.-M., Kim, S.-J., Kim, B.-C., Jin, C., Lim, C.-J., Park, E.-H., 2004. Antiinflammatory effects of genipin, an active principle of gardenia. Eur. J. Pharmacol. 495, 201–208. https://doi.org/10.1016/j.ejphar.2004.05.031

Kuhn, N.Z., Tuan, R.S., 2010. Regulation of stemness and stem cell niche of mesenchymal stem cells: Implications in tumorigenesis and metastasis. J. Cell. Physiol. 222, 268–277. https://doi.org/10.1002/jcp.21940

Kular, J.K., Basu, S., Sharma, R.I., 2014. The extracellular matrix: Structure, composition, age-related differences, tools for analysis and applications for tissue engineering. J. Tissue Eng. 5. https://doi.org/10.1177/2041731414557112

Kulish, E.I., Volodina, V.P., Fatkullina, R.R., Kolesov, S. V., Zaikov, G.E., 2008. Enzymatic degradation of chitosan films under the action of nonspecific enzymes. Polym. Sci. - Ser. B 50, 175–176. https://doi.org/10.1134/S156009040807004X

Lai, J.-Y., Li, Y.-T., Wang, T.-P., 2010. In vitro response of retinal pigment epithelial cells exposed to chitosan materials prepared with different cross-linkers. Int. J. Mol. Sci. 11, 5256–5272. https://doi.org/10.3390/ijms11125256

Langenbach, F., Handschel, J., 2013. Effects of dexamethasone, ascorbic acid and β-glycerophosphate on the osteogenic differentiation of stem cells in vitro. Stem Cell Res. Ther. 4, 117. https://doi.org/10.1186/scrt328

Langner, R., Vacanti, A.R., 1993. Tissue Engineering Articles. Science (80-.). 260, 920–926.

Law, C.H., Li, J.M., Chou, H.C., Chen, Y.H., Chan, H.L., 2013. Hyaluronic acid-dependent protection in H9C2 cardiomyocytes: A cell model of heart ischemia-reperfusion injury and treatment. Toxicology 303, 54–71. https://doi.org/10.1016/j.tox.2012.11.006

Lee, H.P., Gu, L., Mooney, D.J., Levenston, M.E., Chaudhuri, O., 2017. Mechanical confinement regulates cartilage matrix formation by chondrocytes. Nat. Mater. 16, 1243–1251. https://doi.org/10.1038/nmat4993

Lee, K.Y., Mooney, D.J., 2012. Alginate: properties and biomedical applications. Prog. Polym. Sci. 37, 106–126. https://doi.org/10.1016/j.progpolymsci.2011.06.003

Lee, K.Y., Mooney, D.J., 2001. Hydrogels for tissue engineering. Chem. Rev. 101, 1869–1879. https://doi.org/10.1021/cr000108x

Lee, W., Kalashnikov, N., Mok, S., Halaoui, R., Kuzmin, E., Putnam, A.J., Takayama, S., Park, M., McCaffrey, L., Zhao, R., Leask, R.L., Moraes, C., 2019. Dispersible hydrogel force sensors reveal

patterns of solid mechanical stress in multicellular spheroid cultures. Nat. Commun. 10, 1–14. https://doi.org/10.1038/s41467-018-07967-4

Legré-Boyer, V., 2015. Viscosupplementation: Techniques, indications, results. Orthop. Traumatol. Surg. Res. 101, S101–S108. https://doi.org/10.1016/j.otsr.2014.07.027

Leight, J.L., Drain, A.P., Weaver, V.M., 2017. Extracellular matrix remodeling and stiffening modulate tumor phenotype and treatment response. Annu. Rev. Cancer Biol. 1, 313–334. https://doi.org/10.1146/annurev-cancerbio-050216-034431

Li, W., Shepherd, D.E.T., Espino, D.M., 2020. Frequency dependent viscoelastic properties of porcine brain tissue. J. Mech. Behav. Biomed. Mater. 102, 103460. https://doi.org/10.1016/j.jmbbm.2019.103460

Lin, R.Z., Chou, L.F., Chien, C.C.M., Chang, H.Y., 2006. Dynamic analysis of hepatoma spheroid formation: Roles of E-cadherin and β1-integrin. Cell Tissue Res. 324, 411–422. https://doi.org/10.1007/s00441-005-0148-2

Liu, J., Shikhman, A.R., Lotz, M.K., Wong, C.H., 2001. Hexosaminidase inhibitors as new drug candidates for the therapy of osteoarthritis. Chem. Biol. 8, 701–711. https://doi.org/10.1016/S1074-5521(01)00045-X

Loeser, R.F., 2014. Integrins and chondrocyte-matrix interactions in articular cartilage. Matrix Biol. 39, 11–16. https://doi.org/10.1016/j.matbio.2014.08.007

Loeser, R.F., Carlson, C.S., McGee, M.P., 1995. Expression of beta 1 integrins by cultured articular chondrocytes and in osteoarthritic cartilage. Exp. Cell Res. 217, 248–257. https://doi.org/10.1006/excr.1995.1084

Lou, J., Stowers, R., Nam, S., Xia, Y., Chaudhuri, O., 2018. Stress relaxing hyaluronic acid-collagen hydrogels promote cell spreading, fiber remodeling, and focal adhesion formation in 3D cell culture. Biomaterials 154, 213–222. https://doi.org/10.1016/j.biomaterials.2017.11.004

Marcon, P., Marsich, E., Vetere, A., Mozetic, P., Campa, C., Donati, I., Vittur, F., Gamini, A., Paoletti, S., 2005. The role of Galectin-1 in the interaction between chondrocytes and a lactose-modified chitosan. Biomaterials 26. https://doi.org/10.1016/j.biomaterials.2005.01.044

Marinho, A., Nunes, C., Reis, S., 2021. Hyaluronic acid: A key ingredient in the therapy of inflammation. Biomolecules 11, 13–15. https://doi.org/10.3390/biom11101518

Marsich, E.., Borgogna, M.., Donati, I.., Mozetic, P.., Strand, B.L.., Salvador, S.G.., Vittur, F.., Paoletti, S., 2008. Alginate/lactose-modified chitosan hydrogels: A bioactive biomaterial for chondrocyte encapsulation. J. Biomed. Mater. Res. A 84, 364–376. https://doi.org/10.1002/jbm.a

Marsich, E., Travan, A., Feresini, M., Lapasin, R., Paoletti, S., Donati, I., 2013. Polysaccharide-based polyanion-polycation-polyanion ternary systems in the concentrated regime and hydrogel form. Macromol. Chem. Phys. 214, 1309–1320. https://doi.org/10.1002/macp.201300057

Martel-Pelletier, J., 2004. Pathophysiology of osteoarthritis. Osteoarthr. Cartil. 12 Suppl A, S31-3. https://doi.org/10.1016/j.joca.2003.10.002

Martinac, B., Kloda, A., 2003. Evolutionary origins of mechanosensitive ion channels. Prog. Biophys. Mol. Biol. 82, 11–24. https://doi.org/10.1016/s0079-6107(03)00002-6

Mayumi, K., Guo, J., Narita, T., Hui, C.Y., Creton, C., 2016. Fracture of dual crosslink gels with permanent and transient crosslinks. Extrem. Mech. Lett. 6, 52–59. https://doi.org/10.1016/j.eml.2015.12.002

Mayumi, K., Marcellan, A., Ducouret, G., Creton, C., Narita, T., 2013. Stress-strain relationship of highly

stretchable dual cross-link gels: Separability of strain and time effect. ACS Macro Lett. 2, 1065–1068. https://doi.org/10.1021/mz4005106

Medelin, M., Porrelli, D., Aurand, E.R., Scaini, D., Travan, A., Borgogna, M.A., Cok, M., Donati, I., Marsich, E., Scopa, C., Scardigli, R., Paoletti, S., Ballerini, L., 2018. Exploiting natural polysaccharides to enhance in vitro bio-constructs of primary neurons and progenitor cells. Acta Biomater. 73, 285–301. https://doi.org/10.1016/j.actbio.2018.03.041

Medvedeva, E. V, Grebenik, E.A., Gornostaeva, S.N., Telpuhov, V.I., Lychagin, A. V, Timashev, P.S., Chagin, A.S., 2018. Repair of Damaged Articular Cartilage : Current Approaches and Future Directions. Int. J. Mol. Sci. 19, 2366. https://doi.org/10.3390/ijms19082366

Mi, Fwu Long, Sung, H.W., Shyu, S.S., 2001. Release of indomethacin from a novel chitosan microsphere prepared by a naturally occurring crosslinker: Examination of crosslinking and polycation-anionic drug interaction. J. Appl. Polym. Sci. 81, 1700–1711. https://doi.org/10.1002/app.1602

Mi, F L, Tan, Y.C., Liang, H.C., Huang, R.N., Sung, H.W., 2001. In vitro evaluation of a chitosan membrane cross-linked with genipin. J. Biomater. Sci. Polym. Ed. 12, 835–850. https://doi.org/10.1163/156856201753113051

Molinaro, G., Leroux, J.C., Damas, J., Adam, A., 2002. Biocompatibility of thermosensitive chitosan-based hydrogels: An in vivo experimental approach to injectable biomaterials. Biomaterials 23, 2717–2722. https://doi.org/10.1016/S0142-9612(02)00004-2

Muzzarelli, R.A.A., 2009. Genipin-crosslinked chitosan hydrogels as biomedical and pharmaceutical aids. Carbohydr. Polym. 77, 1–9. https://doi.org/https://doi.org/10.1016/j.carbpol.2009.01.016

Muzzarelli, R.A.A., El Mehtedi, M., Bottegoni, C., Gigante, A., 2016. Physical properties imparted by genipin to chitosan for tissue regeneration with human stem cells: A review. Int. J. Biol. Macromol. 93, 1366–1381. https://doi.org/https://doi.org/10.1016/j.ijbiomac.2016.03.075

Nam, S., Lee, J., Brownfield, D.G., Chaudhuri, O., 2016. Viscoplasticity Enables Mechanical Remodeling of Matrix by Cells. Biophys. J. 111, 2296–2308. https://doi.org/10.1016/j.bpj.2016.10.002

Naqvi, S.M., Mcnamara, L.M., 2020. Stem Cell Mechanobiology and the Role of Biomaterials in Governing Mechanotransduction and Matrix Production for Tissue Regeneration 8, 1–27. https://doi.org/10.3389/fbioe.2020.597661

Narita, T., Mayumi, K., Ducouret, G., Hébraud, P., 2013. Viscoelastic properties of poly(vinyl alcohol) hydrogels having permanent and transient cross-links studied by microrheology, clasfile:///Volumes/Chiara Lab /Dottorato/paper meccano/zhao2017.pdfsical rheometry, and dynamic light scattering. Macromolecules 46, 4174–4183. https://doi.org/10.1021/ma400600f

Ofek, G., Dowling, E.P., Raphael, R.M., Mcgarry, J.P., Athanasiou, K.A., 2010. Biomechanics of single chondrocytes under direct shear 153–162. https://doi.org/10.1007/s10237-009-0166-1

Osidak, E.O., Kozhukhov, V.I., Osidak, M.S., Domogatsky, S.P., 2020. Collagen as bioink for bioprinting: A comprehensive review. Int. J. Bioprinting 6, 1–10. https://doi.org/10.18063/IJB.V6I3.270

Osório, J., 2016. Osteoarthritis: Galectin-1 damages cartilage via inflammation. Nat. Rev. Rheumatol. 12, 132–133. https://doi.org/10.1038/nrrheum.2016.12

Otto, S., Engberts, J.B.F.N., 2000. Diels_Alder reactions in water. Pure Appl. Chem. 72, 1365–1372. https://doi.org/https://doi.org/10.1351/pac200072071365

Pásztói, M., Nagy, G., Géher, P., Lakatos, T., Tóth, K., Wellinger, K., Pócza, P., György, B., Holub, M.C., Kittel, Á., Pálóczy, K., Mazán, M., Nyirkos, P., Falus, A., Buzas, E.I., 2009. Gene expression and

activity of cartilage degrading glycosidases in human rheumatoid arthritis and osteoarthritis synovial fibroblasts. Arthritis Res. Ther. 11, 1–13. https://doi.org/10.1186/ar2697

Pelham, R.J.J., Wang, Y. l, 1997. Cell locomotion and focal adhesions are regulated by substrate flexibility. Proc. Natl. Acad. Sci. U. S. A. 94, 13661–13665. https://doi.org/10.1073/pnas.94.25.13661

Peng, Z., Sun, H., Bunpetch, V., Koh, Y., Wen, Y., Wu, D., Ouyang, H., 2021. The regulation of cartilage extracellular matrix homeostasis in joint cartilage degeneration and regeneration. Biomaterials 268, 120555. https://doi.org/10.1016/j.biomaterials.2020.120555

Peppas, B.N.A., Hilt, J.Z., Khademhosseini, A., Langer, R., 2006. Hydrogels in Biology and Medicine : From Molecular Principles to Bionanotechnology. Adv. Mater. 18, 1345–1360. https://doi.org/10.1002/adma.200501612

Pirrung, M.C., 2006. Acceleration of Organic Reactions through Aqueous Solvent Effects. Chem. – A Eur. J. 12, 1312–1317. https://doi.org/10.1002/chem.200500959

Pizzolitto, C., Cok, M., Asaro, F., Scognamiglio, F., Marsich, E., Lopez, F., Donati, I., Sacco, P., 2020. On the mechanism of genipin binding to primary amines in lactose-modified chitosan at neutral pH. Int. J. Mol. Sci. 21, 1–17. https://doi.org/10.3390/ijms21186831

Pizzolitto, C., Esposito, F., Sacco, P., Marsich, E., Gargiulo, V., Bedini, E., Donati, I., 2022. Sulfated lactose-modified chitosan. A novel synthetic glycosaminoglycan-like polysaccharide inducing chondrocyte aggregation. Carbohydr. Polym. 288, 119379. https://doi.org/10.1016/j.carbpol.2022.119379

Pizzolitto, C., Scognamiglio, F., Sacco, P., Lipari, S., Romano, M., Donati, I., Marsich, E., 2023. Immediate stress dissipation in dual cross-link hydrogels controls osteogenic commitment of mesenchymal stem cells. Carbohydr. Polym. 302, 120369. https://doi.org/10.1016/j.carbpol.2022.120369

Rapino, M., Di Valerio, V., Zara, S., Gallorini, M., Marconi, G.D., Sancilio, S., Marsich, E., Ghinassi, B., Di Giacomo, V., Cataldi, A., 2019. Chitlac-coated thermosets enhance osteogenesis and angiogenesis in a co-culture of dental pulp stem cells and endothelial cells. Nanomaterials 9. https://doi.org/10.3390/nano9070928

Rivest, C., Morrison, D.W.G., Ni, B., Rubin, J., Yadav, V., Mahdavi, A., Karp, J.M., Khademhosseini, A., 2007. Mechanics of Materials and Structures. J. Mech. Mater. Struct. 2.

Ryu, N.E., Lee, S.H., Park, H., 2019. Spheroid culture system methods and applications for mesenchymal stem cells. Cells 8, 1–13. https://doi.org/10.3390/cells8121620

Sacco, P., Baj, G., Asaro, F., Marsich, E., Ivan, I., 2020. Substrate Dissipation Energy Regulates Cell Adhesion and Spreading. Adv. Funct. Mater. 30. https://doi.org/10.1002/adfm.202001977

Sacco, Pasquale, Brun, F., Donati, I., Porrelli, D., Paoletti, S., Turco, G., 2018a. On the Correlation between the Microscopic Structure and Properties of Phosphate-Cross-Linked Chitosan Gels. ACS Appl. Mater. Interfaces 10, 10761–10770. https://doi.org/10.1021/acsami.8b01834

Sacco, Pasquale, Cok, M., Asaro, F., Paoletti, S., Donati, I., 2018b. The role played by the molecular weight and acetylation degree in modulating the stiffness and elasticity of chitosan gels. Carbohydr. Polym. 196, 405–413. https://doi.org/10.1016/j.carbpol.2018.05.060

Sacco, P., Cok, M., Asaro, F., Paoletti, S., Donati, I., 2018. The role played by the molecular weight and acetylation degree in modulating the stiffness and elasticity of chitosan gels. Carbohydr. Polym. 196, 405–413. https://doi.org/10.1016/j.carbpol.2018.05.060

Sacco, Pasquale, Cok, M., Scognamiglio, F., Pizzolitto, C., Vecchies, F., Marfoglia, A., Marsich, E., Donati,

I., 2020a. Glycosylated-Chitosan Derivatives: A Systematic Review. Molecules 25, 1534.

Sacco, P., Furlani, F., Cok, M., Travan, A., Borgogna, M., Marsich, E., Paoletti, S., Donati, I., 2017. Boric Acid Induced Transient Cross-Links in Lactose-Modified Chitosan (Chitlac). Biomacromolecules 18, 4206–4213. https://doi.org/10.1021/acs.biomac.7b01237

Sacco, Pasquale, Furlani, F., Marfoglia, A., Cok, M., Pizzolitto, C., Marsich, E., Donati, I., 2020b. Temporary/Permanent Dual Cross-Link Gels Formed of a Bioactive Lactose-Modified Chitosan. Macromol. Biosci. 20, 1–7. https://doi.org/10.1002/mabi.202000236

Sacco, P., Paoletti, S., Cok, M., Asaro, F., Abrami, M., Grassi, M., Donati, I., 2016. Insight into the ionotropic gelation of chitosan using tripolyphosphate and pyrophosphate as cross-linkers. Int. J. Biol. Macromol. 92, 476–483. https://doi.org/10.1016/j.ijbiomac.2016.07.056

Sacco, P., Piazza, F., Pizzolitto, C., Baj, G., Brun, F., Marsich, E., Donati, I., 2022. Regulation of Substrate Dissipation via Tunable Linear Elasticity Controls Cell Activity. Adv. Funct. Mater. 32, 1–12. https://doi.org/10.1002/adfm.202200309

Sack, I., Beierbach, B., Wuerfel, J., Klatt, D., Hamhaber, U., Papazoglou, S., Martus, P., Braun, J., 2009. The impact of aging and gender on brain viscoelasticity. Neuroimage 46, 652–657. https://doi.org/10.1016/j.neuroimage.2009.02.040

Sahoo, D.R., Biswal, T., 2021. Alginate and its application to tissue engineering. SN Appl. Sci. 3, 1–19. https://doi.org/10.1007/s42452-020-04096-w

Salamanna, F., Giavaresi, G., Parrilli, A., Martini, L., Nicoli Aldini, N., Abatangelo, G., Frizziero, A., Fini, M., 2019. Effects of intra-articular hyaluronic acid associated to Chitlac (arty-duo®) in a rat knee osteoarthritis model. J. Orthop. Res. 37, 867–876. https://doi.org/10.1002/jor.24259

Sannan, T., Kurita, K., Iwakura, Y., 1976. Studies on Chitin, - Effect of Deacetylation on Solubility. Die Makromol. Chemie 177, 3589–3600.

Santos, A., Lagares, D., 2018. Matrix Stiffness: the Conductor of Organ Fibrosis. Curr. Rheumatol. Rep. 20, 2. https://doi.org/10.1007/s11926-018-0710-z

Saraswathibhatla, A., Indana, D., Chaudhuri, O., 2023. Cell–extracellular matrix mechanotransduction in 3D. Nat. Rev. Mol. Cell Biol. https://doi.org/10.1038/s41580-023-00583-1

Sargeant, T.D., Desai, A.P., Banerjee, S., Agawu, A., Stopek, J.B., 2012. An in situ forming collagen-PEG hydrogel for tissue regeneration. Acta Biomater. 8, 124–132. https://doi.org/10.1016/j.actbio.2011.07.028

Scognamiglio, F., Cok, M., Piazza, F., Marsich, E., Pacor, S., Aarstad, O.A., Aachmann, F.L., Donati, I., 2023. Hydrogels based on methylated-alginates as a platform to investigate the effect of material properties on cell activity. The role of material compliance. Carbohydr. Polym. 311, 120745. https://doi.org/10.1016/j.carbpol.2023.120745

Scognamiglio, Francesca, Travan, A., Borgogna, M., Donati, I., Marsich, E., 2020. Development of biodegradable membranes for the delivery of a bioactive chitosan-derivative on cartilage defects: A preliminary investigation. J. Biomed. Mater. Res. - Part A 108, 1534–1545. https://doi.org/10.1002/jbm.a.36924

Scognamiglio, F., Travan, A., Bussani, R., Borgogna, M., Donati, I., Bosmans, J.W.A.M., Bouvy, N.D., Marsich, E., 2019. Development of hyaluronan-based membranes for the healing of intestinal surgical wounds: a preliminary study. J. Mater. Sci. Mater. Med. 30. https://doi.org/10.1007/s10856-019-6262-6

Scognamiglio, F., Travan, A., Donati, I., Borgogna, M., Marsich, E., 2020. A hydrogel system based on a

lactose-modified chitosan for viscosupplementation in osteoarthritis. Carbohydr. Polym. 248, 116787. https://doi.org/10.1016/j.carbpol.2020.116787

Sharma, K., Mujawar, M.A., Kaushik, A., 2019. State-of-Art Functional Biomaterials for Tissue Engineering 6, 1–10. https://doi.org/10.3389/fmats.2019.00172

Shikhman, A.R., Brinson, D.C., Lotz, M., 2000. Profile of glycosaminoglycan-degrading glycosidases and glycoside sulfatases secreted by human articular chondrocytes in homeostasis and inflammation. Arthritis Rheum. 43, 1307–1314. https://doi.org/10.1002/1529-0131(200006)43:6<1307::AID-ANR13>3.0.CO;2-3

Shim, J.-H., Jang, K.-M., Hahn, S.K., Park, J.Y., Jung, H., Oh, K., Park, K.M., Yeom, J., Park, S.H., Kim, S.W., Wang, J.H., Kim, K., Cho, D.-W., 2016. Three-dimensional bioprinting of multilayered constructs containing human mesenchymal stromal cells for osteochondral tissue regeneration in the rabbit knee joint. Biofabrication 8, 14102. https://doi.org/10.1088/1758-5090/8/1/014102

Sinkus, R., Siegmann, K., Xydeas, T., Tanter, M., Claussen, C., Fink, M., 2007. MR elastography of breast lesions: understanding the solid/liquid duality can improve the specificity of contrast-enhanced MR mammography. Magn. Reson. Med. 58, 1135–1144. https://doi.org/10.1002/mrm.21404

Sophia Fox, A.J., Bedi, A., Rodeo, S.A., 2009. The basic science of articular cartilage: structure, composition, and function. Sports Health 1, 461–468. https://doi.org/10.1177/1941738109350438

Sorlier, P., Denuzière, A., Viton, C., Domard, A., 2001. Relation between the degree of acetylation and the electrostatic properties of chitin and chitosan. Biomacromolecules 2, 765–772. https://doi.org/10.1021/bm015531+

Sorushanova, A., Delgado, L.M., Wu, Z., Shologu, N., Kshirsagar, A., Raghunath, R., Mullen, A.M., Bayon, Y., Pandit, A., Raghunath, M., Zeugolis, D.I., 2019. The Collagen Suprafamily: From Biosynthesis to Advanced Biomaterial Development. Adv. Mater. 31, 1–39. https://doi.org/10.1002/adma.201801651

Stanton, A.E., Tong, X., Yang, F., 2019. Extracellular matrix type modulates mechanotransduction of stem cells. Acta Biomater. 96, 310–320. https://doi.org/10.1016/j.actbio.2019.06.048

Stavenschi, E., Hoey, D.A., 2019. Pressure-induced mesenchymal stem cell osteogenesis is dependent on intermediate filament remodeling. FASEB J. 33, 4178–4187. https://doi.org/10.1096/fj.201801474RR

Strand, S.P., Tømmeraas, K., Vårum, K.M., Østgaard, K., 2001. Electrophoretic light scattering studies of chitosans with different degrees of N-acetylation. Biomacromolecules 2, 1310–1314. https://doi.org/10.1021/bm015598x

Strecanska, M., Danisovic, L., Ziaran, S., Cehakova, M., 2022. The Role of Extracellular Matrix and Hydrogels in Mesenchymal Stem Cell Chondrogenesis and Cartilage Regeneration. Life 12. https://doi.org/10.3390/life12122066

Streitberger, K.-J., Reiss-Zimmermann, M., Freimann, F.B., Bayerl, S., Guo, J., Arlt, F., Wuerfel, J., Braun, J., Hoffmann, K.-T., Sack, I., 2014. High-resolution mechanical imaging of glioblastoma by multifrequency magnetic resonance elastography. PLoS One 9, e110588. https://doi.org/10.1371/journal.pone.0110588

Sung, H.W., Huang, R.N., Huang, L.H., Tsai, C.C., 1999. In vitro evaluation of cytotoxicity of a naturally occurring cross-linking reagent for biological tissue fixation. J. Biomater. Sci. Polym. Ed. 10, 63–78. https://doi.org/10.1163/156856299X00289

Takeuchi, S., Goto, T., Mikami, K.-I., Miura, K., Ohshima, S., Yoneyama, K., Sato, M., Shibuya, T., Watanabe, D., Kataoka, E., Segawa, D., Endo, A., Sato, W., Yoshino, R., Watanabe, S., 2005. Genipin prevents fulminant hepatic failure resulting in reduction of lethality through the suppression of TNF-

alpha production. Hepatol. Res. 33, 298–305. https://doi.org/10.1016/j.hepres.2005.08.009

Tan, H., Lao, L., Wu, J., Gong, Y., Gao, C., 2008. Biomimetic modification of chitosan with covalently grafted lactose and blended heparin for improvement of in vitro cellular interaction. Polym. Adv. Technol. 19, 15–23. https://doi.org/https://doi.org/10.1002/pat.962

Tarricone, E., Elia, R., Mattiuzzo, E., Faggian, A., Pozzuoli, A., Ruggieri, P., Brun, P., 2021. The Viability and Anti-Inflammatory Effects of Hyaluronic Acid-Chitlac-Tracimolone Acetonide- β-Cyclodextrin Complex on Human Chondrocytes. Cartilage 13, 920S-924S. https://doi.org/10.1177/1947603520908658

Tarricone, E., Mattiuzzo, E., Belluzzi, E., Elia, R., Benetti, A., Venerando, R., Vindigni, V., Ruggieri, P., Brun, P., 2020a. Anti-Inflammatory Performance of Lactose-Modified Osteoarthritis Model. Cells 9, 1328.

Tarricone, E., Mattiuzzo, E., Belluzzi, E., Elia, R., Benetti, A., Venerando, R., Vindigni, V., Ruggieri, P., Brun, P., 2020b. Anti-Inflammatory Performance of Lactose-Modified Chitosan and Hyaluronic Acid Mixtures in an In Vitro Macrophage-Mediated Inflammation Osteoarthritis Model. Cells. https://doi.org/10.3390/cells9061328

Thambiliyagodage, C., Jayanetti, M., Mendis, A., Ekanayake, G., 2023. Recent Advances in Chitosan-Based Applications—A Review 16, 2073.

Toegel, S., Weinmann, D., André, S., Walzer, S.M., Bilban, M., Schmidt, S., Chiari, C., Windhager, R., Krall, C., Bennani-Baiti, I.M., Gabius, H.-J., 2016. Galectin-1 Couples Glycobiology to Inflammation in Osteoarthritis through the Activation of an NF-κB–Regulated Gene Network. J. Immunol. 196, 1910–1921. https://doi.org/10.4049/jimmunol.1501165

Touyama, R.., Inoue, R.. ., Takeda, Y.., Yatsuzuka, M.; Ikumoto, T.; Moritome, N.; Shingu, T.; Yokoi, T.; Inouye, H., 1994. Studies on the Blue Pigments Produced from Genipin and Methylamine. II. On the Formation Mechanisms of Brownish-Red Intermediates Leading to the Blue Pigment Formation. Chem. Pharm. Bull. 42, 1571–1578.

Trappmann, B., Gautrot, J.E., Connelly, J.T., Strange, D.G.T., Li, Y., Oyen, M.L., Cohen Stuart, M.A., Boehm, H., Li, B., Vogel, V., Spatz, J.P., Watt, F.M., Huck, W.T.S., 2012. Extracellular-matrix tethering regulates stem-cell fate. Nat. Mater. 11, 642–649. https://doi.org/10.1038/nmat3339

Travan, A., Marsich, E., Donati, I., Foulc, M.P., Moritz, N., Aro, H.T., Paoletti, S., 2012. Polysaccharide-coated thermosets for orthopedic applications: From material characterization to in vivo tests. Biomacromolecules 13, 1564–1572. https://doi.org/10.1021/bm3002683

Turco, G., Marsich, E., Bellomo, F., Semeraro, S., Donati, I., Brun, F., Grandolfo, M., Accardo, A., Paoletti, S., 2009. Alginate/hydroxyapatite biocomposite for bone ingrowth: A trabecular structure with high and isotropic connectivity. Biomacromolecules 10, 1575–1583. https://doi.org/10.1021/bm900154b

Ullah, F., Othman, M.B.H., Javed, F., Ahmad, Z., Akil, H.M., 2015. Classification, processing and application of hydrogels: A review. Mater. Sci. Eng. C 57, 414–433. https://doi.org/10.1016/j.msec.2015.07.053

Vårum, K.M.; Ottøy, M.H.; Smidsrød, O., 1994. No TitleWater-solubility of partially N-acetylated chitosans as a function of pH: Effect of chemical composition and depolymerisation. Carbohydr. Polym. 25, 65–70.

Vincent, T.L., McClurg, O., Troeberg, L., 2022. The Extracellular Matrix of Articular Cartilage Controls the Bioavailability of Pericellular Matrix-Bound Growth Factors to Drive Tissue Homeostasis and Repair. Int. J. Mol. Sci. 23. https://doi.org/10.3390/ijms23116003

Wang, J., Wang, Z., Gao, J., Wang, L., Yang, Zhiyi, Kong, D., Yang, Zhimou, 2009. Incorporation of supramolecular hydrogels into agarose hydrogels - A potential drug delivery carrier. J. Mater. Chem. 19, 7892–7896. https://doi.org/10.1039/b913158b

Xu, B., Wang, X., Lu, Y., 2006. Surface modification of polyacrylonitrile-based carbon fiber and its interaction with imide. Appl. Surf. Sci. 253, 2695–2701. https://doi.org/https://doi.org/10.1016/j.apsusc.2006.05.044

Xu, J., Strandman, S., Zhu, J.X.X., Barralet, J., Cerruti, M., 2015. Genipin-crosslinked catechol-chitosan mucoadhesive hydrogels for buccal drug delivery. Biomaterials 37, 395–404. https://doi.org/https://doi.org/10.1016/j.biomaterials.2014.10.024

Xu, J., Vilanova, G., Gomez, H., 2016. A mathematical model coupling tumor growth and angiogenesis. PLoS One 11, 1–20. https://doi.org/10.1371/journal.pone.0149422

Yalpani, M., Hall, L.D., 1984. Some Chemical and Analytical Aspects Of Polysaccharide Modifications.1 3. Formation of Branched-Chain, Soluble Chitosan Derivatives2. Macromolecules 17, 272–281. https://doi.org/10.1021/ma00133a003

Yamada, K.M., Sixt, M., 2019. Mechanisms of 3D cell migration. Nat. Rev. Mol. Cell Biol. 20, 738–752. https://doi.org/10.1038/s41580-019-0172-9

Younes, I., Sellimi, S., Rinaudo, M., Jellouli, K., Nasri, M., 2014. Influence of acetylation degree and molecular weight of homogeneous chitosans on antibacterial and antifungal activities. Int. J. Food Microbiol. 185, 57–63. https://doi.org/10.1016/j.ijfoodmicro.2014.04.029

Yu, Y., Xu, S., Yu, S., Li, J., Tan, G., Li, S., Pan, W., 2020. A Hybrid Genipin-Cross-Linked Hydrogel/Nanostructured Lipid Carrier for Ocular Drug Delivery: Cellular, ex Vivo, and in Vivo Evaluation. ACS Biomater. Sci. Eng. 6, 1543–1552. https://doi.org/10.1021/acsbiomaterials.9b01800

Yuan, Y., Chesnutt, B.M., Utturkar, G., Haggard, W.O., Yang, Y., Ong, J.L., Bumgardner, J.D., 2007. The effect of cross-linking of chitosan microspheres with genipin on protein release. Carbohydr. Polym. 68, 561–567. https://doi.org/https://doi.org/10.1016/j.carbpol.2006.10.023

Zhang, C.-Y., Parton, L.E., Ye, C.P., Krauss, S., Shen, R., Lin, C.-T., Porco, J.A.J., Lowell, B.B., 2006. Genipin inhibits UCP2-mediated proton leak and acutely reverses obesity- and high glucose-induced beta cell dysfunction in isolated pancreatic islets. Cell Metab. 3, 417–427. https://doi.org/10.1016/j.cmet.2006.04.010

Zhang, C., Shi, G., Zhang, J., Song, H., Niu, J., Shi, S., Huang, P., Wang, Y., Wang, W., Li, C., Kong, D., 2017. Targeted antigen delivery to dendritic cell via functionalized alginate nanoparticles for cancer immunotherapy. J. Control. release Off. J. Control. Release Soc. 256, 170–181. https://doi.org/10.1016/j.jconrel.2017.04.020

Zhang, C., Wang, W., Liu, T., Wu, Y., Guo, H., Wang, P., Tian, Q., Wang, Y., Yuan, Z., 2012. Doxorubicin-loaded glycyrrhetinic acid-modified alginate nanoparticles for liver tumor chemotherapy. Biomaterials 33, 2187–2196. https://doi.org/10.1016/j.biomaterials.2011.11.045

Zhang, H., Cheng, J., Ao, Q., 2021. Preparation of Alginate-Based Biomaterials and Their Applications in Biomedicine. Mar. Drugs 19, 264.

Zhang, L., Hu, J., Athanasiou, K.A., 2009. The role of tissue engineering in articular cartilage repair and regeneration. Crit. Rev. Biomed. Eng. 37, 1–57. https://doi.org/10.1615/critrevbiomedeng.v37.i1-2.10

Zhang, M., Zhao, X., 2020. Alginate hydrogel dressings for advanced wound management. Int. J. Biol. Macromol. 162, 1414–1428. https://doi.org/10.1016/j.ijbiomac.2020.07.311

Zhang, Y.S., Khademhosseini, A., 2017. Advances in engineering hydrogels. Science (80-.). 356, 139–148. https://doi.org/10.1126/science.aaf3627.Advances

Zhao, J., Mayumi, K., Creton, C., Narita, T., 2017. Rheological properties of tough hydrogels based on an associating polymer with permanent and transient crosslinks: Effects of crosslinking density. J. Rheol. (N. Y. N. Y). 61, 1371–1383. https://doi.org/10.1122/1.4997589

Zheng, L.Y., Zhu, J.F., 2003. Study on antimicrobial activity of chitosan with different molecular weights. Carbohydr. Polym. 54, 527–530. https://doi.org/10.1016/j.carbpol.2003.07.009

Zubillaga, V., Alonso-varona, A., Fernandes, S.C.M., Salaberria, A.M., Palomares, T., 2020. Adipose-derived mesenchymal stem cell chondrospheroids cultured in hypoxia and a 3D porous chitosan/chitin nanocrystal scaffold as a platform for cartilage tissue engineering. Int. J. Mol. Sci. 21, 1–17. https://doi.org/10.3390/ijms21031004

AKNOWLEDGEMENTS

“Hai mai pensato di fare il dottorato?” Ed è con questa frase che il mio percorso verso il dottorato è cominciato. Poche parole dette tra un esperimento e l’altro mi hanno portata ad intraprendere questa sfida. Ricordo ancora quel maggio 2019 quando all’ultimo momento mi sono ritrovata ad abbozzare un progetto di dottorato e provare a partecipare al concorso. Ricordo poi l’ansia a settembre quando, felice per la posizione in graduatoria, mi sono resa conto di dovermi però prima laureare. Non so ancora come ci sia riuscita in un mese a finire gli ultimi esami e a scrivere la tesi di laurea. Forse in realtà ci sono riuscita grazie alla grinta che ho, quella grinta che vedono più gli altri in me e che a volte io mi dimentico di avere. Ed è con questa grinta che ho affrontato questi 3 anni, bellissimi ma non sempre facili. Le paure di non essere all’altezza del ruolo nel primo periodo, le prime sicurezze prese, la voglia di tornare in laboratorio durante il lockdown, il pensiero fisso del “paper dei condrociti” pure in sala parto e nei mesi successivi dove, tra una poppata e l’altra rispondevo ai Referee, ed infine le corse negli ultimi mesi per riuscire a fare combaciare il tutto per terminare questo incredibile percorso.
Oltre alla grinta però tutto questo è stato possibile anche grazie a diverse persone che voglio ringraziare nelle prossime righe.

Un primo grazie va al mio Supervisor, Ivan e al mio Co-Supervisor Gianluca, per avermi dato la possibilità di raggiungere questo importante traguardo permettendomi di frequentare i loro laboratori ed essendo stati costantemente presenti.

Un grazie va poi ad Eleonora per essere stata sempre disponibile per un consiglio e per il preziosissimo contributo per la realizzazione del progetto sugli sferoidi.

Sempre per il progetto sferoidi un grazie va anche a piccola Fra, colei che mi fece frullare per la testa l’ipotesi del dottorato. Ne abbiamo passate parecchie in questi 3 anni ma nonostante tutto siamo sempre riuscite a chiarirci e a trovare sempre il tempo per parlarci e raccontarci i vari cambiamenti della nostra vita.

Un grazie va poi a Sara, la nostra marachella-girl, nonché prima tesista che mi sono trovata a seguire. Ammetto all’inizio ero un po’ nel panico perché avevo davanti una ragazza brava e avevo paura di non essere all’altezza nel darle l’’aiuto per realizzare un buon progetto di tesi. Fortunatamente mi sono trovata davanti una ragazza tosta e l’averti accompagnata durante il tuo periodo di internato mi ha permesso di crescere molto e mi ha spronato a cercare di fare sempre meglio.

Un grazie va poi a tutti i ragazzi (tesisti, tirocinanti, dottorandi e assegnisti) che negli anni si sono susseguiti nel TEAM 105 per avermi donato un sacco di momenti divertenti e di svago tra un esperimento e l'altro: Adriana, Alberto, Andrea, Beatrice, Davide, Dede, Federica V, Francesco, Franco, Gigi, Julia, Lara, Lorenzo, Luigi, Mario, Marco, Martina C., Martina G., Michela, Michele, Riccardo.

Per la realizzazione di questo progetto di tesi vorrei poi ringrazia diversi collaboratori che hanno contribuito a vario titolo all’esecuzione di alcuni esperimenti e all’interpretazione di

alcuni risultat: Prof. Maurizio Romano per gli esperimenti sulla qRT-PCR, Dr.sse Roberta Bulla e Giovanna Baldini per l'analisi TEM, Prof.ssa Vanessa Nicolin per l'interpretazione dei dati istologici nel progetto sferoidi, Prof.ssa Susi Zara dell'Università di Chieti per la realizzazione delle immagini di istologia per gli sferoidi con cellule mesenchimali.

Un grazie va poi alla mia famiglia e in particolare a mia mamma, a mio papà e a mia sorella che mi hanno sempre supportato in questo percorso e in tutto il resto della mia vita. Ora siete diventati dei nonni e una zia fantastica per Bianca e sono grata per l'aiuto che mi state dando.

Un grazie in più anche ai miei nonni che in questi anni mi hanno sempre chiesto come procedeva il laboratorio.

Un grazie ai miei zii, ai miei cugini (Carlos con Mariam e la piccola Soleil, Emma e Matilde) e a mia zia Giorgia che con le varie difficoltà di questi ultimi anni ha sempre trovato il tempo ogni sera per chiedermi come era andata la giornata.

Un grazie anche a tutti i miei amici (dal Secret Santa alle Asciugapozzanghere, passando dal gruppo di AC e a quelle amiche che conosco da una vita) so che nell'ultimo anno sono cambiate parecchie cose nella mia vita e vi ho trascurato un pochino ma sappiate che avete ci sono sempre per qualsiasi cosa.
Un pensiero finale lo devo poi ai miei due nonni che mi stanno guardando da la su e che sono sicura essere orgogliosi nel vedermi vivere nella loro casa con la mia famiglia, quella famiglia che nel profondo ho sempre sognato ma che ho avevo paura di cercare fino in fondo. Ed è qui che arrivano gli ultimi due grazie, quelli alle due persone che non ho ancora nominato fino ad ora: Pasquale e Bianca. Pasquale, se dovessi scriverti qua tutti i grazie che dovrei dirti uscirebbe un'ulteriore tesi ma fortunatamente già li sai. Quindi ne dirò solo uno: grazie per ricordarmi ogni giorno che sono "Chiara cazzuta" e "Chiara cuore d'oro". Ricordati, tu e Bianca siete la migliore cosa che mi potesse mai capitare nella vita. Ed è quindi che concludo con grazie piccola Bianca, grazie per averci scelto come tua mamma e tuo papà, per essere arrivata tra noi e per donarci spensieratezza e gioia ogni volta che incrociamo il tuo sguardo. Ti amiamo.